Politecnico di Torino

Master’s degree in Energy and Nuclear Engineering
A.a. 2024/2025
Sessione di Laurea Marzo 2025

Direct Air Capture (DAC)-Sourced CO_2 and Green Hydrogen: A Synergistic Route to Sustainable E-Fuels

Relatori:
Prof. Massimo Santarelli
Prof. Salvatore Cannone

Candidati:
Federico Cavallo

SUMMARY

ABSTRACT

The increasing urgency of climate change mitigation has led to growing interest in Direct Air Capture (DAC) as a viable solution for reducing atmospheric CO_2 levels. This study focuses on the modeling of a DAC process employing an alkali sorbent, specifically implementing a modified Kraft process. The objective is to develop a simulation of the upscaled Carbon Engineering ‘s DAC plant assessing its energy consumption and integration with downstream CO_2 utilization. The captured CO_2 is subsequently used in methanol synthesis process combining it with green hydrogen, exploring a potential pathway for sustainable e-fuel production.

The process was modeled using Aspen Plus®, a professional software developed by AspenTech, with a focus on replicating the thermodynamic and operational characteristics of the large-scale DAC system. Special attention was given to thermal integration strategies aimed at recovering thermal energy in order to reduce consumption. The DAC model was validated by comparing its energy demand per unit of CO_2 captured against reference values from literature and existing pilot-scale systems. Additionally, an analysis was conducted to evaluate energy conversion efficiencies, particularly, regarding the utilization section, properly methanol conversion ratio and electrical conversion into chemical power were assessed.

The results provide valuable insights into the feasibility of large-scale DAC deployment and its integration with e-fuel production, clarifying the implications of utilization strategies for DAC systems. Specifically, the study calculates energy consumption per unit of methanol produced and per unit of CO_2 captured, offering a clear estimate of the energy requirements involved. Additionally, the analysis includes a detailed comparison between plants with and without the utilization facility, highlighting how the energy demand increases with the utilization process and how other factors are impacted. These factors include the potential removal of obsolete auxiliary components and changes in the purity of some streams like the CO_2 available. The findings underscore key considerations that provide a basis for future research, aimed at improving energy efficiency and assessing the role of DAC technologies within a sustainable carbon management framework.

1 OVERVIEW

1.1 INTRODUCTION

Environmental pollution encompasses a wide range of detrimental impacts caused by human activities, adversely affecting air, water, soil, and ecosystems. Among the most pressing types are air pollution, water contamination, soil degradation, and hazardous waste accumulation. Air pollution, driven by emissions from fossil fuels, industrial processes, emission vehicles, energy generation and deforestation, significantly contributes to climate change. Among various pollutants, greenhouse gases (GHGs) play a central role in altering the Earth's climate system.

1.1.1 GREENHOUSE GASES AND THE ROLE OF CO_2

The greenhouse effect is a natural process that takes place in the Earth's atmosphere due to solar radiation. The sun emits energy in the form of ultraviolet rays, visible light, infrared radiation, which pass through the atmosphere, primarily made up of nitrogen, oxygen, water vapor and GHGs. The interaction between these gases and infrared radiation is essential in sustaining the greenhouse effect[1].

Solar radiation, mostly in the form of visible light, moves through the atmosphere and reaches the Earth's surface. At this stage, the sun's energy is absorbed by land, water, and vegetation, and is then released as heat in the form of long-wave infrared radiation.
Normally, this radiation would escape into space. However, GHGs such as carbon dioxide (CO_2), methane (CH_4), nitrous oxide (N_2O), and others, have the ability to absorb some of the infrared radiation emitted by the Earth. These gases, confined in the atmosphere for many years or even centuries, trap the heat, intensifying the natural greenhouse effect. It's effect directly deriving, from this heat being unable to radiate back into cosmos, contribute to global warming[1].

As already anticipated Carbon dioxide, is primarily emitted through several processes:

- Combustion of fossil fuels: burning coal, oil and natural gas for electricity, transportation and heating releases CO_2.
- Deforestation: trees absorb CO_2 during photosynthesis. When forests are cut down or burned, the stored carbon is released back into the air.
- Industrial activities: manufacturing processes, such as steel, cement production and chemical refining, generate CO_2 as a byproduct.

Since the pre-industrial era, atmospheric CO_2 concentrations have risen sharply, reaching levels not observed in at least two million years. In 2019, CO_2 concentrations overcomes 410 parts per million (ppm), representing a 50% increase compared to pre-industrial levels[2].

The contribution of CO_2 to global warming is substantial due to its high emission volume and long atmospheric lifespan. While CH_4 and N_2O have a higher global warming potential (GWP), respectively around 25 and 273 times, their lifespan is much shorter, and emissions are considerably lower. For these reasons, CO_2 remains the dominant driver of climate change, responsible for most of the human-induced warming. Historical cumulative CO_2 emissions since 1850 have been estimated at approximately 2400 gigatons of CO_2 (Gton-CO_2), with over half occurring after 1989. This underscores the accelerating pace of industrialization and its environmental consequences[2].

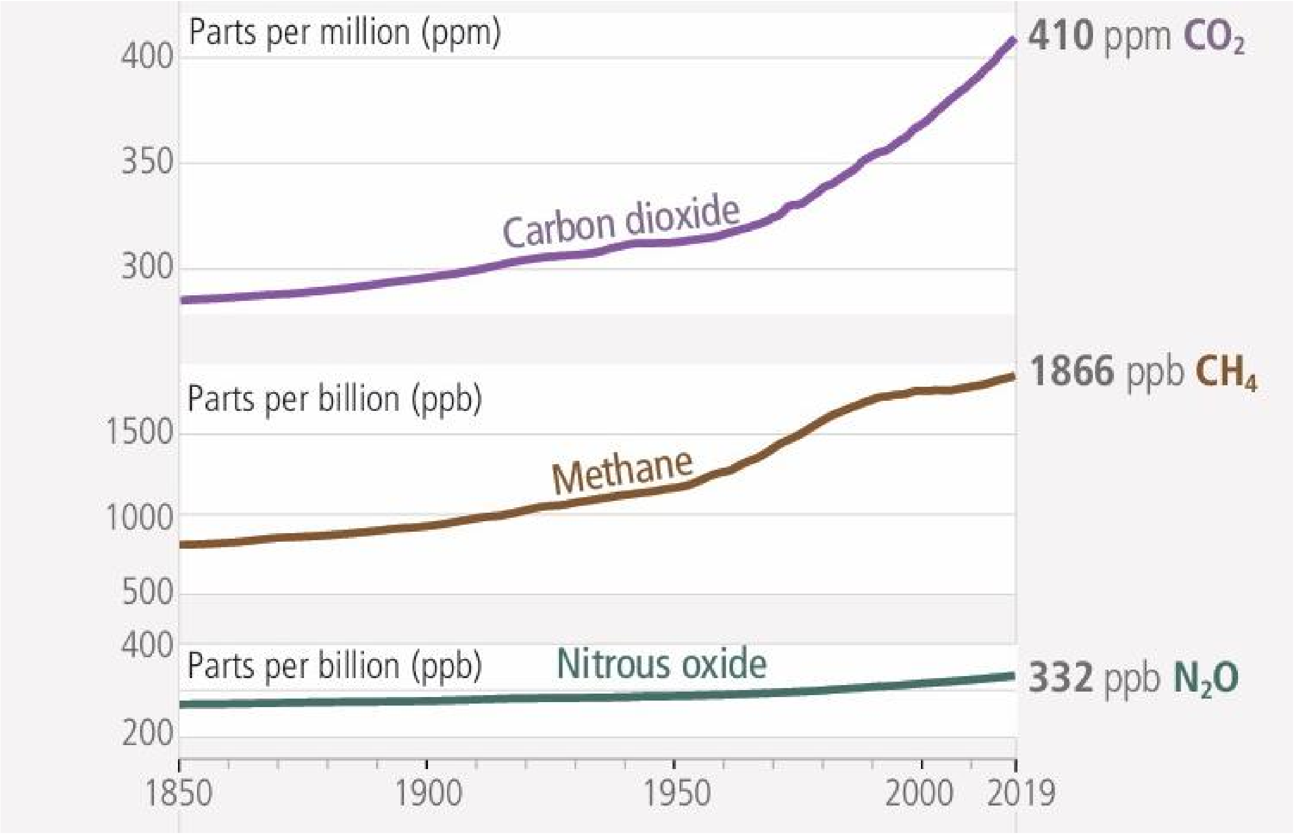

Figure 1 CO_2, methane and nitrous oxide emissions over the years[2]

To give an idea on how much CO_2 emissions have increased, the International Panel for Climate Change (IPCC) report that in 2019 overall GHG emissions were about 59 ± 6.6 Gton-CO_2 -eq, 12% higher compared to 2010 and 54% higher compared to 1990, with the largest share occurring in CO_2 from fossil fuel combustion and industrial processes[2].

1.1.2 EFFECT OF RISING GREENHOUSE GASES EMISSIONS

The rapid increase in GHG emissions has led to profound changes in the Earth's climate and ecosystems, especially when compared to pre-industrial conditions, which can be direct observed on mean global temperature, impact on animals and life in general, natural disasters and so on. All of these have huge consequences on many other aspects, which in general are not associated with climate change

1. **Temperature Changes**: Since the late 19th century, global surface temperatures have risen by approximately 1.1°C. This warming is more pronounced over land (1.6°C) than over oceans (0.9°C), with recent decades witnessing the fastest rate of temperature increase in the past 2,000 years. The mean global temperature projections indicate that if current trends continue, temperatures could rise further, breaching the critical 1.5°C threshold as early as the 2030s. Overcome the 2°C threshold would lead to an irreversible damage for the entire planet[2].

2. **Ecosystem Impacts**: Climate change has significantly disrupted terrestrial and marine ecosystems. Species migration, loss of biodiversity, and changes in seasonal patterns are some of the observable effects. In the oceans, warming and acidification have led to coral bleaching and reduced fishery yields, threatening marine biodiversity and food security[2].

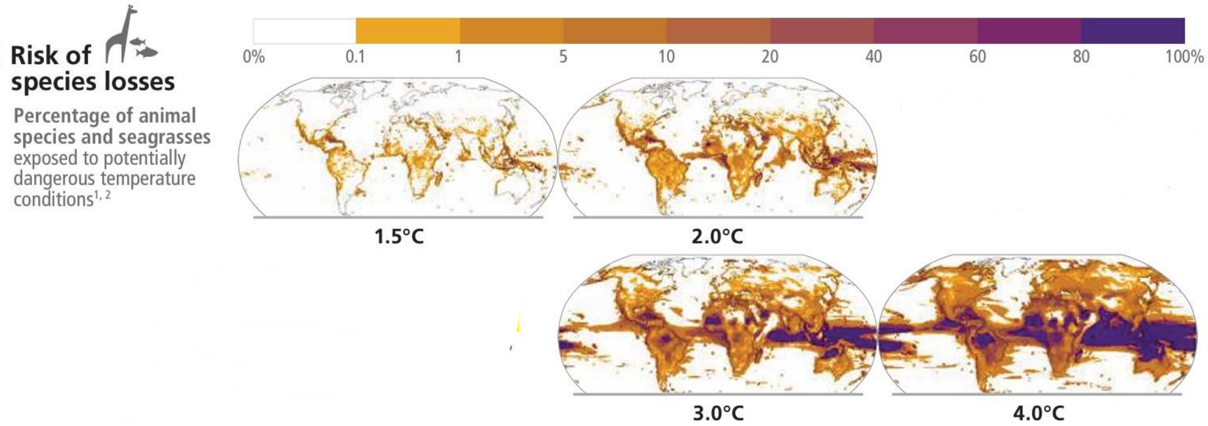

Figure 2 Risk of species losses on different location of world based on different temperature scenarios[2]

3. **Human Systems**: Rising temperatures and extreme weather events exacerbate vulnerabilities in human systems. Between 2010 and 2020, extreme events such as heatwaves, floods, and droughts increased mortality rates in high-risk regions by up to 15 times compared to less vulnerable areas. Food and water insecurities have deepened, particularly in developing regions, where adaptive capacities are limited. Health challenges, including heat-related illnesses, vector-borne diseases, and mental health impacts, have also intensified[2].

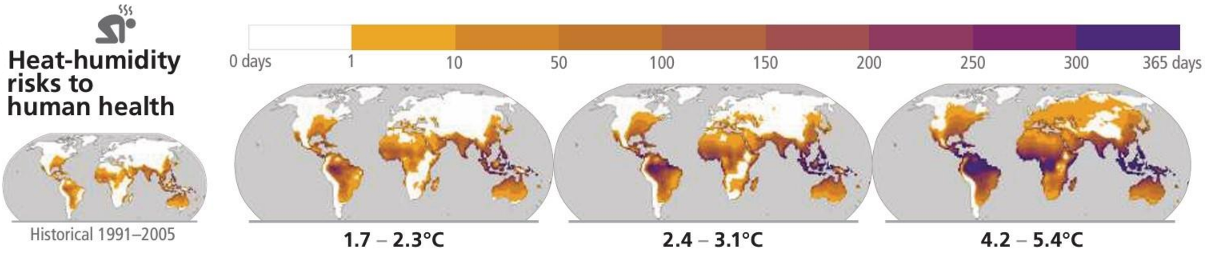

Figure 3 Human health hazard on different location of world based on different temperature scenarios[2]

4. **Sea Level Rise and Glacier retraction**: Since 1901, global mean sea level has risen by approximately 0.2 meters due to thermal expansion and glacial melting. The rate of sea level rise has accelerated, doubling from 1.3 mm per year between 1901 and 1971 to 3.7 mm per year between 2006 and 2018. This poses severe risks to coastal communities and ecosystems. On the other hand, this causes inevitable damage of the cryosphere and harness for the species living in the polar regions[2].

5. **Resource security and social Injustice**: As previously mentioned, climate change can lead to not so obvious consequences. Apart from the decrease in food and water security, AR6 shows how increasing temperature will impact differently the different regions of the world. The higher risk is for the equatorial regions which would witness the most detrimental effect in terms of human health hazard and scarcity of water and food. Also, agriculture and fisheries would be affected, increasing the capacity towards northern and southern regions and decreasing in the equatorial one[2].

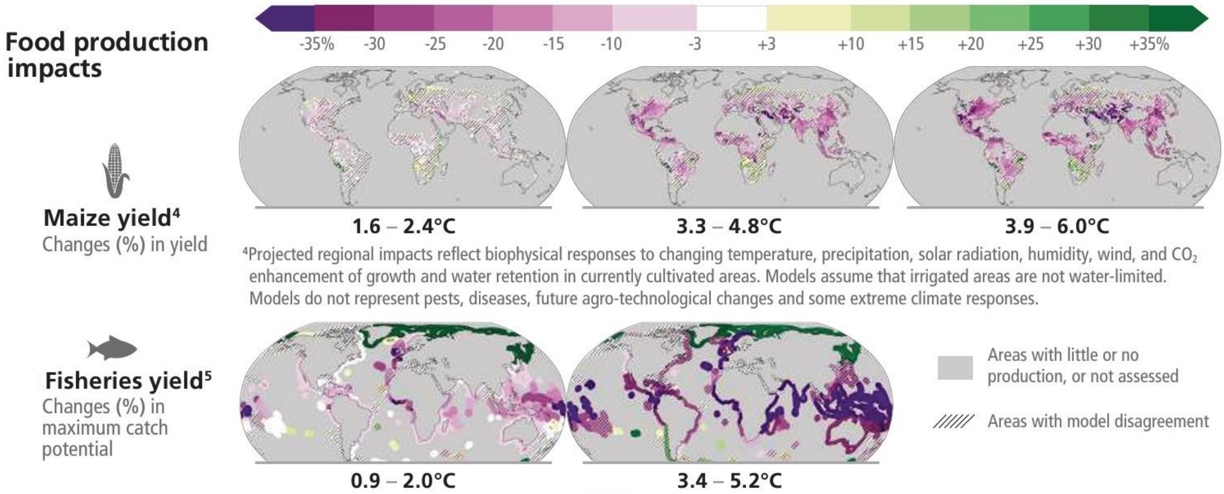

Figure 4 Change in food production on different location of world based on different temperature scenarios[2]

1.1.3 POLICIES AND GREEN HOUSE GASES EMISSION REDUCTION

All these aspects have been recognized by almost the entire world during the 'Paris agreement', held on 12th December 2015. The agreement, within United Nations Framework Convention on Climate Change (UNFCCC), aim to deal with greenhouse gas emissions mitigation starting from 2020.

The Paris Agreement is built on several key aspects. One of its main goals is to limit the rise in global temperature to well below 2°C above pre-industrial levels, with efforts to keep the increase within 1.5°C. Achieving this target is crucial to reducing the risks of climate change[3].

A central feature of the agreement is the Nationally Determined Contributions (NDCs), where each country sets its own goals for reducing GHGs emissions. These plans are reviewed and updated every five years, with increasing levels of ambition. To assess collective progress, the agreement includes a Global Stock take process, to ensure accountability and drive further action[3].

The Paris Agreement also emphasizes achieving net-zero emissions by the second half of the century, balancing GHG emissions with removal mechanisms like reforestation or carbon capture[4].

Additionally, it promotes adaptation and resilience efforts, especially for vulnerable nations, to help them manage the impacts of climate change.

Financial and technological support for developing countries is another cornerstone, with developed nations committing to mobilizing at least $100 billion annually to assist in mitigation and adaptation efforts. Transparency is ensured through a standardized Transparency Framework, requiring countries to report on their emissions and progress toward their commitments[3].

Finally, the agreement encourages international cooperation, including mechanisms for carbon trading, and recognizes the importance of addressing loss and damage caused by climate impacts[4].

The 2030 Agenda for Sustainable Development, adopted by all United Nations (UN) Member States in September 2015, is an action program which offers a transformative framework to guide global progress toward addressing the world's most pressing issues, giving an insight into what actions must be taken

Figure 5 2030 AGENDA SDGs[5]

to reach targets. It comprises 17 Sustainable Development Goals (SDGs) aimed at ending poverty, reducing inequalities, and protecting the planet.

Each of these goals is linked to specific targets that must be achieved by 2030. Among the most crucial for addressing climate change are SDG 7 (Affordable and Clean Energy) and SDG 13 (Climate Action), which emphasize the need for sustainable energy systems and urgent action to combat climate change[5].

One of the most significant challenges of the 21st century is, in fact, the transition from fossil fuels to cleaner, renewable energy sources. This energy transition is fundamental to achieving several of the SDGs and plays a central role in SDG 7, which also seeks to ensure universal access to affordable, reliable, and sustainable energy. The transition involves increasing the share of renewable energy sources, such as solar, wind, and hydropower, in the global energy mix while improving energy efficiency across all sectors, from industrial processes to transport and housing. Renewable energy not only helps mitigate climate change by reducing greenhouse gas emissions but also has the potential to provide access to electricity and clean energy solutions for communities that still lack reliable energy, especially in developing regions[5].

However, while the shift to renewables is essential, there are still challenges, particularly in industries that are difficult to decarbonize, and heavy transport. This is where Carbon Capture and Storage (CCS) and Carbon Capture, Utilization, and Storage (CCUS) technologies come into play. These technologies involve capturing CO_2 emissions from industrial sources and either storing them underground or utilizing them in new applications, like creating synthetic fuels or enhancing agricultural productivity[6].

The inclusion of CCUS in the European Union (EU) SET-Plan highlights its importance in the energy transition. The EU's SET-Plan, which focuses on research and innovation in energy technologies, emphasizes actions to drive the deployment of carbon capture and storage alongside renewable energy sources. This initiative is crucial to support industries that cannot immediately decarbonize through energy transition alone. As the energy transition evolves, the integration of CCUS technologies will help manage the carbon emissions that remain from industries reliant on fossil fuels, creating a more effective approach to reducing global emissions[6].

1.2 CARBON CAPTURE STORAGE AND UTILIZATION

The concept of CCS emerged in the 1970s as a response to growing concerns about rising atmospheric CO_2 levels and their link to climate change. Initial research and development were driven by the recognition that curbing CO_2 emissions was crucial for climate stability. During this period, early CCS projects focused on capturing CO_2 from industrial processes to prevent its release into the atmosphere[2]. This foundational research laid the groundwork for contemporary CCS technology, which now encompasses advanced capture, transport, and storage techniques.

Throughout the 1980s and 1990s, interest in CCS expanded, with significant contributions from energy and environmental organizations. The International Energy Agency (IEA) and the IPCC played pivotal roles in endorsing CCS as a critical strategy for mitigating emissions[7].

Different approaches exist based on different types of technologies and process procedures.

They can be mainly divided into:

- Pre-combustion
- Post-combustion
- Oxy-fuel combustion
- Direct air capture (DAC)

1.2.1 PRE-COMBUSTION

Pre-combustion carbon capture is a process that captures CO_2 before the combustion of fuel. The fuel, whether it is coal, natural gas, or biomass, is first converted into a gaseous mixture known as syngas (synthesis gas), which primarily consists of carbon monoxide (CO) and hydrogen (H_2). This is done through a gasification process, where the fuel is heated in the presence of oxygen and steam to break down the chemical bonds. The carbon monoxide in the syngas is then shifted by reacting with steam (in a reaction called “water-gas shift reaction") to produce additional hydrogen and carbon dioxide. The CO_2 is then separated from the remaining gases, primarily hydrogen, which is now a clean fuel.

Pre-combustion capture is typically used in Integrated Gasification Combined Cycle (IGCC) power plants, where the syngas produced is used to generate electricity. This method is also used in hydrogen production facilities, which aim to produce hydrogen for use as a clean energy carrier. The main advantages of pre-combustion capture are the high capture efficiency and the ability to generate hydrogen as a by-product, which is a significant component in the future of clean energy systems. However, this method has some challenges, particularly the high initial capital cost of the technology, as well as the complexity of integrating gasification processes into existing infrastructure. The gasification process is complex and requires advanced equipment, making it more expensive to implement on a large scale compared to other methods[7].

1.2.2 POST-COMBUSTION

Post-combustion carbon capture is the process of removing CO_2 from the exhaust gases of combustion. After fuel such as coal, oil, or natural gas is burnt in power plants or industrial facilities, the exhaust gases contain a mixture of CO_2, water vapor, nitrogen, and other pollutant traces. In post-combustion capture, CO_2 is extracted from these gases using various methods, most commonly by using chemical solvents like amines. The flue gas is passed through a solvent that binds to the CO_2, forming a compound. The CO_2-loaded solvent is then heated in a separate unit (a stripper column), causing the CO_2 to be released. The CO_2 is then compressed for storage, while the solvent can be reused in the process.

Post-combustion capture is particularly advantageous for industries and power plants that want to retrofit existing infrastructure. Since this technology can be applied to existing coal- and gas-fired power plants, it allows for emissions reduction without the need for building new facilities. This makes post-combustion capture a very appealing option for reducing emissions in the short-term. However, it is energy-intensive because regenerating the solvents and maintaining the absorption process requires significant energy input, which can reduce the overall efficiency of the system. Furthermore, the capture efficiency of post-combustion systems is typically lower than pre-combustion technologies, and large-scale implementation can be challenging due to the scale of the exhaust gas flows that need to be processed[2], [8].

1.2.3 OXY-FUEL COMBUSTION

Oxy-fuel combustion is a method that involves burning fuel in pure oxygen rather than in air. Normally, when fuel is burned in air, the combustion produces a mixture of gases, including carbon dioxide, nitrogen, and water vapor. In an oxy-fuel combustion process, the combustion occurs in an atmosphere of nearly 100% oxygen, which results in a flue gas that is predominantly CO_2 and water vapor. The water vapor is then condensed, leaving behind almost pure CO_2, which can be easily captured and stored.

The main advantage of oxy-fuel combustion is that it produces a high-purity CO_2 stream with very little nitrogen, making the CO_2 separation process much simpler and more efficient. This makes oxy-fuel combustion particularly useful in power plants and large industrial furnaces where the goal is to produce a high-purity CO_2 stream with minimal additional separation steps. However, the downside of this method is the significant energy required to produce pure oxygen. Oxygen production typically relies on cryogenic air separation or pressure swing adsorption, both of which are energy-intensive processes. This makes oxy-fuel combustion more costly than other methods, especially at the scale required for industrial applications [8], [9], [10].

1.2.4 DIRECT AIR CAPTURE (DAC)

DAC is a technology that captures CO_2 directly from the atmosphere, as opposed to from point-source emissions like the ones previously mentioned. This process is designed to address the legacy emissions in the atmosphere that have already contributed to climate change, as well as current emissions. DAC systems use chemical sorbents or filters that selectively absorb CO_2 from ambient air.

One of the key advantages of DAC is that it can be applied to a wide range of sources of CO_2 emissions, including hard-to-reduce emissions from sectors like transportation, agriculture, and buildings. It also provides a means of reducing the overall CO_2 concentration in the atmosphere, which is crucial for achieving long-term climate targets.

However, the major challenge with DAC is the high cost related. Unlike post-combustion capture, where CO_2 concentrations are relatively high in exhaust gases, ambient air contains only about 0.04% CO_2 in mass, which means DAC systems must process vast amounts of air to capture significant quantities of CO_2. This requires large infrastructure which results in high costs, making DAC a less economically viable option compared to other carbon capture technologies. Additionally, the infrastructure required for large-scale deployment is still under development, and further innovations are needed to improve efficiency and so reduce cost related to the energy consumption [11], [12]. For these reasons DAC is the less mature technology among the others, with a Technologies readiness level (TRL) of 5. Further research will be needed to improve the technology in order to upgrade it to full commercial scale.

1.2.5 STORAGE AND UTILIZATION STRATEGIES

Once the CO_2 stream is separated thanks the Carbon Capture process, two different approaches can be used: Storage solution or Utilization.

CCU and CCS represent two distinct but complementary approaches to addressing CO_2 emissions. While CCS focuses on capturing and permanently storing carbon dioxide to prevent its re-entry into the atmosphere, CCU seeks to repurpose the captured CO_2 into valuable products, thus promoting its integration into the industrial and economic ecosystem.

In CCS, once CO_2 is captured, it is compressed and transported to a storage site, typically via pipelines. The storage process involves injecting CO_2 into deep geological formations such as depleted oil and gas reservoirs, deep saline aquifers, or not mineable coal seams. These formations provide natural barriers, such as impermeable cap rock, to prevent CO_2 from escaping back into the atmosphere [2], [8]. Over time, CO_2 several storage mechanisms were explored, like: structural trapping, where CO_2 is physically confined beneath impermeable rock layers; solubility trapping, where CO_2 dissolves into subsurface brine; and mineral trapping, where CO_2 reacts with minerals to form stable carbonates[9], [12].

Among these mechanisms, mineralization ensures that CO_2 is permanently fixed in solid form, effectively eliminating the risk of re-release into the atmosphere, thereby making this form of storage highly secure and long-lasting[11].Geological sequestration has been successfully implemented in various projects worldwide. For example, Enhanced Oil Recovery (EOR) projects utilize injected CO_2 to improve the extraction of oil from aging reservoirs and, at the same time, store the CO_2 in the depleted well. This approach not only provides economic incentives but also demonstrates the feasibility of long-term CO_2 storage [8]. Large-scale CCS projects, such as the Sleipner project in Norway, have demonstrated that geological storage can be both safe and effective when properly managed [2], [8]. Despite its effectiveness, CCS still faces significant challenges related to cost, energy consumption, and public acceptance.

Costs for CCS implementation range between \$50 and \$150 per tons of CO_2, depending on factors such as the capture process and the distance to suitable storage sites [12]. Moreover, concerns surrounding potential CO_2 leakage and seismic activity necessitate rigorous monitoring systems and safety protocols to ensure long-term stability and environmental security, adding further complexity to large-scale deployment[11].

CCU, on the other hand, gives the opportunity to increase economic revenues from capture procedure and avoid the previously cited issues of long-term stability of the storage. It gives also the possibility to further reduce indirectly the emissions by producing goods that inevitably would lead to other emissions during production. The most debated aspect related to CCU is the energy requirements for the processes which, in some cases, lead to unviability of it economically speaking. For these reasons, research focused a lot of attention on increasing energy efficiency and reduction of costs for both processes. Actually, the CO_2-EOR is considered mainly as a utilization strategy as oil is extracted as consequence of the storage. It accounts for a total usage of 17 Mtons per year of anthropogenic CO_2 which is more than 60% of the total. Despite being economically beneficial the debate remains open on the effectiveness of this strategy for climate action[13].

The non-EOR applications, instead, include the utilization to produce[13]:

- Minerals: making the CO_2 reacting to forms carbonate which can be used in pharmaceutical and building sector.
- Concrete: using the CO_2 as feedstock to produce or enhancing the properties of cement.
- Fuels: converting CO_2 in carbon-based fuels, including diesel, jet fuels, ethanol, and natural gas using for example Fisher-Tropsch processes.
- Chemicals: Converting CO_2 into valuable organic chemicals, such as methanol, ethylene, and carbamates or carbon monoxide. For example, using hydrogenation reaction and electrochemical- CO_2 reduction.
- Polymers: polymerizing the CO_2 directly to form plastics and resins, offering a sustainable alternative to traditional petrochemical-based polymers.
- Carbon Fibers and Composites: CO_2 can be used directly or indirectly (via chemical intermediaries) use to produce carbon fibers, carbon composites, and other advanced materials like graphene.

This aspect will be further analyzed in another section as a particular utilization strategy will be modelled and discussed as part of this work.

1.3 THERMODYNAMIC OF DIRECT AIR CAPTURE

Before starting the actual analysis, it can be useful to examine the separation process of CO_2 from a mixture—in our case, air—to determine the minimum thermodynamic work required for the separation. This will provide insight into the fundamental energy demands of the process.

We assume an incoming air stream that undergoes separation, yielding a pure CO_2 stream and a purified air stream. The minimum theoretical work required for this separation can be determined by evaluating the exergy balance of the system. The total work requirement is given by the algebraic summation of the exergy associated with the three streams, expressed as follows:

$$W_{min} = \pm \sum_i \psi_i$$

The separation process will be discussed under the hypothesis of isobaric and isothermal conditions, which implies that the outlet streams will have the same thermal and manometric energy as the inlet one. In this case the exergy will be equal to the Gibbs free energy, and so we can rewrite the previous equation in this way:

$$W_{min} = \mp RT \sum_{i=1\ldots n} (N_i \sum_{j=1\ldots m} X_{i,j} \ln\left(X_{i,j}\right))$$

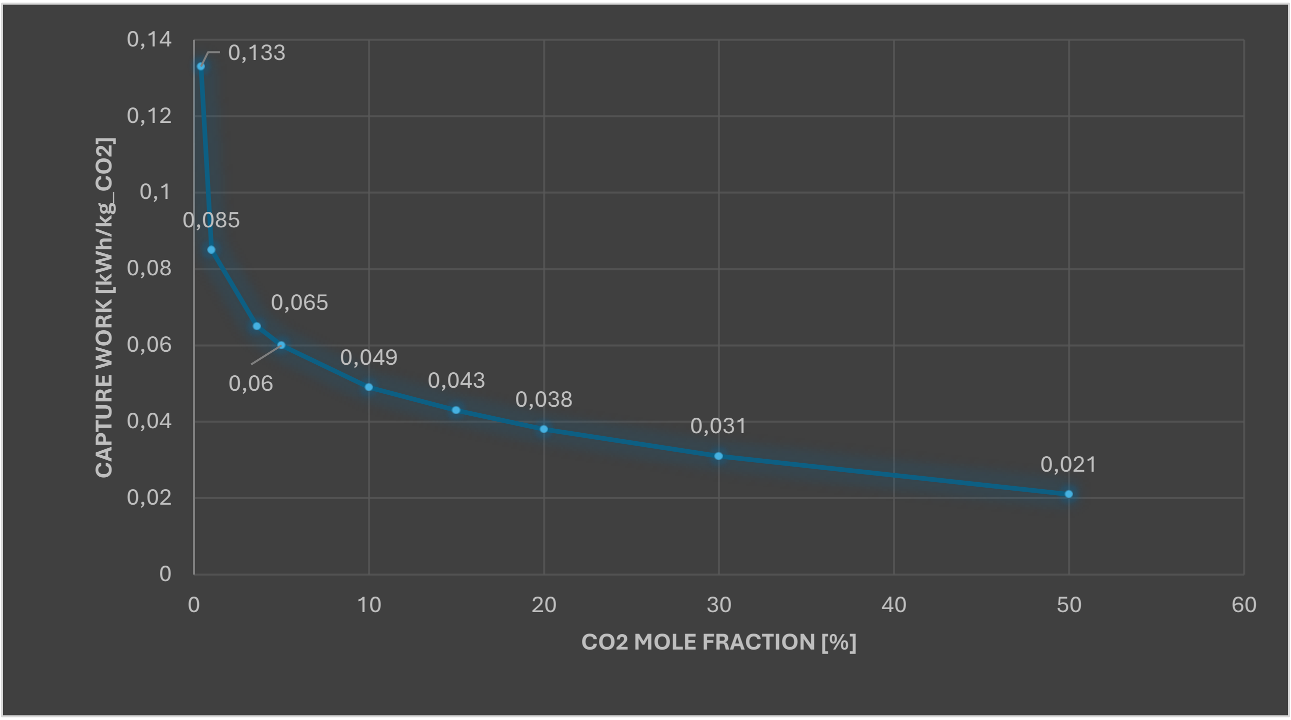

Figure 6 Minimum work required to separate CO_2 from a mixture as function of the molar concentration[14]

Where:

- R is the perfect gas constant
- T is the temperature
- N_i is the molar flow rate associated to the i-th stream
- $X_{i,j}$ is the molar fraction of the j-th substance in the i-th stream

Assuming that there are only three streams, one as inlet and two as outlet, where one of the outlets is CO_2 with high purity the equation can be simplified as:

$$W_{min} = -RT(N_1 \sum_{j=1\ldots m} X_{1,j} \ln(X_{1,j}) - N_2 \sum_{j=1\ldots m} X_{2,j} \ln(X_{2,j}) - N_3 \sum_{j=1\ldots m} X_{3,j} \ln(X_{3,j})$$

As it is possible to note, the work required to separate CO_2 from the mixture decrease drastically as the concentration of the CO_2 increases. The trend is strongly nonlinear and asymptotically tends to zero as the concentration approaches 100%. This shows the first big problem of the DAC systems which have to work with very low concentration of CO_2, leading to much higher work required compared to post-combustion technique.

The theoretical minimum work needed to separate a stream of air containing 400 ppm CO_2 (the CO_2 concentration assumed in the developed model) into one stream with low CO_2 content and another stream with high CO_2 concentration (e.g., 99% purity), under the same temperature and pressure conditions, is approximately 20 kJ/mol or 0.126 kWh/kg or 0.45 Gj/ton of CO_2. However, achieving this theoretical minimum is not possible in real processes. This because, achieving complete reversibility of the process requires infinitesimally small mass transport driving forces, which would necessitate equipment of infinite size and cost[14].

1.4 THE DIRECT AIR CAPTURE SYSTEMS STATE OF ART

As seen previously, DAC is one of the less mature technologies for CO_2 capture, mainly due to the high cost per unit of CO_2 captured. Several concepts have been developed over the years based on different chemical and physical phenomena, many of which are also used in Post-combustion processes due to the similarity of the methods.

For this reason, DAC and Post-combustion tend to be often considered as a single strategy. However, this is far from the truth because their applications and purposes are very different. Additionally, because the CO_2 concentration in the mixture treated by the plant differs significantly—exhaust gases are orders of magnitude richer in CO_2 than air—the components designed for similar purposes must be tailored in very different ways to handle these specific requirements. While Post-combustion aims at reducing CO_2 locally, directly from industrial processes, DAC allows the reduction of overall CO_2 in the atmosphere, being one of the only technologies capable of achieving negative emissions, meaning it can actively remove CO_2 from the air rather than merely preventing additional emissions. This is particularly crucial for long-term climate goals, as simply reducing emissions may not be sufficient to limit global warming. Instead, actively removing CO_2 can help compensate for hard-to-abate sectors and even allow a return to pre-industrial CO_2 levels if necessary.

This might seem irrelevant, but risks for the environment exist even at current CO_2 levels, and in the future, the ability to return to previous states could be extremely valuable.

Apart from DAC, the only other technology capable of achieving negative emissions is Bioenergy with Carbon Capture and Storage (BECCS). BECCS involves capturing CO_2 from biomass combustion or processing, where plants have already absorbed CO_2 from the atmosphere during their growth. By capturing and storing the emissions rather than releasing them back, BECCS effectively removes CO_2 from the carbon cycle. When developed in parallel with DAC, these two technologies provide complementary pathways to mitigate climate change, making their advancement crucial for achieving net-zero and even net-negative emissions in the future[15].

Nonetheless, for the goals set, developing all the CCSU technologies in parallel remains the most effective way to proceed.

DAC can vary significantly from one another, and various classifications can be made. However, for our analysis, we will divide them into two categories: liquid sorbent processes (Alkali based scrubbing process, Amine-based scrubbing process…) and solid sorbent processes.

All sorbents have different capabilities based on their nature and obviously operative conditions. The key requirements to evaluate the effectiveness of the solvent are[16], [17], [18]:

- Selectivity: The ability of the sorbent to preferentially bind with CO_2 compared to other gases present.
- Capacity: The amount of CO_2 that the sorbent can absorb or adsorb per unit of mass or volume.
- Transport and Kinetic Properties: The rate at which CO_2 can be captured, which depends on diffusion and the chemical reaction.
- Thermal and Chemical Stability: The ability of the sorbent to maintain its effectiveness at high temperatures and in complex chemical environments.
- Mechanical Properties (if the sorbent is solid): Resistance to breakage, compaction, and hardness.
- Ease of Loading (if the sorbent is solid): How easily the sorbent can be loaded into the capture system.

- Resistance to Fouling: The sorbent's ability to resist contamination and accumulation of materials that may reduce its efficiency.
- Ease of Regeneration: How easily the captured CO_2 can be removed from the sorbent to allow for a new capture cycle.
- Cost: The overall cost of the sorbent, which includes both the initial cost and operational costs (for example, regeneration or maintenance).

All the different processes will be described briefly concentrating on the pros and cons of each technology and state of the art.

1.4.1 ALKALI BASED LIQUID SORBENT PROCESSES

Alkali like potassium hydroxide (KOH), and sodium hydroxide (NaOH), are generally the most used for DAC systems. These are used dissolved in an aqueous solution to have dissociation of the alkali in ions, allowing the reaction with the CO_2.

The strong affinity of the compounds with CO_2 guarantees among the best performance in terms of capture rate and this is the main reason behind utilization. On the other hand, the regeneration process is much more complicated compared to amine solvent and must be performed in two different steps, which are highly energy consuming. For this reason, plants based on this process require precise optimization in order to be economically viable[16].

This regeneration process is based on the Kraft process, which has been widely used in the paper industry since the 19th century.

The overall process consists of four main steps. First, an aqueous solution is brought into contact with carbon dioxide in a dedicated device known as the Air Contactor. During this step, sodium carbonate (Na_2CO_3) is formed alongside water and heat, as the reaction is exothermic. A similar reaction involving KOH will be discussed later, as it plays a central role in this work[19].

Next, the sodium carbonate undergoes a reaction with calcium hydroxide ($Ca(OH)_2$) in a process known as causticization. This term originates from the use of calcium hydroxide, a highly basic and "caustic" compound. Through this reaction, NaOH is regenerated, enabling its reuse in subsequent cycles. Additionally, calcium carbonate ($CaCO_3$) is produced as a byproduct, necessitating a separate regeneration process to release the captured CO_2.

The final two steps, which are common to both NaOH- and KOH-based processes, include:

1. Thermal dissociation of $CaCO_3$: In this step, calcium carbonate is decomposed into calcium oxide (CaO) and CO_2. This reaction—typically carried out in a lime kiln similar to those used in the cement industry—is highly endothermic and requires a high temperature of approximately 900°C. As result, it represents the most energy-intensive stage of the process.

2. Hydration of calcium oxide: The final step involves the reaction of calcium oxide with water to regenerate calcium hydroxide. The regenerated calcium hydroxide is then reused in the causticization process, ensuring the continuity of the cycle.[15].

The reactions which summarize the NaOH DAC process are[19]:

$$2NaOH + CO_2 \rightarrow Na_2CO_3 + H_{2O} \qquad \Delta H° = -109{,}4\,Kj/mol \;\; AIR\ CONTACTOR$$

$$Na_2CO_3 + Ca(OH)_2 \rightarrow 2NaOH + CaCO_3 \qquad \Delta H° = -5{,}3\,Kj/mol \;\; CAUSTICIZER$$

$$CaCO_3 \rightarrow CaO + CO_2 \quad \Delta H° = +179{,}2\ Kj/mol \text{ CALCINER (or LIME KILN)}$$

$$CaO + H_{2O} \rightarrow Ca(OH)_2 \quad \Delta H° = -64{,}5\ Kj/mol \text{ SLAKER}$$

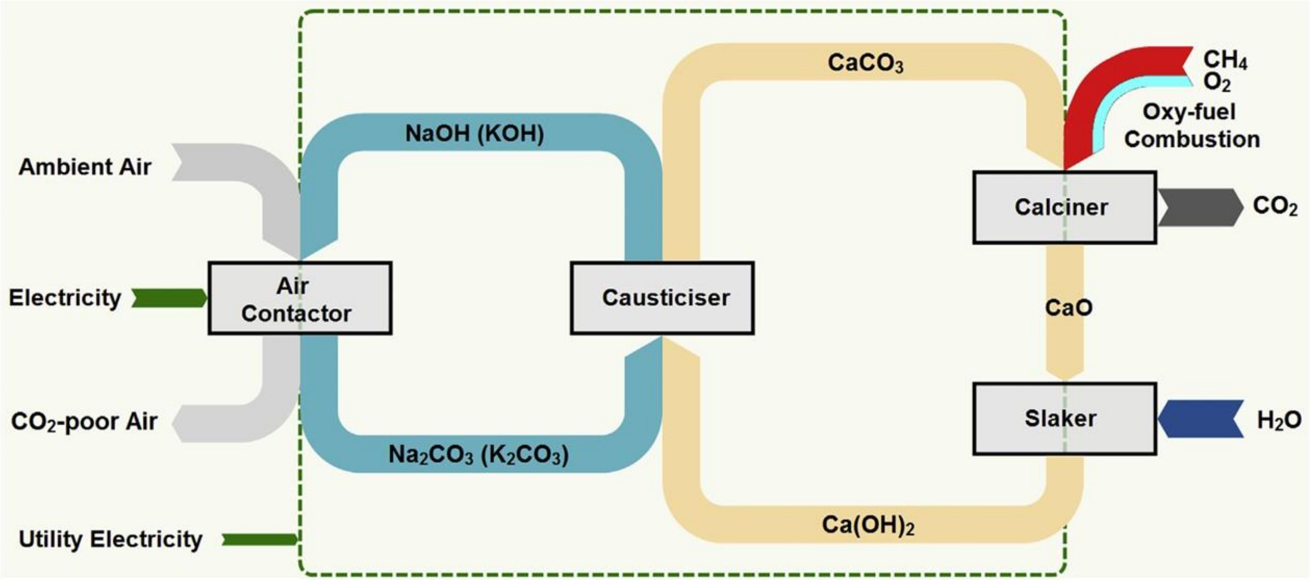

Figure 7 NaOH based solvent DAC process[19]

PROS[16], [19]

- High Selectivity for CO_2: Alkali react mainly with CO_2, other reactions with compounds inside air are absent or negligible.
- High Affinity for CO_2: Alkali solutions also have a high affinity for CO_2, meaning they can effectively absorb CO_2 even at low concentrations, making more suitable for DAC applications.
- High Absorption Capacity: Alkali-based solvents can absorb a large amount of CO_2, which is essential for large-scale CO_2 removal.
- High efficiency in the regeneration of solvent: The captured CO_2 can be released by regenerating the alkali solution, allowing the solvent to be reused in multiple cycles with minimal amount of make-up.
- Established Technology: Alkali-based solutions are already widely used in CO_2 capture from industrial emissions, making them a proven and reliable technology.

CONS[16], [19]

- Energy-Intensive Regeneration: The regeneration of alkali solutions requires significant energy, especially for the Calcination step.
- Corrosion Issues: Alkali solutions are highly corrosive, which can lead to damage to equipment and increase maintenance costs.
- Environmental Concerns: The disposal or recycling of by-products, such as calcium carbonate can present environmental challenges.

1.4.2 AMINE-BASED LIQUID SORBENT PROCESSES

As the name suggests these processes use different types of amines as solvent to capture the CO_2.

One of the most used is Monoethanolamine (MEA) which is already used for CO_2 capture at point sources. It has been found to be less effective for DAC, as the CO_2 concentration are low, around as 400 ppm [16]. Alkanolamines, like MEA, generally exhibit slower absorption rates compared to alkaline liquid sorbents, and their performance is hindered by issues like degradation in oxygen and high energy demands for regeneration due to water absorption. Additionally, these sorbents can be environmentally harmful[16].

However, recent research has shown that certain amines, when tested under DAC conditions, can achieve similar CO_2 absorption rates to NaOH and exhibit high adsorption capacity after a day of exposure. These amines also have the advantage of requiring less thermal energy for regeneration compared to traditional aqueous alkali hydroxides. In other experiments, pyrrolizidine-based sorbents effectively absorbed CO_2 from compressed air at low concentrations over several days, showing no signs of oxidation. Furthermore, alkylamines with hydrophobic phenyl groups, such as OXDA, MXDA, and PXDA, demonstrated no water absorption when exposed to CO_2 under DAC conditions solving the problem of the regeneration energy surplus required. Anyway, scale up processes based on these amines have been found to be too much expensive[16].

Amine-based solvents tend to be much less stable than alkali based, being prone to easy degrade when exposed to oxygen or pollutants like NOx and SOx. For this reason, the amine type has to be chosen carefully for each application, accounting for the composition of the gas to be purified[17]. Being the air much richer in oxygen than typical exhaust gasses amine oxygen degradation has to be properly assessed when utilized this type of solvent in DAC applications.

The chemical absorption of CO_2 in the aqueous MEA solution occurs through a reaction involving hydroxide ions, as described by the following reactions[18]:

$$MEA + CO_{2,aq} + H_{2O} \rightleftharpoons MEACOO^{-} + H_{3O}^{+}$$

$$MEA + H_{3O}^{+} \rightleftharpoons MEAH^{+} + H_{2O}$$

PROS[16], [17], [18]

- High Selectivity for CO_2: Ammine react mainly with CO_2, other reactions with compounds inside air are absent or negligible.
- Established Technology: The use of amines for CO_2 capture is well-researched and has been successfully applied in industrial-scale applications like power plants and natural gas processing.
- Energy Efficiency Potential: Recent studies suggest that certain amines could reduce the amount of low-grade thermal energy required for regeneration, making the regeneration process potentially more energy-efficient than other sorbents like aqueous alkali hydroxides.
- Versatility: Amine-based systems can be modified or combined with other substances to improve absorption rates or minimize degradation, offering flexibility in system design for different DAC applications

CONS [16], [17], [18]

- Less affinity: Amines like MEA are less effective at capturing CO_2 in low concentrations (e.g., 400 ppm), which is a significant challenge for DAC applications where the CO_2 concentration is much lower than in industrial point sources and the ones which exhibits potential similar to NaOH are generally too expensive after a scale-up of the process.

- Degradation and Environmental Impact: Amines are prone to degradation when exposed to oxygen, leading to the formation of harmful by-products. This limits their long-term effectiveness and can increase operational costs due to the need for frequent replenishment.
- Corrosiveness: Amines can be corrosive, especially in high concentrations, which can increase the maintenance requirements and operational costs of DAC systems.
- Regeneration complication due to water absorption: Amines like MEA tend to absorb water, which complicates the regeneration process and can further reduce their efficiency when used in DAC systems.

1.4.3 SOLID SORBENT BASED PROCESSES

Solid-based sorption can operate using physisorption or chemisorption and can be further divided into organic and inorganic types.

Physisorption using inorganic compounds represents a promising alternative to liquid sorbents. Unlike solid sorbents that rely on chemisorption, physisorption offers advantages such as lower regeneration temperatures. Chemisorption-based solid sorbents often face challenges, including high-temperature regeneration requirements (sometimes exceeding those of alkaline solutions), slower reaction kinetics (as seen with $Mg(OH)_2$), or, in some cases, the inability to regenerate the sorbent (such as $Zn(OH)_2$). In fact, recent studies suggest that while $Mg(OH)_2$ captures CO_2 more slowly than some alternatives, but have a kinetic still faster than those of MgO and $Zn(OH)_2$ can react with CO_2, but its regeneration from the carbonate form may be challenging, potentially limiting its practical use in cyclic CO_2 capture processes[16].

Inorganic physisorption relies on trapping CO_2 within solid-state, open-structured systems, such as microporous materials like metal-organic frameworks (MOFs) and zeolites. This process is driven by adsorption, a surface-based phenomenon in which gas molecules adhere to a material's surface through weak physical forces, such as Van der Waals interactions. The efficiency of CO_2 capture largely depends on the presence of active sites—specific regions on the material's surface or within its pores that exhibit a higher affinity for CO_2 molecules[16].

These systems enable the adjustment of CO_2 equilibrium with ease, particularly under specific environmental conditions. This approach offers an energy-efficient solution for storing and releasing CO_2 through the material's pores. Zeolites, for instance, can be fine-tuned to efficiently and selectively adsorb or desorb CO_2, even at low concentrations, thanks to their unique characteristics, such as pore structure, extra-framework cations, affordability, crystal size, and chemical composition[16].

One of the most relevant projects based on solid sorbent is the concept developed by Climeworks. The Climeworks DAC design, also known as Carbfix, relies on an adsorption/desorption process using alkaline-functionalized adsorbents.

The incoming air is not treated prior to CO_2 adsorption, which takes place directly on the adsorbent. For desorption, a temperature-vacuum-swing (TVS) process is employed: the system's pressure is reduced, and the temperature is increased from 80°C to 120°C, causing the captured CO_2 to be released. After the cooling phase, the process is repeated[20].

The entire procedure occurs inside a compact module called "Collector" allowing to have a modular design, which can support easily scalability and reducing operation costs. The only moving parts are constituted by the fans, used to push the air through the device and two lids. The temperature required for regeneration is around 80°-120° allowing the coupling of this device with low-grade temperature source of heat, like geothermal ones as in the case of the Carbfix2 project[20].

Several others solid Sorbent are currently under investigation for potential use but most of them are only tested on a lab scale. By the fact that the work focuses on other points, minor's sorbent solution will not be discussed.

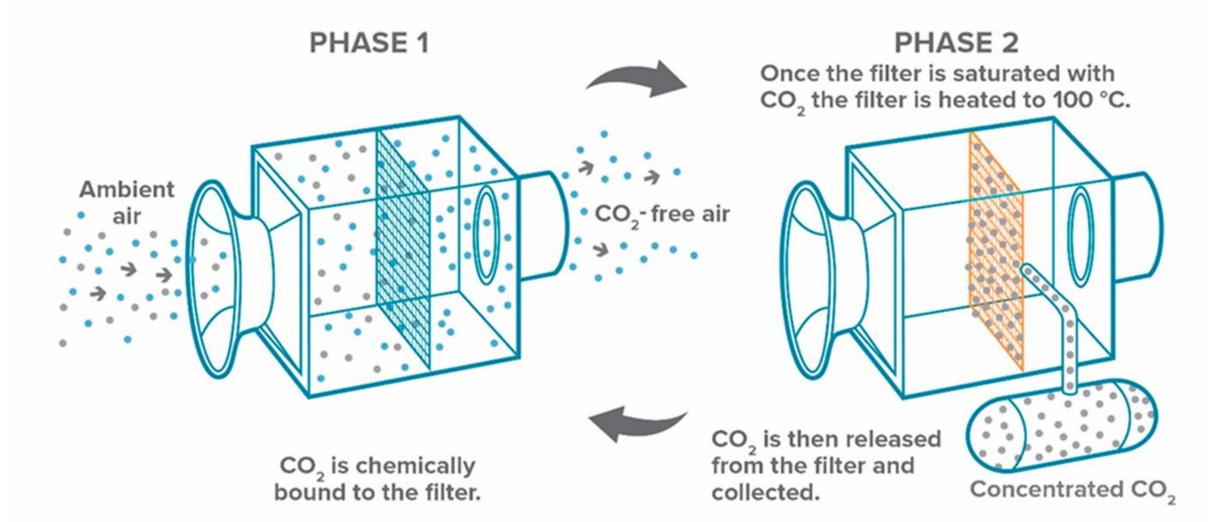

Figure 8 Carbix developed by Climeworks scheme process[20]

PROS[16], [20], [21]

- Less energy intensive: Temperature range required low grade heat and in general less amount of energy is required for the regeneration
- Low operating costs
- Scalability: Possibility to scale-up easily the system thanks the module composure

CONS [16], [20], [21]

- Auxiliary structure: need for a big supportive structure at low cost
- Need to allow the entire structure to be periodically sealed from ambient air during the regeneration step
- Difficult conditions of work: The system must cope with vacuum and humidity conditions
- Need to overcome the conflicting requirements of high sorbent performance, low cost, and long economic life in impure ambient air
- No continuous operation

1.5 DAC REFERENCE CASE OF STUDY

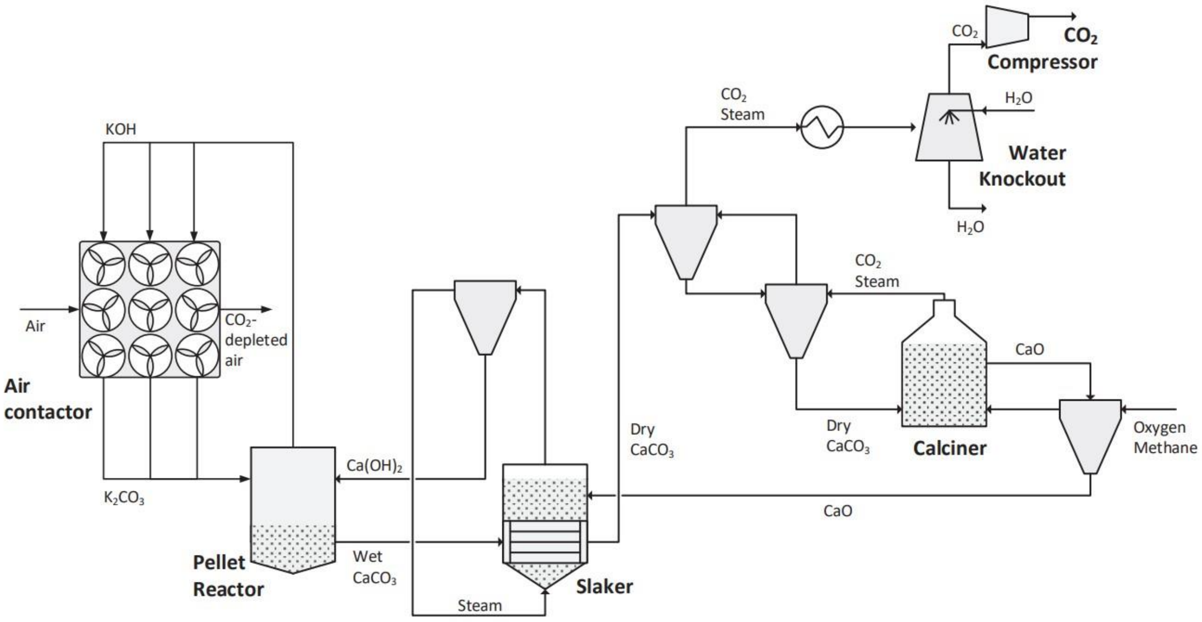

Figure 9 Scheme of DAC plant based on KOH solvent[11]

The reference system used by this study is based on the Carbon engineering project, which use potassium hydroxide, a liquid alkali solvent, as sorbent to capture CO_2. The plant has been discussed in detail in the work of Keith et al [11] and is capable of capture 1 ton-CO_2/day. The plant started its operation in 2015.

As previously said KOH has a very similar behavior compared to NaOH and the last two steps of the plant are common. Generally, KOH has a higher affinity compared to NaOH and tends to perform better at lower concentration of CO_2. On the other hand, potassium hydroxide is more expensive, in fact, in Post-combustion technique, is generally preferable to use NaOH. By this reason it is not so simple to determine which of them can perform better from an economically point of view, so research have focused on both[22].

The process begins with an Air Contactor that captures CO_2 from the ambient air using a liquid sorbent (KOH) solution, with ionic concentrations of roughly 1.0 M OH-, 0.5 M CO_3^{2-}, and 2.0 M K+. As air flows over the contactor, the CO_2 reacts with KOH to form potassium carbonate (K_2CO_3)[11].

Next, the carbonate-rich solution undergoes processing in a Pellet reactor. In this stage, calcium hydroxide is introduced to the solution, leading to the precipitation of calcium carbonate pellets while regenerating the KOH solution for reuse. This step is the counterpart of the caustization described in the classical Kraft process and serves as a critical link in the closed-loop system, allowing for continuous operation [11].

Calcium carbonate pellets are then transferred to a high temperature Calciner, where they are subjected to calcination at approximately 900°C. This process decomposes the calcium carbonate into calcium oxide (CaO) and releases concentrated CO_2 gas. The CO_2 can be compressed for sequestration or utilized in various industrial applications as we will see later. The remaining calcium oxide is hydrated in the Slaker to regenerate calcium hydroxide, completing the chemical loop[11].

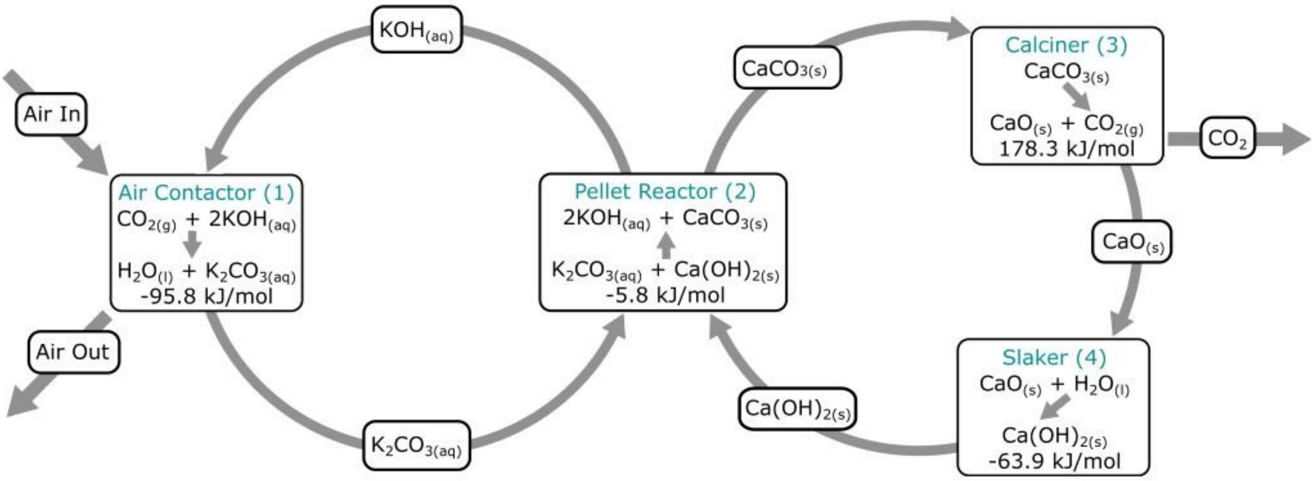

Figure 10 Scheme of the process of the DAC based on KOH solvent[11]

The reactions which summarize the KOH DAC process are[11]:

$$2KOH\ +\ CO_2 \rightarrow K_2CO_3 +\ H_{2O} \qquad \Delta H° = -95.8\ Kj/mol \quad \text{AIR CONTACTOR}$$

$$K_2CO_3 +\ Ca(OH)_2 \rightarrow\ 2KOH\ +\ CaCO_3 \quad \Delta H° = -5.8\ Kj/mol\ \ \text{PELLET REACTOR}$$

$$CaCO_3 \rightarrow\ CaO\ +\ CO_2 \quad \Delta H° = +178{,}3\ Kj/mol\ \ \text{CALCINER (or LIME KILN)}$$

$$CaO\ +\ H_{2O} \rightarrow Ca(OH)_2 \quad \Delta H° = -63.9\ Kj/mol\ \ SLAKER$$

The plant modelled by Keith et al., is an upscaled version of the Carbon engineering DAC and is estimated to have a capacity of roughly 1 Mton-CO_2/year captured, roughly 2750 times the original. The authors emphasize that this capacity can be further increased through advancements in capture technologies and energy integration processes. In terms of performance, Keith et al. estimated that the DAC system could capture CO_2 at costs ranging from \$94 to \$232 per ton, depending on energy prices and operational parameters, while previous study found a cost of roughly \$600 per ton. The system's energy demand is approximately 8.81 GJ per ton of CO_2 to be supplied with NG, or 5.26 Gj thermally supplied supplemented by around 366 kWh of electricity per ton. Another version—completely electrically supplied—is proposed with a consumption of 1500 KWh per ton of CO_2[11].

The Air Contactor, as previously mentioned, is a specific component that varies significantly in design across different DAC technologies. The version proposed by Keith et al. resembles the behavior of an absorber while incorporating a structure similar to a cooling tower. Its design is simple and fundamentally consists of a large wall made up of massive fans. The interior of the Air Contactor is filled with materials similar to those used in Absorber columns. Several optimization techniques are required to ensure a low pressure drop, with particular focus on the design of the packing. The Air Contactor's interior is wet with solvent to facilitate the reaction process[23], [24], [25].

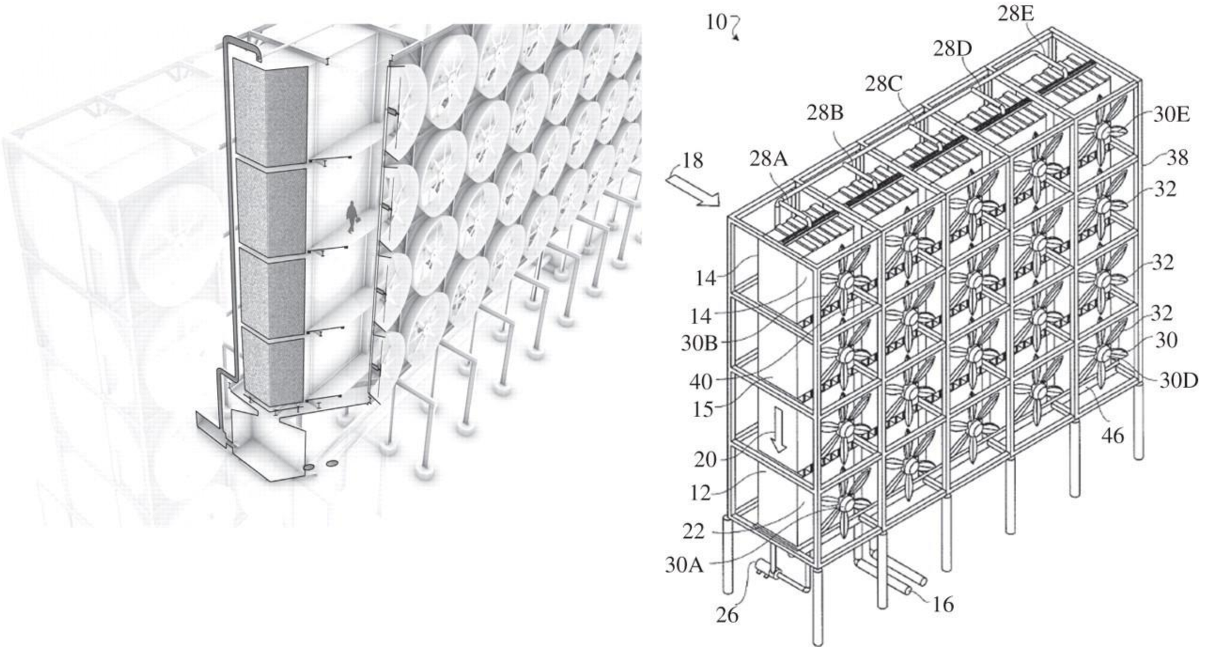

Figure 11 Scheme of the Air contactor component structure[25]

The Pellet Reactor is a Fluidized bed reactor which substitutes the caustization procedure. In this way it is possible to waste less energy as the calcite precipitate in small pellet crystal instead of forming the typical “lime mud” of causticization process. In this way, the removal of lime from Pellet Reactor is easier and less energy intensive. Also, pellets formation has the advantage of retaining less calcium hydroxide leading to a more efficient washing procedure. Unreacted ions such as the carbonates ones are filtrated using similar components used in the wastewater treatment plant. Roughly 10% of the calcium in form of lime is collected with fine filters as fines[11].

The formation of the Pellet allows the usage of an oxy-fired Circulating Fluidized Bed Reactor (CFB) instead of a rotary kiln for the Calcination procedure. The Calciner and preheat cyclones are large steel vessels lined with refractory brick. Fluidizing are supplied with a refractory distribution plate, and natural gas is injected via lances above it. CFB offers several advantages; heat recovery is highly efficient due to the preheating cyclones and steam superheaters, reducing fuel consumption. Heat integration follows a conservative approach that lowers technical risk and capital costs compared to more complex solutions. Thermal control is optimized through gradual preheating of materials and controlled gas cooling, ensuring a stable reaction and high-quality product. Also, the usage of CFB instead of rotary kiln doesn’t require vacuum filtration as “lime mud” is no more present in the system. The refractory linings in the steel components enhance resistance to high temperatures, reducing maintenance. Incoming oxygen is preheated using the heat from outgoing CaO, improving energy efficiency[11].

Heat from the slaking reaction is used to dry and preheat the pellets, generating steam to sustain the process. Steam slaking is thermodynamically advantageous over conventional water slaking, as it releases enthalpy at higher temperatures. Operating at 300°C ensures fast reaction kinetics, while the maximum temperature for slaking in 100-kPa steam is 520°C. The Slaker is a refractory-lined bubbling fluidized bed which used recirculating steam as fluidized gases. It receives hot CaO at 674°C from the calciner’s oxygen preheat cyclone. Quicklime (CaO) particles react to form $Ca(OH)_2$, with small particles recirculated through a cyclone and loop seal, while finer slaked particles are captured in a dust collector. The 300°C hydrated lime stream provides heat for drying and warming the pellets, which are then transported via a closed-loop pneumatic conveyor[11].

The plant incorporates auxiliary components to supply the energy and specific streams required for its operation. A power island, powered by a gas turbine, generates the electrical energy needed by the system. The flue gas from the turbine is directed to an absorber, where a post-combustion carbon capture process is employed to remove CO_2 emissions. The cleaned flue gas is then mixed with the inlet air of the air contactor, enabling additional CO_2 capture.

A Rankine cycle is also integrated to recover a portion of the waste heat and to produce steam, as it is required by the Slaker to regenerate calcium hydroxide. An Air separation unit (ASU) is also included to produce pure oxygen, which is used for Oxy-combustion in the calciner. Oxy-combustion—instead of conventional combustion with air—minimizes the formation of NOx and other pollutants, reducing the need for additional gas cleaning processes. The flue gas from the Oxy-combustor is subsequently mixed with the main stream within the Calciner. Last but not least, a compression train is included to compress the captured CO_2 to 150 bars, making it ready for utilization or storage.

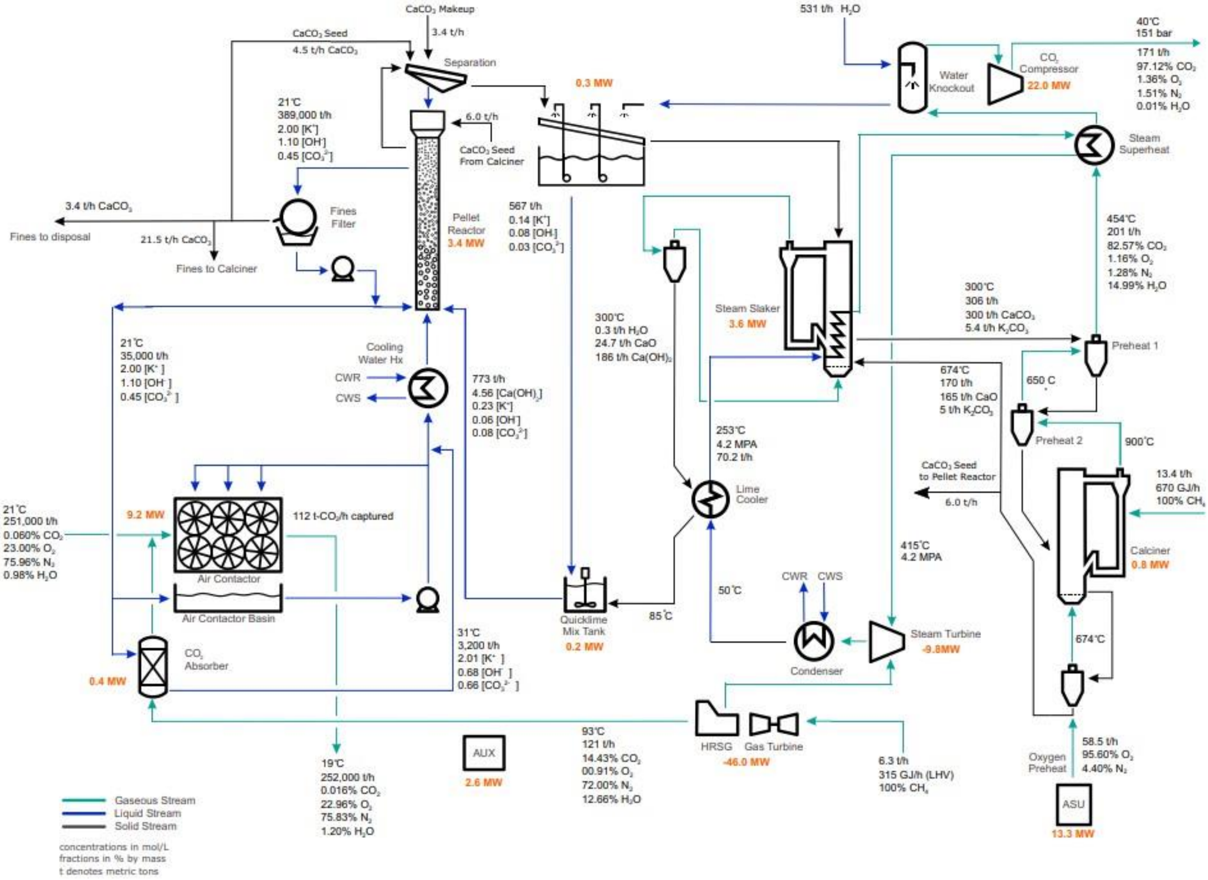

Figure 12 scheme of the DAC plant modelled by Keith et al.[11]

1.6 PRODUCTION OF CHEMICALS FROM CO_2

The annual production of chemicals, such as solvents and plastics, contributes approximately to 2 gigatons of CO_2 emissions per year. Utilize CO_2 as a feedstock offers a promising opportunity to reduce GHG emissions by displacing the need for fossil fuel-derived chemicals. Currently, the production of these chemicals is tightly linked to petroleum, which ensures extremely low costs for these commodities. However, this reliance on fossil fuels comes at a significant environmental cost. Several pathways exist for using CO_2 as an alternative feedstock, but many of these processes are highly energy-intensive. The amount of energy required relies on the type of reactions involved, in fact, when the CO_2 is simply incorporated in an organic molecule, the energy required is relatively small as the oxidation state of the CO_2 does not change. In most of the chemicals considered, instead, a reduction of the CO_2 is required involving a high amount of energy. The reduction generally takes place by making the CO_2 reacting directly with hydrogen or with an electrochemical conversion. In both cases the energy requested is very high due to electricity consumption of the cell and to the heat to supply the reaction. The CO_2 reduction can be performed with different type of reaction, which are summarized as follows[13]:

- Thermo-catalytic: In which the reaction is driven by the high temperature and pressure. Generally, the reaction rate is increased with a catalyst.
- Electrochemical: In which energy is provided as an electrical current inside the cell
- Biochemical: In which the CO_2 is reduced using living organisms and enzymes
- Photochemical: In which energy is provided by the sun, thermally or electrically by using aphotovoltaic cell.

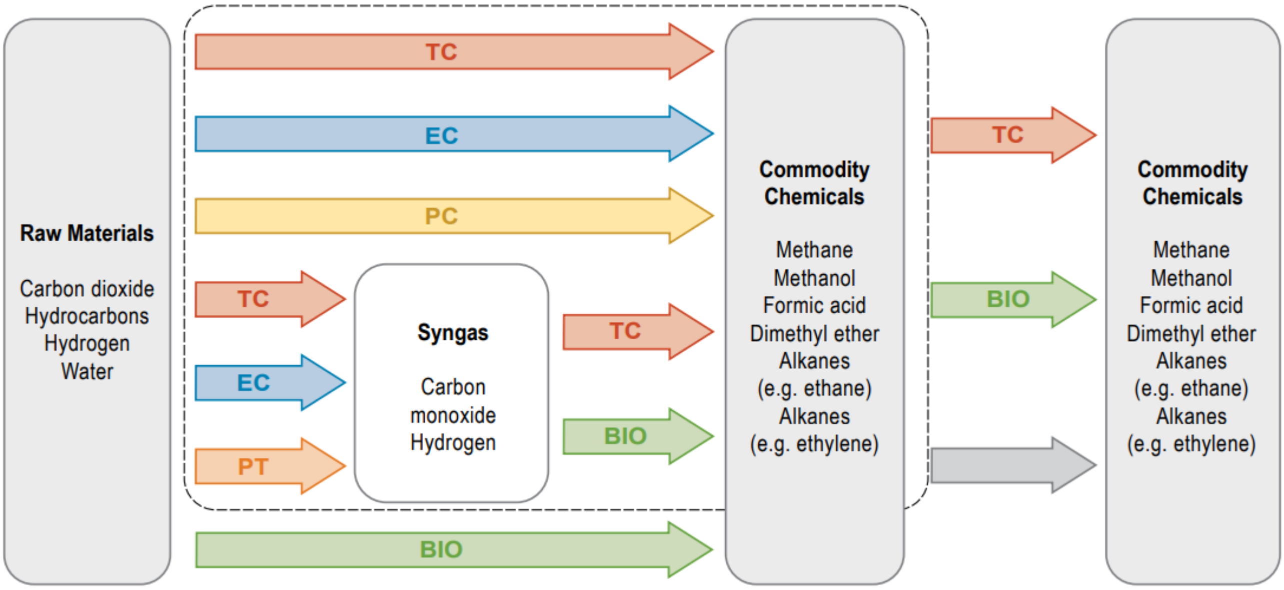

Figure 13 Pathways to produce Chemicals from CO_2[13]

The first two are the most widely used as explored pathways.

Aside from the one step procedure, in which one of the previous patterns is used to synthesize one of the products (methane, methanol, formic acid and dimethyl ether), it is possible to obtain the same product via 2 steps. In the first step carbon monoxide is obtained, generally involving a reverse water gas shift reaction (RWGS) or an electrochemical reduction of the CO_2. The second step involves a hydrogenation reaction. As shown in figure, the second step can't be performed with an electrochemical reduction. The product from the first step can be syngas, in this case the resulting mixture will be composed by both carbon monoxide and hydrogen, ready for the second step. To obtain this result the CO_2 can be make react together with water in order to reduce both of them. The syngas alone has a poor price on the market, so generally it is preferable to perform the second step. Carbon monoxide has instead a higher value on the market but only if high purity is obtained. Achieving this is not so simple as it's required high purity of the CO_2 stream and high selectivity of the process.

1.6.1 SYNTHETIC METHANE

Methane (CH_4) stands out among the chemical which can be obtained thanks to its high energy density (55.5 MJ/kg), extensive global consumption, and dominance in the energy market—accounting for nearly 23% of worldwide energy use. The potential to synthesize CH_4 using renewable electricity presents a compelling opportunity to transform carbon emissions into a valuable energy carrier[26].

Several problems, mainly related to profitability and scalability, are currently under investigation. The synthetic methane is currently not price competitive compared to the fossil-based one. As seen in the figure shown in the previous section, many pathways can be explored for production, in particular thermo-catalytic and electrochemical conversion are the most interesting ones.

The CO_2 methanation, also known as the Sabatier reaction, is a chemical process in which carbon dioxide reacts with hydrogen to form methane and water.

$$CO_2 + 4H_2 \rightleftharpoons CH_4 + 2H_2O \quad \Delta H^\circ = -164 kJ/mol\ (298\ K) \quad Sabatier\ reaction$$

Other two reactions aside from this takes place during the methanation process, which concur to the methane production. The first is the RWGS in which CO_2 react forming carbon monoxide, while the second is the methanation of carbon monoxide:

$$CO_2 + H2 \rightleftharpoons CO + H_2O \quad \Delta H^\circ = +41.2kJ/mol \quad RWGS$$

$$CO + 3H_2 \rightleftharpoons CH_4 + H_2O \quad \Delta H^\circ = -206\ kJ/mol\ (298\ K) \quad Methanation\ of\ CO$$

These pathways could be implemented only in high renewable energy sources (RES) penetration due to the necessity of hydrogen. The hydrogen produced by fossil fuels, also known as grey hydrogen, produce a certain amount of CO_2 during the process. To maintain effective the carbon capture procedure also the production plant of hydrogen would have to be coupled with a Post-combustion carbon capture system. The other alternative is to produce hydrogen via electrolysis, but this would require a high amount of electricity, only available and cost competitive with high-RES penetration[13].

Methanation reactors uses commonly nickel based catalysts which are cost-effective. The problem related to this catalyst, as shown in a ENEA study[27], is the degradation of it, which can lead to dispersion of particles influencing the catalytic activity and so the conversion efficiency and product purity. The reaction generally takes place at a temperature between 200°C-550°C and a pressure between 1 and 100 bars which summed with the exothermicity of the reaction required proper thermal management. Generally, isothermal reactors are the best choice for this process, with a cooling system provided by an external fluid[28].

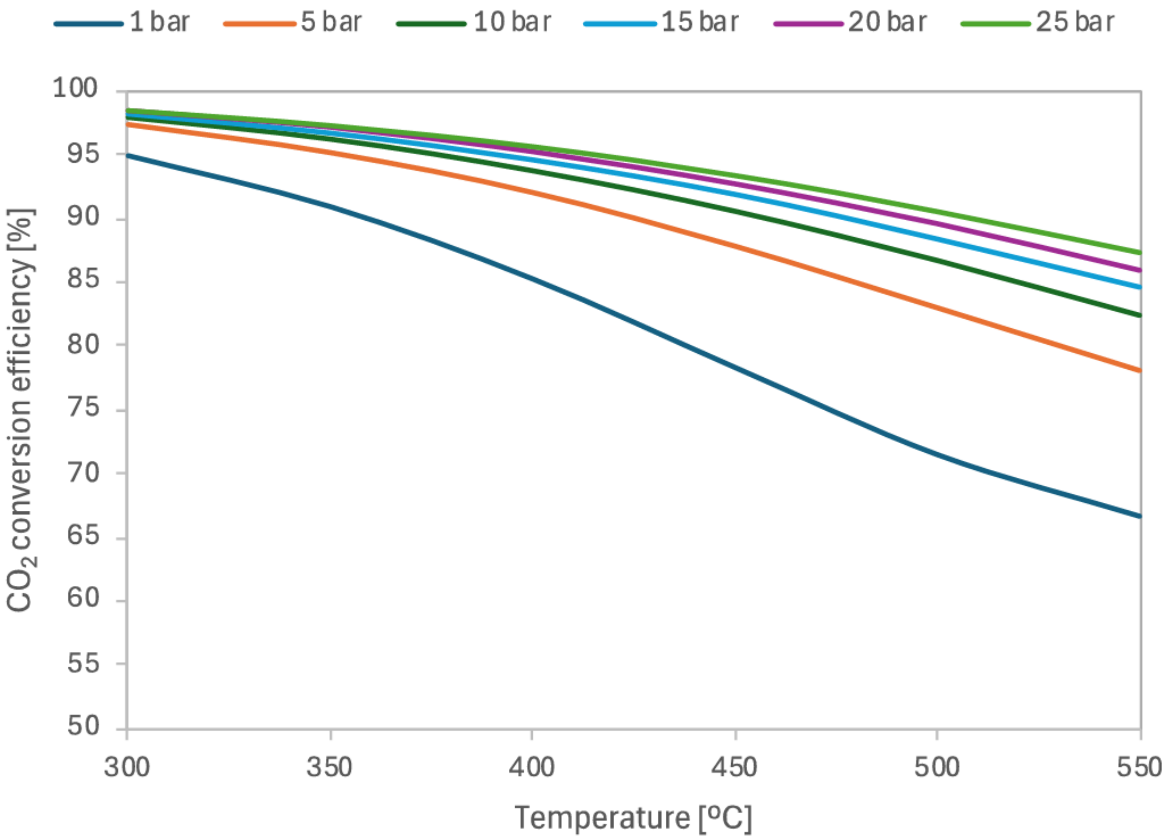

Figure 14 Sabatier methanation CO_2 conversion as function of temperature and pressure[29]

As shown in the graph, the Sabatier reaction, being exothermic, benefits from lower temperatures. However, the temperature cannot be too low, as this would negatively impact the reaction kinetics. As previously mentioned, the reaction also benefits from higher pressure. Increasing the pressure leads to higher CO_2 conversion, and overall, the function's profile decreases less sharply as temperature increases. The results shown in the figure are based on the study of Varandas et al.[29], using a ratio of moles of H_2/CO_2 stoichiometric of 4:1.

On the other hand, we have the electrochemical carbon dioxide reduction (ECR), which is less mature compared to the first and less explored.

The process is performed using an electrolyzer, typically an alkaline electrolytes membrane (AEM) cell, with a Cu-based catalyst[30]. In those cells, the CO_2 is fed to the cathode in which an electrochemical reaction with water occurs as follows:

$$CO_2 + 6H_2O + 8e^- \rightarrow \; CH_4 + 8OH^-$$

The oxydrilic group, then, cross the membrane, reaching the anode in which occurs the other half reaction:

$$8OH^- \rightarrow \; 2O_2 + 4H_2O + 8e^-$$

The total reaction is:

$$CO_2 + 2H_2O \rightleftharpoons \; 2O_2 + CH_4 \quad \Delta H° = +891 kJ/mol$$

ECR systems present technical difficulties as mainly used alkaline electrolytes and anion exchange membrane cells. Those systems work at high current densities, generally above >300 mA/cm^2, which allows higher selectivity and Faraidic efficiency in the range of 60% to 70%. As drawback, crossover phenomena and carbonate or bicarbonate formation must be considered[26].

Crossover phenomena refer to the capability of the CO_2 to cross the membrane and migrate from the cathode to the anode. The main driving force is the formation of carbonate and bicarbonate ions—which can cross the alkaline electrolyte due to the negative charge—formed as side effect reaction between the CO_2 and the oxydrilic group. Other factors include the pressure and concentration gradient which can lead to crossover based on diffusion. The effect of crossover includes[30] :

- Reduction in CO_2 conversion efficiency: mainly due to the less amount available of CO_2
- Increasing of the energy required: to recover the carbonate ions formed
- Decrease in selectivity: which impacts on the purity of the product

General approach to reduce the crossover phenomena includes optimization of the membranes and fine-tuning parameters adjustment of the PH, current density and other operation parameters[30]. A similar procedure can be conducted to produce methanol and other chemicals. Anyway, as the focus of this study is on the thermo-catalytic pathways, the ER won't be further analyzed for the others.

1.6.2 METHANOL

Methanol is a widely used chemical, forming the basis for many industrial products. It is essential in manufacturing polymer fibers for textiles, plastics for packaging, adhesives, paints, solvents, and absorbents. Those includes[31]:

- Formaldehyde: Used in resins, adhesives, plywood, and insulation materials
- Acetic Acid: A key component in making synthetic fibers, plastics, and food preservatives.
- Methyl Tert-Butyl Ether (MTBE) / Methyl Methacrylate (MMA): Used as fuel additives and in the production of acrylic plastics.
- Olefin Production: Methanol is converted into ethylene and propylene, which are used in plastics, packaging, and textiles.

Methanol is also used as fuel, directly burning it in modified engines or to feed fuel cells as hydrogen carrier. It's usage as fuel is particularly research in the marine sector. It can also be used in process to manufacture others such as gasoline or biodiesel[32].

Nowadays, the total annual production of this chemical is 75 Mton with a global market value of 369 billion $. This makes methanol the second most produced chemical explored and the leader in terms of global market value[33].

Currently, based on Report1 of the International Methanol Producers and Consumers Association (IMPCA), the methanol production accounts for 165 Mton-CO_2/year emitted which is roughly 0.3% of the total yearly emissions[31].

This is because the methanol is mainly produced from natural gas and coal. Similarly to hydrogen, different pathways are under investigation including the usage of municipal waste, sewage from water treatment plants and captured CO_2, all fed by RES electricity[32].

Like methanation process the methanol can be synthesized using thermo-catalytic reactions or direct electrochemical reduction of CO_2.

Today, methanol is commercially synthesized from natural gas using the syngas route.

This process occurs in two steps:

1. Steam reforming of methane(SMR)
2. Methanol production

The first step is the most energy-expensive, as it requires very high temperatures and pressures.

$$CH_4 + H_2O \rightleftharpoons CO + 3H_2 \quad \Delta H° = 206\ kJ/mol\ \ SMR$$

The second step for producing methanol is through the hydrogenation of carbon monoxide and carbon dioxide which is obtained as consequence of water gas shift reaction (WGS) [34].

$$CO + 2H_2 \rightleftharpoons CH_3OH \quad \Delta H° = -90.7 kJ/mol \quad Hydrogenation\ of\ CO$$

$$CO_2 + 3H_2 \rightleftharpoons CH_3\,OH + H_2O \quad \Delta H° = -49.5\ kJ/mol\ \ Hydrogenation\ of\ CO_2$$

$$CO + H2 \rightleftharpoons CO_2 + H_2O \quad \Delta H° = -41.2kJ/mol\ \ WGS$$

In the hydrogenation of CO, Carbon monoxide reacts with two molecules of hydrogen to form methanol (CH_3OH). This process is more direct and efficient compared to CO_2 hydrogenation, as it does not produce water.

In contrast, hydrogenation of CO_2 requires three hydrogen molecules to produce methanol and water.

Industrially, on the other hand, the methanol from CO_2 can be obtain in two steps: CO_2 is often first converted into CO as an intermediate step via the RWGS reaction or electrochemical reduction.

$$CO_2 + H2 \rightleftharpoons CO + H_2O \quad \Delta H° = +41.2kJ/mol \quad RWGS$$

And then the conversion in methanol through hydrogenation of CO is performed.

$$CO + 2H_2 \rightleftharpoons CH_3OH \quad \Delta H° = -90.7kJ/mol\ \ Hydrogenation\ of\ CO$$

As previously stated, furthermore, there is an alternative method in which methanol is produced in a single step.
In this case the hydrogenation of CO_2 is the main reaction, although the RWGS reaction and the hydrogenation of CO occur to a minimal extent.

$$CO_2 + 3H_2 \rightleftharpoons CH_3\,OH + H_2O \quad \Delta H° = -49.5\ kJ/mol\ \ Hydrogenation\ of\ CO_2$$

$$CO_2 + H2 \rightleftharpoons CO + H_2O \quad \Delta H° = +41.2kJ/mol\ \ RWGS$$

$$CO + 2H_2 \rightleftharpoons CH_3OH \quad \Delta H° = -90.7kJ/mol\ \ Hydrogenation\ of\ CO$$

The optimal reaction's temperature for maximum performance, range from 200 to 300°C, while the pressure should be between 50 and 100 bar[35].

The most commonly used catalyst for this pathway is $Cu/ZnO/Al_2O_3$ (copper oxide, zinc oxide, and alumina). Copper is the main active component for the hydrogenation reaction, promoting the reaction between CO and H_2 to produce methanol. Zinc (ZnO) and alumina (Al_2O_3) mainly serve as supports, dispersing the copper and improving the catalyst's stability at relatively moderate temperatures and pressures[36].

A drawback that could affect the efficiency is the presence of water, which could deactivate the catalyst. To address this issue, two different approaches can be considered: the first is to use separation systems to remove H_2O, while the second is to use catalysts that are not affected by it[37].
An example of the latter is zirconia.

Zirconia is a heat-resistant oxide that, unlike the commonly used alumina, has lower hydrophilicity. It also improves the dispersion of copper, thereby increasing the catalyst's activity and the selectivity towards methanol. Commercially, alumina is most used because much more inexpensive than Zirconia[38].

Another potential catalyst could be the ruthenium (Ru) instead of copper. The ruthenium is more efficient at lower temperatures and pressures, but its average cost tends to be higher and economic feasibility at industrial scale could not be possible[39].

1.6.3 DIMETHYL-ETHER

Dimethyl ether (DME) is a non-toxic, non-carcinogenic molecule, typically derived from natural gas or methanol[40]. DME account for a total annual demand of 6.3 Mtons with a market value of 3.2 billion $. Even if the share is lower DME have an higher CO_2 potential reduction—of 1.913 tons-CO_2/tons-product—compared to methanol[33].

It is used as an "eco-friendly" aerosol propellant as an alternative to ozone-depleting Chlorofluorocarbons(CFC) compounds[41].

Due to its physical and chemical properties similar to liquefied petroleum gas (LPG), DME has gained increasing attention in recent years as an alternative liquid fuel to diesel and LPG[40], [41].

In this regard, during the 1990s, researchers demonstrated that DME is a suitable fuel for diesel engines, as it produces lower emissions of NOx and particulate matter, with zero SOx emissions, unlike conventional fuels[40], [41].

The diesel engine injection system would require only minor modifications, while significantly improving emissions without excessive efficiency losses[41].

Dimethyl ether is a direct byproduct of methanol, obtained through its dehydration. Therefore, it can be synthesized directly from CO_2 and H_2, or from CO and H_2 when using hybrid catalysts[42].

- synthesis of DME from CO_2 and H_2[42]:

$$CO_2 + 3H_2 \rightleftharpoons CH_3OH + H_2O \quad \Delta H° = -49{,}5kJ/mol \;\; Hydrogenation\ of\ CO_2$$

$$2CH_3OH \rightleftharpoons CH_3OCH_3 + H_2O \quad \Delta H° = -40{,}7kJ/mol \;\; DME\ from\ methanol$$

$$CO_2 + H_2 \rightleftharpoons CO + H_2O \quad \Delta H° = 41{,}2kJ/mol \;\; RWGS$$

- synthesis of DME from CO and H_2[42]:

$$CO + 2H_2 \rightleftharpoons CH_3OH \quad \Delta H° = -90{,}7kJ/mol \;\; Hydrogenation\ of\ CO$$

$$2CH_3OH \rightleftharpoons CH_3OCH_3 + H_2O \quad \Delta H° = -40{,}7kJ/mol \;\; DME\ from\ methanol$$

$$CO + H_2\mathrm{O} \rightleftharpoons CO_2 + H_2 \quad \Delta H° = -41{,}2kJ/mol \;\; WGS$$

As this is a one-step procedure, all the reactions occur parallelly and compete against each other. For this reason, DME Yield is generally lower compared to methanol. The reaction requires a proper catalyst, and it is enhanced by slightly lower temperature and pressure of the ones used for methanol. Aside from catalysts used in methanol production, reactors require materials like Nafion or zeolites which demonstrated high capability in dehydration of methanol [33].

Although DME shows promise as a future alternative fuel, it has not yet been developed in the market due to technical issues related to engine components and distribution infrastructure. There are also factors that limit its success. DME has a much lower LHV than conventional diesel, which means a significantly larger volume must be injected into the engine to provide the same amount of energy. Another drawback is its low viscosity and solvent capacity, which require a careful selection of sealing materials[40].

1.6.4 FORMIC ACID

Another produced chemical synthesised from CO_2 is Formic acid, which is the simplest carboxylic acid. It is mainly used in chemical and pharmaceutical sector, for example as precursor for the synthesis of esters

Although ants and other insects produce a significant amount of this chemical, the majority of the world's production is industrially derived. This is done either through the base-catalysed reaction of carbon monoxide and methanol to produce methyl formate, which is then hydrolysed to formic acid, or by heating CO with sodium hydroxide to produce sodium formate, which is subsequently acidified[43].

- Methyl formate process[43]:
    - *Methyl formate (via basic catalyst)*

      $$CO + CH_3OH \rightarrow CH_3OCHO \quad \Delta H° = 150.2 kJ/mol$$

    - *Hydrolysis to obtain formic acid*

      $$CH_3OCHO + H_2O \rightarrow HCOOH + CH_3OH \quad \Delta H° - 223.5 kJ/mol$$

- Sodium formate process[43]:
    - *Sodium formate (by heat)*

      $$CO + NaOH \rightarrow HCOONa \quad \Delta H° = -110.5 kJ/mol$$

    - *Acidification to obtain formic acid*

      $$HCOONa + H_2SO_4 \rightarrow HCOOH + Na_2SO_4 \quad \Delta H° = -352.0 kJ/mol$$

The reaction, however, requires a significant amount of energy, as it is disfavoured by a very negative entropy, which causes the chemical equilibrium to shift strongly to the left, resulting in a ΔG of 32.8 kJ/mol[44].

1.7 THESIS OUTLINE

Before proceeding further, it is useful to discuss the goal of this study. This work aims to explore potential utilization pathways for CO_2 captured by the DAC system. As we have seen, DAC systems face significant challenges in achieving economic viability. The goal is to integrate a utilization facility that produces a valuable chemical, analyzing the plant from a thermodynamic perspective, and understanding the potential decrease in energy efficiency when coupled with a DAC system, as capturing CO_2 adds an additional energy requirement.

As discussed in the previous section, many different chemicals can be obtained using various strategies. In our work, we have chosen to produce methanol through thermo-catalytic reduction. DME and Formic Acid are for sure interesting, especially the less explored electrochemical pathway of the last one. Anyway, analyzing their market share and total annual production they are not the most strategic choice. Also—being subproduct of methanol—the added reaction led to more complex reactor design and smaller yielding. Methane, on the other hand, could be a good choice but due to low selling price synthetic way is not so competitive.

For the plant modeling Aspen Plus® (V14), a software developed by AspenTech, is utilized. The software includes a variety of blocks designed to simulate the behavior of real components accurately. Aspen Plus® also offers tools such as calculators and design specifications, enabling iterative computations to determine specific target values efficiently. All the thermodynamics, the method implemented for the model as well as the entire design procedure will be discussed in the next two Chapters.

2 THERMODYNAMIC MODELS AND METHODS

The accuracy of simulation results is closely tied to the selection of appropriate thermodynamic models, as these are the foundation for calculating the properties required by unit operation models. While basic calculations, such as flash and enthalpy, often suffice to establish mass and energy balances, the software also evaluates additional properties like transport characteristics for all process streams. As a result, it is crucial to choose thermodynamic models that effectively represent the physical behavior of the components being simulated.

One of the most frequent phenomena in the plant involves interactions between gaseous and aqueous streams. This occurs primarily in the air contactor and absorber units, where CO_2 is separated from gas mixtures. To accurately model the vapor-liquid equilibrium (VLE) in these areas, two thermodynamic models are utilized:

- Electrolyte NRTL (Non-Random Two-Liquid) for the liquid phase, capturing non-idealities in aqueous solutions.
- SRK EoS (Soave-Redlich-Kwong Equation of State) for the gas phase, suitable for describing gas mixture behavior.

Instead, for the components where electrolyte solutions were not involved classical PENG-ROB (Peng-Robinson Equation of State) is used.

2.1 ELECTROLYTE NON-RANDOM TWO-LIQUID MODEL

The Electrolyte Non-Random Two-Liquid (e-NRTL) model is a thermodynamic framework specifically designed to describe the behavior of electrolyte solutions. Unlike simpler models, it takes into account the interactions that occur in systems involving ions and neutral molecules. This model is built upon the local composition theory introduced in the original NRTL model [45] and incorporates additional terms to account for long-range electrostatic interactions using Debye-Hückel theory [45]. These features make the e-NRTL model particularly suitable for systems where ionic dissociation and non-ideal solution behavior are prominent [45].

The model's fundamental goal is to predict the activity coefficients for species in a solution, which are critical for understanding phase equilibria and solubility. To achieve this, the e-NRTL approach divides the excess Gibbs free energy into two contributions: one describing short-range molecular-level interactions and the other capturing long-range ionic interactions. This dual contribution allows the model to effectively describe the thermodynamic behavior of electrolytic systems over a wide range of concentrations and temperatures.

The model is based on two assumptions[15]:

- Like-ion repulsion: repulsion force due to charge are assume extremely big. This has the consequence of having almost zero concentration of anions around anions and cations around cations.
- Local electroneutrality: distribution of anionic and cationic species are homogeneous around a molecule species, so net local ionic charge is zero

The excess Gibbs free energy G_{ex} is the cornerstone of the eNRTL model. It is defined as the difference between Gibbs free energy of the electrolyte system—which is the thermodynamic potential related to the maximum reversible work at certain conditions maintaining temperature and pressure constant—and The Gibbs free energy of an ideal solution at same conditions. It is divided into short-range and long-range terms, as follows[46]:

$$G_{ex} = G_{ex}^{short-range} + G_{ex}^{long-range}$$

The short-range interactions are modeled using the NRTL framework, which accounts for local molecular interactions. Inside the mixture three different species can be found: molecular, anionic, cationic. The first one type maintains the electroneutrality in the neighborhood region, while the others are based on like-ionic assumption and the center of the specie can be an anion or a cation. The $G_{ex}^{short-range}$ can be calculated as follows, with a term for each type of specie (molecular, anionic, cationic):

$$\frac{G_{ex}^{short-range}}{RT} = \sum_{I}\sum_{m} r_{m,I}\, n_I (\frac{\sum_j X_j G_{jm} \tau_{jm}}{\sum_k X_k G_{km}})$$
$$+ \sum_{I}\sum_{c} z_c\, r_{c,I} n_I (\sum_{a} Y_a \frac{\sum_j X_j G_{jc,ac} \tau_{jc,ac}}{\sum_k X_k G_{kc,ac}}) + \sum_{I}\sum_{a} z_a\, r_{a,I} n_I (\sum_{c} Y_c \frac{\sum_j X_j G_{ja,ca} \tau_{ja,ca}}{\sum_k X_k G_{ka,ca}})$$

With:

$$X_j = C_j x_j$$

$$x_j = \frac{\sum_j x_j r_{j,j}}{\sum_k X_k G_{km}}$$

Where:

- letters $m, a\ and\ c$ refer to molecular species, anions and cations while $i\ and\ j$ indexes refer to segment-based species (functional groups)

- letters $I\ and\ J$ are component indexes
- n_I is the mole number of component I
- x is the segment base mole fraction
- z is the charge number
- C_j is a coefficient equal to z_j for ionic species and equal to 1 for molecular species
- r is a parameter which is the overall number of species present of all types
- Y is the cationic/anionic charge composition fraction quantity
- τ is the asymettric binary interaction energy parameter, it is related to G by a non-random factor parameter named a following an expontial law:

$$G = \exp(-\alpha\tau)$$

τ is defined as the difference between interaction energies of the specie i in the neighborhood of the j specie. Aspen uses this two-temperature related correlation to both calculate τ and α[47] :

$$\tau_{i,j} = a_{i,j} + \frac{b_{i,j}}{T} + e_{i,j}\ln(T) + f_{i,j}T$$

$$\alpha_{i,j} = c_{i,j} + d_{i,j}(\mathrm{T} - 273{,}15\mathrm{K})$$

The second term, which accounts for the long-distance interaction, is expressed by the Pitzer-Debye-Huckel equation[15]:

$$\frac{G_{ex}^{long-range}}{RT} = -\sum_i n_i \left(\frac{1000}{M_s}\right)^{\frac{1}{2}} \frac{4A_\varphi I_x}{\rho} \ln(1 + \rho I_x{}^{\frac{1}{2}})$$

with:

$$A_\varphi = \frac{1}{3}\left(\frac{2\pi N_A d_s}{1000}\right)^{\frac{1}{2}} \left(\frac{Q_e{}^2}{\varepsilon_s k_b T}\right)^{\frac{3}{2}}$$

$$I_x = \frac{1}{2}\sum_i x_i z_i{}^2$$

Where:

- A_φ is the Debye-Hückel parameter
- I_x is the ionic strength
- M_s is the molecular weight of the solvent
- N_A is the Avogadro's number
- ρ is the closest approach parameter
- d_s is the density of the solvent
- Q_e is the electron charge
- ε_s is the dielectric constant of the solvent
- k_b is the Boltzmann constant

Finally, it is possible to express the activity coefficient, of the generical I specie, thanks to the relation with Gibbs free energy. It is also possible to split the term into two different, each one accounting for short distance and long-distance interaction respectively:

$$\ln(\gamma_I) = \frac{1}{RT}\frac{\partial G_{ex}}{\partial n_I} = \ln\left({\gamma_I}^{short}\right) + \ln\left({\gamma_I}^{long}\right)$$

2.1.1 DIFFERENCES BETWEEN ELECNTRL AND ENTRL-RK

The e-NRTL method is implemented in Aspen through two models, namely ELECNTRL and ENTRL-RK. Both methods utilize RK-Soave for vapor phase calculations and the same asymmetric reference state for ions. However, there are theoretical differences between the two models that may influence the choice of one over the other.

Firstly, ENTRL-RK addresses certain inconsistencies observed in the original ELECNTRL, particularly related to the liquid-liquid equilibrium of electrolytes in mixed solvents and the phase equilibrium of non-electrolyte solutions. Additionally, ENTRL-RK provides more accurate enthalpy calculations for non-electrolyte organic mixtures[47].

Another distinction is how the two models treat zwitterions—species that carry both positive and negative charges but have a net charge of zero. ELECNTRL treats zwitterions as cations, while ENTRL-RK models them as molecular species. This difference in treatment can result in slightly different calculations for Gibbs free energy[47].

Lastly, ENTRL-RK is more computationally demanding due to its more complex ideal gas approach, which makes the optimization process more resource-intensive compared to ELECNTRL[47].

2.2 REDLICH-KWONG-SOAVE EQUATION OF STATE

RK-SOAVE method is based on the Redlich-Kwong equation of state, proposed for the first time in 1949. This equation represented a marked improvement in describing the gas phase, especially under high pressure or low temperature conditions, even though, like previous models developed, it is not capable of calculating the liquid-vapor equilibrium. It represents a better alternative to classical Van der Walls equation of state and other second- order virial equations, providing more accurate results and being more practical to use[48]. This is the first formulation of the RK equation of state:

$$P = \frac{RT}{V_M - b} - \frac{a}{\sqrt{T}V_M(V_M - b)}$$

Where:

- P is the gas pressure
- R is the universal gas constat
- T is the temperature
- V_M is the molar volume
- a and b are corrective coefficient which account respectively for the attractive potential of molecules and volume.

Several modifications of the equation have been proposed over the years. The one used by RK-SOAVE, as the name suggests, is the Soave's correction reported below[15] :

$$P = \frac{RT}{V_M - b} - \frac{a_c\alpha(T)}{V_M(V_M - b)}$$

Where:

$$a_c = 0{,}42747\frac{R^2{T_c}^2}{P_c}$$

$$b = 0{,}8664\frac{RT_c}{P_c}$$

As we can note Soave substitute the $\sqrt{T}$ term with a the $\alpha(T)$ term, which generalizes the formula. $\alpha(T)$ is still function of temperature:

$$\alpha(T) = \left[1 + m\left(1 - \sqrt{\frac{T}{T_c}}\right)\right]$$

Where:

$$m = 0{,}48 + 1{,}574w - 0{,}176w^2$$

Where w is the acentric factor of the component.

2.3 PENG-ROBINSON EQUATION OF STATE

The Peng-Robinson equation of state (PR-EOS) is a thermodynamic model developed in 1976 by Ding-Yu Peng and Donald B. Robinson. It is widely used to predict the behavior of real gases, particularly for hydrocarbon mixtures, and is often applied in the petroleum and chemical industries.

This equation is an improvement over previous equations of state as it provides a better balance between accuracy and simplicity in describing the phase behavior of substances, especially near the critical point. The PR-EOS is very similar to SRK-EOS and maintains also the same $\alpha(T)$ with some variations. The equation is reported below[49]:

$$P = \frac{RT}{V_M - b} - \frac{a\alpha(T)}{{V_M}^2 + 2V_M b - b^2}$$

Where:

- P is the gas pressure
- R is the universal gas constat
- T is the temperature
- V_M is the molar volume
- a and b are corrective coefficient which account respectively for the attractive potential of molecules and volume.

With:

$$a_c = 0{,}45724\frac{R^2{T_c}^2}{P_c}$$

$$b = 0{,}07780\frac{RT_c}{P_c}$$

$$\alpha(T) = \left[1 + m\left(1 - \sqrt{\frac{T}{T_c}}\right)\right]^2$$

$$m = 0{,}37464 + 1{,}54226w - 0{,}269926w^2$$

Where w is the acentric factor of the component.

2.4 CHEMICAL REACTIONS AND HENRY COMPONENTS

As described in the REFERENCE MODEL section, the overall reactions which take place are only apparent and several sub reactions occur involving the ionic species. The reactions also include the formation and dissociation of salt. To account for all these aspects, based on the references[11], [15], [22], ENTRL-RK and RK-SOAVE thermodynamic models have been chosen. The method selected, based on our version of ASPEN plus, automatically incorporates the property database APV101 (an expansion of the APV88 used by references) which contains the following databanks: ASPENCPD, AQUEOUS, SOLIDS, INORGANIC, PURE26 and PURE32.

To account for the chemical reactions the tool "Electrolyte Wizard", provided by ASPEN plus, has been chosen[15].

The tool automatically generates all reactions related to a given component, including salt formation and water dissociation reactions. It also prompts the user to select the reference ionic state, with an unsymmetrical approach chosen in our case. Additionally, it is necessary to specify the hydrogen ion for the reactions, and the hydronium ion (H_3O^+) has been selected.

The generated reactions are organized within a section called "Chemistry", each assigned a unique ID. When this ID is referenced within a block, the associated reactions are assumed to occur, and the software applies them automatically during calculations.

A key feature of the tool is that reactions in the Chemistry section are not confined to specific blocks; they also take place in broader system interactions, such as when two streams are simply mixed.

The reaction generated are equilibrium reactions and the constant of equilibrium, which will be used for the computation, is calculated using the following formula:

$$lnK_j = A_j + \frac{B_j}{T} + C_j\ln(T) + D_jT$$

As we can note, the equilibrium constant is strictly related to temperature and to $A, B, C \text{ and } D$ coefficient which are provided by the databanks selected.

Reaction	Type	Number
$H_2O + HCO_3^- \leftrightarrow CO_3^{2-} + H_3O^+$	Equilibrium	1
$CaOH^+ \leftrightarrow Ca^{2+} + OH^-$	Equilibrium	2
$2\,H_2O + CO_2 \leftrightarrow HCO_3^- + H_3O^+$	Equilibrium	3
$2\,H_2O \leftrightarrow OH^- + H_3O^+$	Equilibrium	4
$K_2CO_3 \leftrightarrow CO_3^{2-} + 2\,K^+$	Salt	5
$CaCO_3 \leftrightarrow CO_3^{2-} + Ca^{2+}$	Salt	6
$KOH \rightarrow OH^- + K^+$	Dissociation	7
$Ca(OH)_2 \rightarrow CaOH^+ + OH^-$	Dissociation	8

Table 1 Reactions generated with the Electrolyte Wizard Tool

Reaction	A	B	C	D
1	216.05	-12431.7	-354.819	0
3	-231.465	12092.1	-12092.1	0
4	-132.899	-13445.9	-224.773	0
5	-175.998	17765.2	216.865	0

Table 2 Coefficients of the reactions generated with the Electrolyte Wizard Tool

Last but not least, to ensure correct calculations, it is necessary to specify which components should be treated as Henry's components, in our case, N_2, O_2, and CO_2. These components are modeled following Henry's Law, represented by the equation:

$$C = k_h P$$

where:

- C is the concentration of the dissolved gas in the liquid phase,
- P is the partial pressure of the gas in the vapor phase,
- k_h is the Henry's constant, specific to the gas-liquid pair and temperature-dependent.

This designation is essential because Henry's components are assumed not to form chemical bonds with the electrolyte present in the liquid phase. The interaction is therefore purely physical, described as simple dissolution, which remains very limited (low solubility)[50].

If Henry's components are not specified in Aspen, the following issues may arise[50]:

- The gas may be treated as highly soluble or completely miscible with the liquid, leading to significant errors in the calculations.
- Inappropriate thermodynamic models might be used (e.g., activity coefficient models or equations of state that fail to account for the gas's low solubility).

- Gas concentrations in the liquid phase could be overestimated, resulting in unrealistic predictions for vapor-liquid equilibrium and overall system behavior.

2.5 COLUMN BEHAVIOUR: RATE BASED VS EQUILIBRIUM BASE MODEL

Before proceeding further, it is useful to explain how columns are modeled in Aspen to better understand how VLE is calculated. As mentioned earlier, ionic species do not directly participate in the VLE because they are accounted by the e-NRTL model, which describes only the liquid phase behavior[15].

In Aspen, we use RADFRAC blocks to simulate both distillation processes (e.g., the ASU/UTILIZATION section) and absorption processes (e.g., the AIR CONTACTOR section). Two different modeling approaches can be applied to them: the equilibrium-based model or the rate-based model.

- The equilibrium-based model assumes that equilibrium between the vapor and liquid phases is reached at each stage (or tray) of the column. Additionally, perfect mixing of the two phases is assumed at each stage. By combining these assumptions with chemical equilibrium and mass and energy balances, the software calculates the compositions and conditions of the outlet streams.
  However, since this theoretical approach does not reflect real-world behavior, stage efficiency coefficients are introduced to correct the results and account for deviations from ideal equilibrium. Despite these corrections, the equilibrium-based model often fails to provide accurate results, particularly for reactive columns, where chemical reactions occur alongside mass and heat transfer[51].
- The rate-based approach, on the other hand, assumes that vapor-liquid equilibrium occurs at the interface between the two phases. The mass transfer between them is modeled using the two-film theory and the Maxwell-Stefan formulation. This approach enables highly accurate results by incorporating enhancement factors, empirical mass transfer correlations, and effective interfacial area. In fact, unlike the equilibrium-based model, the rate-based model requires the specification of the column dimensions, such as its height and diameter. Additionally, it takes into account hydraulic and transport properties and allows the type of packing selection, which impacts mainly on pressure drop calculations[51].

The two-film theory, proposed by Whitman in 1923, is a development of the classic film theory and describes the mass transfer of a species between two phases (e.g., gas and liquid) in contact. It assumes the presence of a thin film in both the gas and liquid phases near the interface. Within these films, mass transfer occurs primarily through molecular diffusion. Beyond the films, in the bulk of the gas and liquid phases, convection dominates, ensuring relatively uniform concentrations.

At the interface, the concentrations in the two phases are assumed to be in equilibrium. This means the concentration of the species in the liquid phase at the interface is related to its partial pressure in the gas phase by Henry's law[52]:

$$C_{A,i} = \frac{p_{A,i}}{H_A}$$

Where:

- $C_{A,i}$ is the concentration of the species in the liquid at the interface
- $p_{A,i}$ is the partial pressure in the gas phase at the interface
- H_A is Henry's constant

The widely used assumption of phase equilibrium at the interface may not always be true, especially when gradients in interfacial tension arise during the mass transfer process. These gradients often lead to interfacial turbulence, which significantly enhances mass-transfer coefficients. This phenomenon, commonly referred to as the Marangoni effect.

In the gas phase, the molar flux N_A of the species A across the film is proportional to the difference in partial pressures between the bulk gas and the interface[52]:

$$N_A = k_p(p_{A,b} - p_{A,i})$$

Where:

- k_p is the mass transfer coefficient in the gas film
- $p_{A,b}$ is the bulk partial pressure
- $p_{A,i}$ is the partial pressure at the interface

Similarly, in the liquid phase, the molar flux N_A is proportional to the concentration difference:

$$N_A = k_c(c_{A,b} - c_{A,i})$$

Where:

- k_c is the mass transfer coefficient in the liquid film
- $c_{A,i}$ is the concentration at the interface
- $c_{A,b}$ is the bulk concentration

The overall mass transfer resistance includes contributions from both films. This resistance is expressed as follows:

$$\frac{1}{K_o} = \frac{1}{k_p} + \frac{1}{k_c H_A}$$

Where:

- K_o is the overall mass transfer coefficient
- k_p and k_c are the mass transfer coefficients for the gas and liquid films
- H_A is Henry's constant

The Two film theory is described in a very detailed way in the work of Seader et al.[52].

2.6 LANGMUIR-HINSHELWOOD-HOUGEN-WATSON KINETIC MODEL

The LHHW (Langmuir-Hinshelwood-Hougen-Watson) model is a kinetic model used to describe heterogeneous catalytic reactions involving fluid or solid catalysts. The model assumes that the reaction proceeds through three key steps: first, the reactants adsorb onto the catalyst surface (chemisorption); second, the adsorbed reactants undergo a chemical reaction on the surface; and third, the products desorb from the surface and return to the surrounding phase (desorption).

One of the advantages of the LHHW model is that it takes into account both the adsorption-desorption process and the surface reaction, which are critical for understanding the behavior of reactions on solid catalysts. This is especially important because the interactions between reactants and the catalyst surface play a central role in controlling the rate of the reaction. Additionally, the rate equation derived from this model can be extrapolated to predict reaction rates even at concentrations beyond the experimental range, which makes it useful in industrial applications where conditions often exceed those tested in the lab[53].

In this model, physical transport steps, such as the movement of reactants from the bulk phase (gas or liquid) to the catalyst surface, or the diffusion of reactants within the pores of the catalyst, are excluded. The reason for this simplification is that it is assumed these transport processes are much faster than the chemical reaction occurring on the catalyst surface. Therefore, only the chemical rate process, which depends on chemisorption, surface reactions, and desorption, is considered in the rate equation[53].

The chemical rate process in the LHHW model is governed by three factors: the rate of chemisorption (how reactants adsorb onto the surface), the surface reaction (the actual chemical reaction occurring between adsorbed molecules), and the desorption rate (the rate at which the products leave the surface). The model also assumes that the system is isothermal, meaning the temperature is uniform both on the catalyst surface and within the catalyst particle, with no temperature gradient present[53].

The rate equation in the LHHW model is derived by considering the surface concentration of adsorbed species and the number of vacant sites available for adsorption. The adsorption process follows a Langmuir isotherm, which states that the number of available adsorption sites depends on the partial pressure (or concentration) of the reactants. The resulting rate expression is therefore based on the concentration of the adsorbed species and vacant sites, which can be used to describe the reaction rate in practical conditions[53].

The rate of reaction is generally expressed in $\frac{mol}{Kgcat.s}$ and is function of the kinetic constants, evaluated experimentally, and the partial pressure of reactants and product. The LHHV model has a temperature and pressure range of applicability so operating conditions have to be accounted in the choice of the model. This model will be used during the simulation of the utilization facility to account for the kinetics of methanol reaction inside the reactor.

2.7 PLANT DESIGN AND SIMULATION

2.7.1 PROCESS LAYOUT

The entire system is modeled by dividing different sections of the plant into Aspen blocks called Hierarchies. This approach simplifies the procedure and reduces errors caused by conflicting variables or functions. The plant has been re-drawn in an editor and will first be presented with all components connected. To keep the system manageable while allowing for the representation of complex components several simplifications have been made, which will be discussed for each section. The first Hierarchy is called AIR CONTACTOR and focuses on modeling the air contactor component. It is integrated inside an Absorber which has the purpose of capturing the carbon dioxide produced in the POWER ISLAND. The spent solvent is sent to the PELLET REACTOR Hierarchy to recover the KOH base solvent. The Calcite produced is washed and sent to the CALCINER Hierarchy to extract the CO_2. The calcium oxide produced in the CALCINER is hydrated in the SLAKER section and the CO_2 is compressed in the COMPRESSION TRAIN section. The modelling integrates also a Hierarchy for the ASU, POWER ISLAND and STEAM CYCLE which have the function described in the REFERENCE MODEL section. In a second version of the plant, a UTILIZATION Hierarchy is added to use the CO_2 to produce methanol.

For the modelling of this study, three main references are used: Bianchi at al. [15] and Zolfaghari et al.[22] and Keith et al.[11]. The last one has been described in the REFERENCE MODEL section.

The first one use as reference the Keith et al. plant, introducing some assumptions and semplification in the modelling of complex components—like the Air contactor—proceding than performing a thermal integration strategy and a validation of the model. The second one, instead, use the model of Bianchi et al. as starting point, to optimize the thermal integration, achieving better performances and reducing costs. For the layout of main component, Air contactor, Pellet reactor, Slaker, Calciner, Power island, Bianchi et al. scheme will be used. Also some assumptions, which will be discussed later, will be taken from these two studies. Unlike the two references [15], [22]heat exchangers have not been included within the Aspen simulation. This decision is made because the pinch analysis, which will be discussed later, resulted in a high number of units. Including all heat exchangers in the Aspen model would have made the diagram overly complex and less clear. Also, the computational cost would be too high leading to convergence issues. Instead, the heat exchangers network (HEN) will be presented separately during the pinch analysis discussion. Within the Aspen model, only one heater/cooler is used for each temperature transition. The only exception is made for steam streams, where three heaters are used in series to more accurately account for variations in specific heat capacity.

A table containing the stream specifications (mass flow, temperature, pressure, and composition) will be provided in the APPENDIX section. Each Hierarchy use one of the different methods provided previously which are:

- AIR CONTACTOR : ENTRL-RK
- PELLET REACTOR : ENTRL-RK
- WASHER-SLAKER : ENTRL-RK
- CALCINER : PENG-ROB
- POWER-ISLAND : PENG-ROB
- STEAM-CYCLE : PENG-ROB
- ASU : PENG-ROB
- COMPRESSION TRAIN : PENG-ROB
- UTILIZATION : PENG-ROB

Figure 15 Scheme of Standalone DAC plant modelled

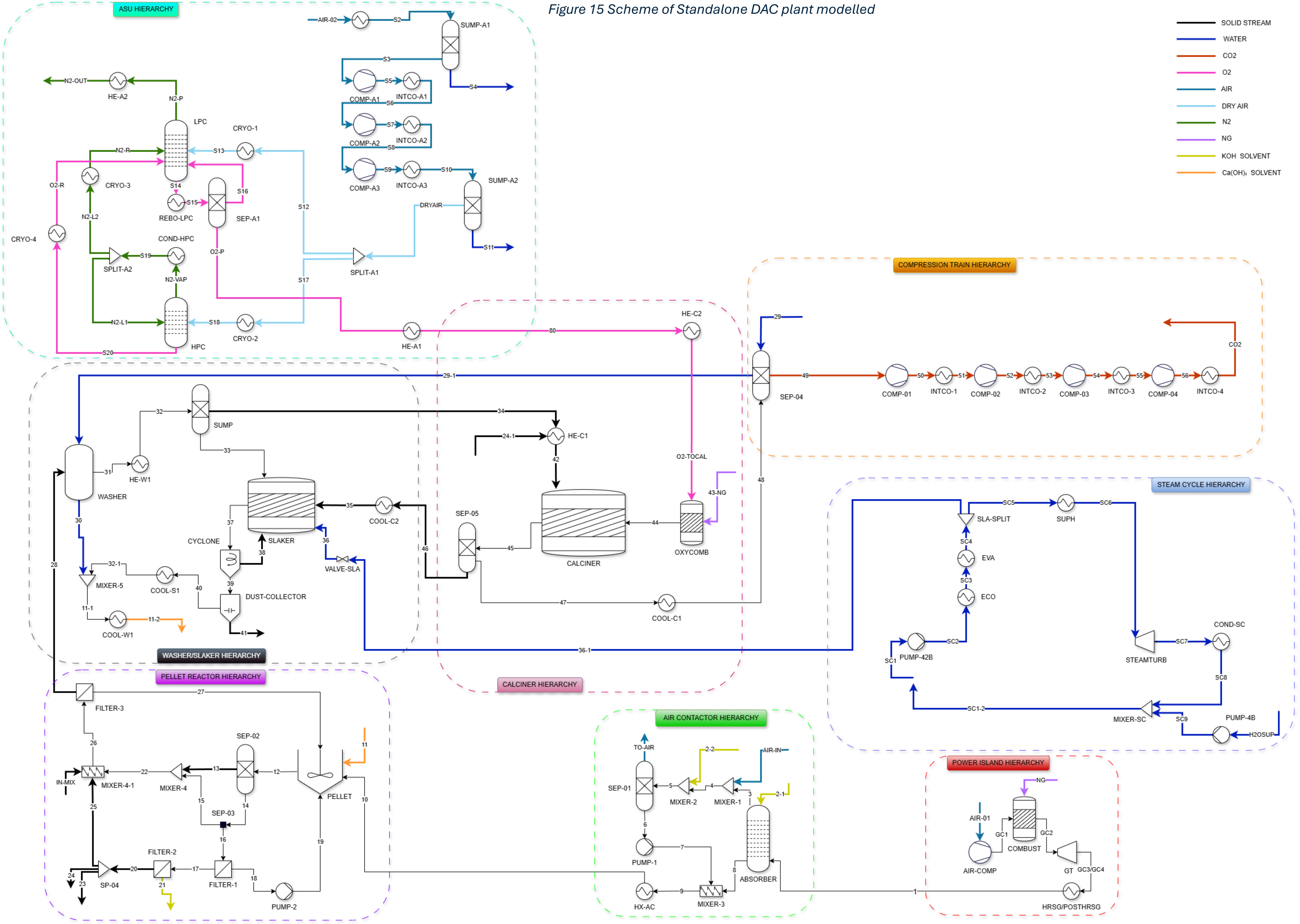

2.7.2 AIR CONTACTOR HIEARARCHY

The process begins with exhaust gas from the GAS CYCLE section, which is sent to the absorber block via stream 1. The absorber is modeled using a RADFRAC block, where a rate-based model approach is implemented. The column has dimensions of 12 x 7.5 m (height x diameter) and is filled with structured packing material provided by BERL Ceramic.

Several input parameters are required for the RADFRAC block when operating in a rate-based model, as in this case. Specifically, the column is divided into 16 stages, with a reaction condition factor of 0.9, a film discretization ratio of 5, an interfacial area factor of 1.2, and liquid film discretization points set to 5, following the reference methodology [15], [22].

The reaction condition factor, ranging from 0 to 1, accounts for the position of the liquid phase within the film. Lower values indicate liquid conditions closer to the vapor phase, while higher values suggest liquid conditions closer to the bulk. This parameter is crucial because it directly affects mass transport phenomena and consequently changes the chemical reactions. As explained in the previous sections, the chemical reaction takes place only in the liquid phase and not in the vapor phase [15].

The film discretization ratio defines the thickness of the adjacent discretization regions, where values greater than 1 indicate a thinner film near the vapor-liquid interface. The interfacial area factor corrects the actual interfacial area by multiplying it by the specified factor [15].

According to the reference, these parameter values are adopted from other models of amine scrubbing processes for CO_2 capture. This approach is reasonable since the mass transfer phenomena involved are quite similar in both amine-based and alkali-based solvent processes [15].

The RADFRAC column is fed from the top (stage 1 in the Aspen convention) with a KOH-based solvent, the same used in the air contactor. The solvent composition is 2.00 M K^+, 1.10 M OH^-, and 0.45 M CO_3^{2-}, as reported in the references [11], [15], [22]. To determine the appropriate solvent flow rate required to achieve a 90% CO_2 capture ratio, a design specification is implemented. This specification adjusts the inlet solvent mass flow rate until the ratio of CO_2 mass flow at the outlet to CO_2 mass flow at the inlet reaches 0.1.

As previously mentioned, the chemical reaction occurs without requiring additional parameters, as it is predefined in the chemistry section using the electrolyte wizard. Thus, it is only necessary to reference the predefined chemistry in the Hierarchy's method section to activate the reactions.

From the top of the absorber block, the purified exhaust gas is sent to a mixer, while from the bottom (stage 16), the spent solvent exits with the captured CO_2. The purified gas is mixed in the MIXER-1 block with 250,000 ton/h of air, having a similar CO_2 concentration. The CO_2 concentration in the incoming air is set to 400 ppm, based on reference values that approximate current atmospheric levels (423 ppm).

The mixture is then sent to MIXER-2, where it is mixed again with the solvent before passing through SEP-01. SEP-01 is modeled using a 0/1 logic to account for the separation process. A second design specification is implemented to adjust the solvent flow rate (stream 2-2) until a CO_2 capture ratio of 74.39% is achieved. This is done by setting the CO_2 mass flow rate in the TO-AIR stream divided by the CO_2 mass flow rate in stream 4 equal to 0.2561.

To better account for real system pressure conditions, a pressure drop of 0.5 bar is applied in SEP-01. To compensate for this, a pump is placed after the separator. These last three components aim to replicate the behavior of the real Air contactor. This simplification is necessary because the Air contactor is an innovative component that cannot be directly modeled in the software.

After separation, the solvent from the separator and the Absorber is mixed in MIXER-3 and then cooled to 19.20°C, as indicated in the reference.

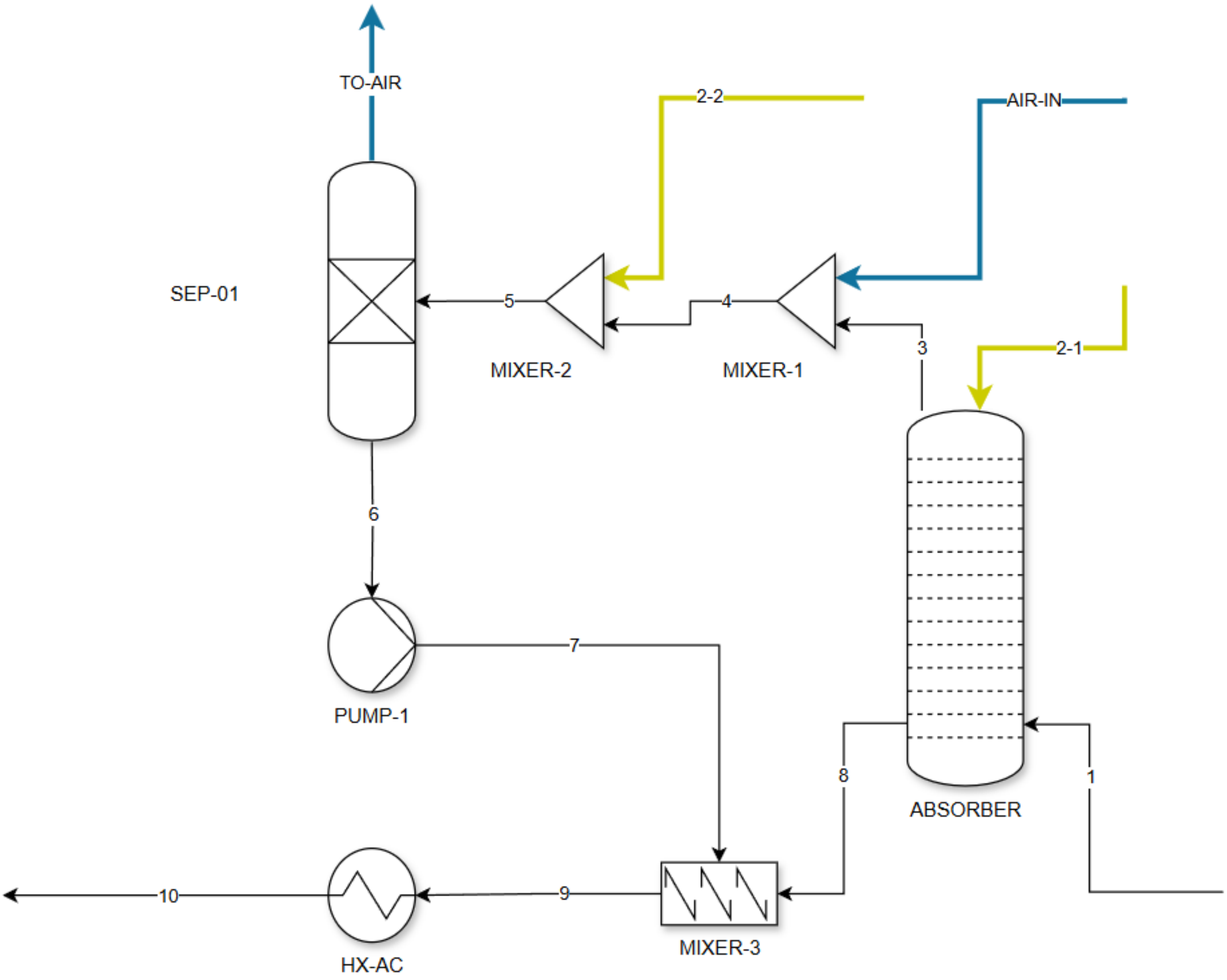

Figure 16 AIR CONTACTOR Hierarchy

2.7.3 PELLET REACTOR HIERARCHY

The Pellet Reactor is the second Hierarchy of the system, responsible for recovering the CO_2 contained in carbonate ions (CO_3^{2-}) from the spent solvent stream. The process involves the crystallization of calcium carbonate ($CaCO_3$), where carbonate ions react with calcium from calcium hydroxide, forming solid calcite.

The actual Pellet Reactor is a fluidized bed, a component available in Aspen simulation under the name of "FLUIDBED." However, this model requires numerous input parameters that are not provided in references[11], [15]. For this reason, as done by Bianchi et al.[15] , a Crystallizer block (named PELLET) is used instead.

This block operates under relatively simple conditions, requiring only the pressure and temperature at which the reaction occurs, set at 25°C and 1 bar. Additionally, it needs a "saturation calculation method," which can either be defined manually by inserting the solubility function or, as in our case, defined using the chemistry generated by the electrolyte wizard, specifying the compound to be recalled.

The calcium required for crystallization is supplied by Stream 11, which consists primarily of water and calcium hydroxide. This stream follows the reference values, with:

- Mass flow rate = 770 ton/h
- Mass fraction of calcium hydroxide = 0.277

Calcium hydroxide is provided in excess to ensure the maximum amount of carbonate ions can react. As a result, Stream 12, which exits the PELLET block, contains a certain amount of calcium hydroxide (in its dissociated ion form).

Similar to the AIR CONTACTOR section, this stream would normally be recirculated from another section (SLAKER/WASHER) corresponding to Stream 11-2. However, to prevent convergence issues, the two streams are separated in the model.

Bianchi et al. originally uses a design specification to adjust the split fraction inside SEP-02 to assess the "calcium retention" parameter, which is fixed by reference at 90%[15][11]. However, as the procedure to create the design spec is unclear, we adjust the split fraction iteratively to match the mass flow rate reported in the study.

Additionally, the values of the mass flow rate of streams 23 and 24 are changed. The values proposed by Bianchi et al., in fact, seem unreasonably high, leading to excessive waste of $CaCO_3$. Even if, as we will see, this does not significantly affect the validation of the model—since the energy requirement is weighed on the CO_2 available in the outlet stream of the plant—it has major consequences on the actual amount of CO_2 available.

To assess the problem, the values of streams 23 and 24 are taken from Keith et al. and readjusted proportionally based on the CO_2 captured in the AIR CONTACTOR section (Keith et al. capture slightly less CO_2 due to the composition of the exhaust gases from POWER ISLAND).

Streams 23 and 24, which are pure calcium carbonate, are roughly 10% of the $CaCO_3$ inside Stream 12, accounting for the calcium retention parameter.

After leaving the PELLET block, Stream 12 is directed to the first separator (SEP-02). This step models a function of the real Pellet Reactor, which partially separates $CaCO_3$ and sends it directly to the upper loop.

The next separator (SEP-03) recirculates approximately 0.1% of Stream 14's liquid to MIXER-4 via Stream 15, where it is mixed with Stream 13, forming Stream 16.

Those steps mimic the real behavior of the Pellet Reactor, which can separate some calcium carbonate but not in perfectly pure form. While this could be done with a single separator without any mixer, we maintain the same configuration as the reference for easier result checking.

Stream 16 is sent to FILTER-1, modeled with a solid separator; this block can separate most of the liquid, introducing a pressure drop. The liquid fraction (Stream 18) passes through PUMP-2, restoring its pressure to 1 bar before being recirculated into the PELLET block via Stream 19.

The solid fraction (Stream 20, mostly $CaCO_3$) is sent to FILTER-2—which completes the solid-liquid separation—where Stream 21 represents the solvent that would be sent to the AIR CONTACTOR. The difference in mass compared to Streams 2-1 and 2-2 is mainly due to higher water content; in fact, the content of KOH (in dissociated ion form) almost perfectly matches while carbonates ions are slightly higher due to small inefficiency of the PELLET block.

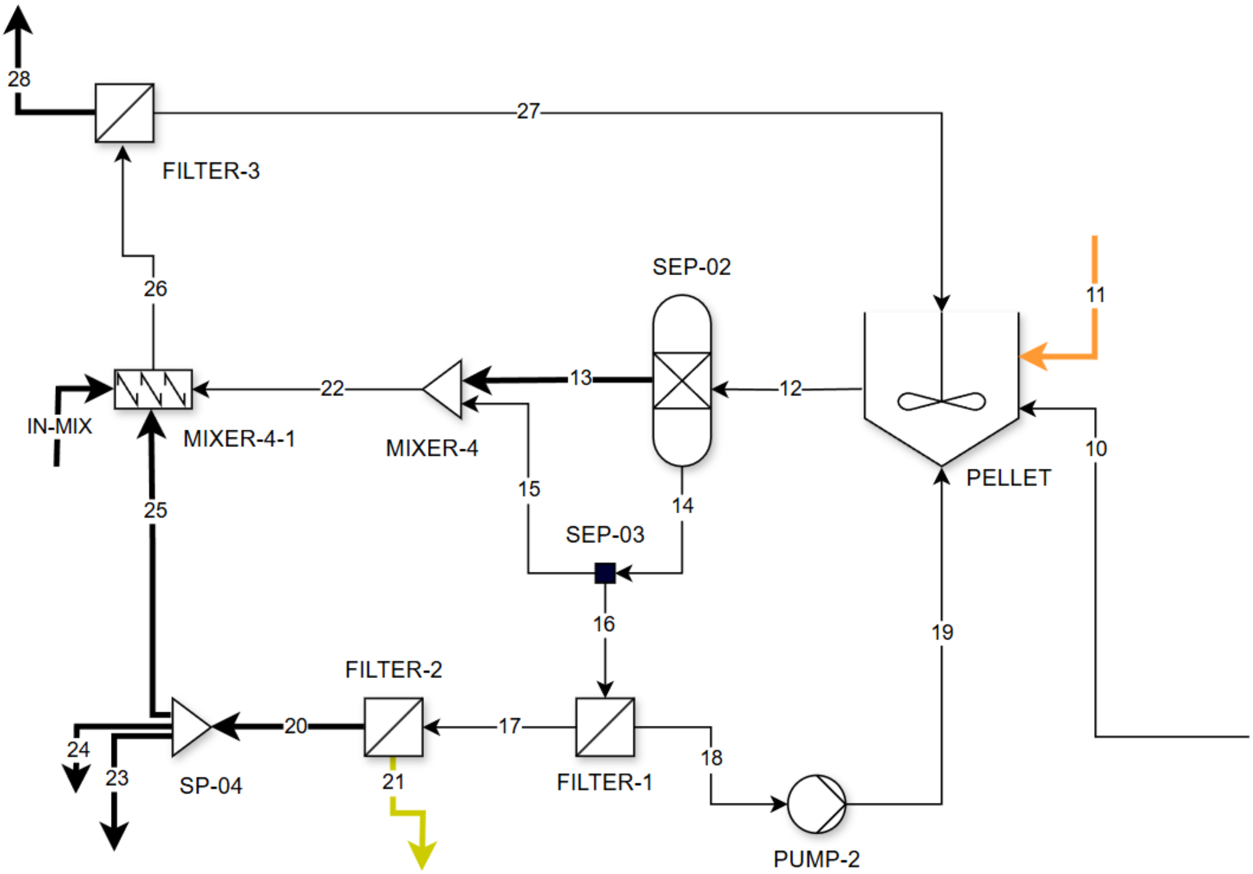

Figure 17 PELLET REACTOR Hierarchy

The resulting solid stream is then divided in a splitter into three different flows:

- Stream 23 which are the fines disposed
- Stream 24 which are the fines directly sent to the calciner
- Stream 25, which is mixed with Stream 22 from MIXER-3 and IN-MIX stream in MIXER-4.

The IN-MIX stream is a make-up of $CaCO_3$ which is required to account for the loss of mass in the system. In particular, this stream contains the amount of calcite lost in the stream 23, the seeds coming from the calciner and the small loss which occurs inside the crystallizer due to unreacted carbonate ions. This last amount of calcite corresponds to the excess of carbonate ions in stream 21. The seeds from the calciner, instead, correspond to the unreacted $CaCO_3$ inside the CALCINER block. As can be seen these are contained in the stream 11-2. The IN-MIX stream is crucial to maintain the plant balanced in mass and so, in the results section, a calculation of the error introduced by this stream will be computed.

The Stream 26 is then sent to FILTER-3, where a complete solid-liquid separation occurs. The liquid is recirculated to the PELLET block via stream 27 while the solid is sent to the WASHER/SLAKER Hierarchy for further processing via stream 28.

2.7.4 WASHER and SLAKER HIERARCHIES

The next Hierarchy is the SLAKER/WASHER one, which in the reference[15] is accounted as a single unit. In our modeling, these correspond to two different Hierarchies; however, the methods used are the same, and since they work synergistically together, they will be treated as one.

Stream 28, coming from the PELLET REACTOR section, is sent to the WASHER, modeled with a SWASH block. The block is also fed with water by stream 29, which comes from another component that will be discussed in the COMPRESSION TRAIN section.

The main purpose of the block is to wash away traces of calcium hydroxide from the calcite pellets. However, this process is not explicitly modeled in the simulation; in fact, stream 28 consists purely of $CaCO_3$. Part of the water exits the Washer via stream 30, while the wet pellet comes out via stream 31.

Stream 31 is then heated up to 300°C to completely remove the water. This is achieved using a HEATER and a FLASH separator block. The references claim that the heater uses the heat from the SLAKER block, which produces a large amount of heat due to the exothermic reaction occurring inside. In our modeling, a different approach is used, as this heater requires a very high amount of heat, which cannot be provided by the SLAKER alone. For this reason, as we will see, this heat will be provided by other streams in the Pinch Analysis.

The reason of this high heat capacity is the high mass flow rate of water mixed with the calcite inside the stream. Instead of simply removing the water physically, the entire stream is heated, and the steam is used to feed the slaking reaction.

Stream 32 passes through the SUMP block (FLASH), which completely separates the solid from the vapor, sending the steam to the SLAKER via stream 33. Stream 34, now pure calcite, is mixed with the stream 24-1, which account for the fines collected by stream 24, and heated up to 674°C before being sent to the CALCINER BLOCK.

The SLAKER block is a fluidized bed reactor, but in our simulation, it is modeled using a simple RSTOIC block. RSTOIC requires only the operating conditions—set to 1 bar and 300°C as a reference—and the reaction with a conversion factor. The main purpose of this block is to hydrate the CaO coming from the CALCINER to produce the calcium hydroxide required by the PELLET REACTOR.

The reaction that takes place is:

$$CaO + H_2O(g) \rightarrow Ca(OH)_2$$

With a conversion factor of 85% taken from[15][11].

The SLAKER is fed with CaO coming from the CALCINER via stream 35 at a temperature of 674°C and with steam via stream 36. The steam is produced in the STEAM CYCLE Hierarchy, which will be discussed in a further section. The product of the SLAKER exits via stream 37 and enters the CYCLONE block, modeled with a SEP block, which recirculates a small amount of calcium oxide into the SLAKER. The purified stream 39, exiting the CYCLONE, is sent to a second SEP block called DUST-COLLECTOR, which separates the remaining calcium oxide from the main stream.

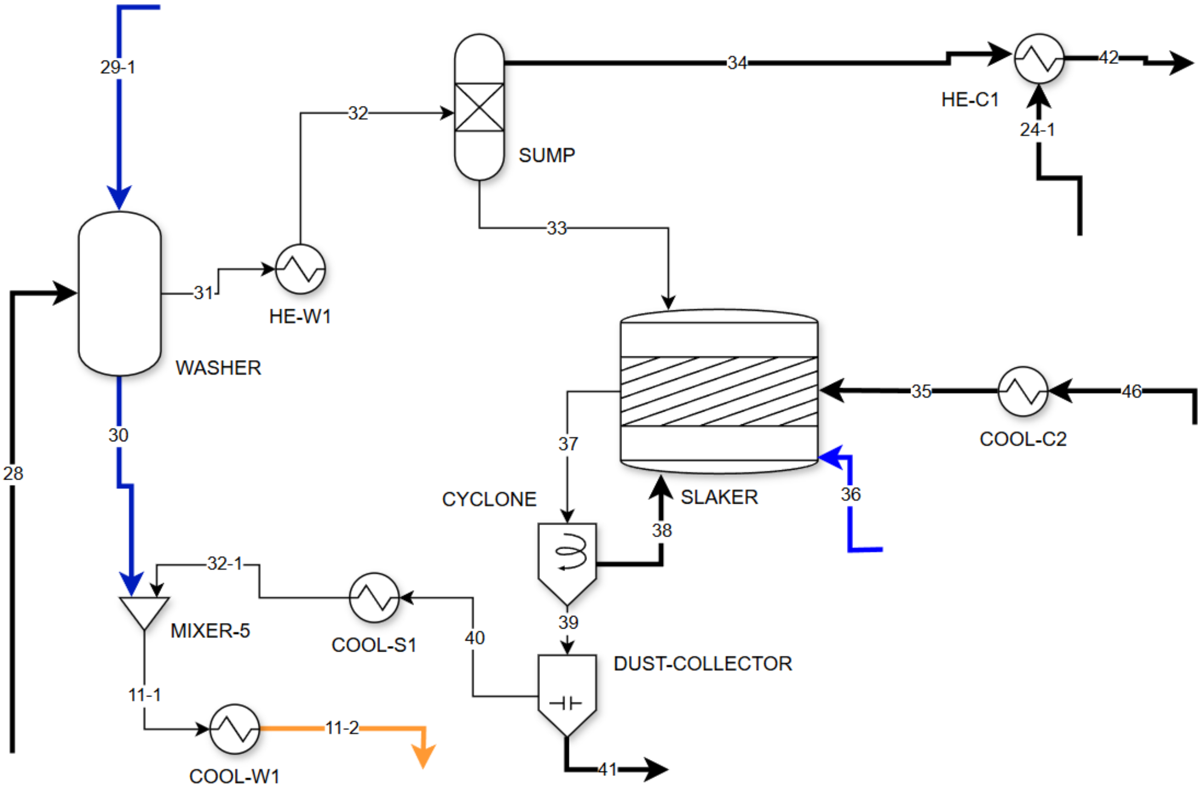

Figure 18 SLAKER/WASHER Hierarchy

Stream 41 is then cooled to 85°C in the COOL-S1 block and sent to MIXER-5 via stream 32-1 where mix with the water from the WASHER. The heat from COOL-S1 will be recovered in the Pinch Analysis.

Stream 11-1, coming out from MIXER-5, is cooled again with the COOL-W1 to match the temperature conditions of stream 11. Since this heat is at a very low temperature and cannot be recovered, part of it can be used to feed the PELLET REACTOR. However, this will be discussed further in the Pinch Analysis section.

2.7.5 CALCINER HIERARCHY

The CALCINER section represents the final stage of the Kraft process, where CO_2 is extracted from Calcite. The stream 42, exiting HE-C1 at 645,88°C, is directed into the CALCINER block. Additionally, the CALCINER receives exhaust gases from the OXYCOMB block, where oxy-combustion occurs to generate the necessary heat.

The CALCINER can be heated either externally or internally, with combustion occurring inside the unit. Even if this last option is the one selected, in fact the exhaust gases are sent to CALCINER from the OXYCOMB, the two components are modelled as two separated for clarity reasons.

The CALCINER is modeled similarly to the SLAKER, using an RSTOIC block under operating conditions of 1 bar and 900°C. Maintaining this temperature is crucial, as the decomposition of $CaCO_3$ into CO_2 and CaO achieves its highest conversion rate at this temperature. The reaction is implemented within the model, with a fixed conversion rate of 98%[11].

$$CaCO_3 \rightarrow CO_2 + CaO$$

The CALCINER is assumed to be adiabatic, meaning no heat losses are considered. Since the reaction is endothermic.

The OXYCOMB block is modeled using an RSTOIC block, under the same operating conditions of the CALCINER. The combustion reactions of methane and ethane are implemented, both with an assumed conversion factor of 100%.

The OXYCOMB is fed with natural gas (NG) through stream 43-NG, with the following mass fractions, taken from Zolfaghari et al.[22]:

- CH_4 = 79.6%
- C_2H_6 = 6.5%
- CO_2 = 7.5%
- N_2 = 6.4%

While oxygen is supplied via stream O2-TOCAL, produced within the ASU, with the following composition:

- O_2 = 96.5%
- N_2 = 3.2%
- CO_2 = 0.263%

In the reference study[15], a design specification is used to determine the NG flow rate required to meet the heat demand. Oxygen, instead, is considered a fixed parameter, taken from Keith et al.[11], set at 58.5 ton/h.

A different approach is adopted in this study, similar to the methodology of Zolfaghari et al. Instead of fixing the oxygen supply, both oxygen and NG flow rates are iteratively adjusted to generate the exact heat requirement for the CALCINER and ensure an almost stoichiometric combustion, minimizing residual oxygen in the exhaust gases.

This adjustment is critical for obtaining a pure CO_2 stream, essential for the next stage of the process.

Oxygen, initially supplied by the ASU at 93°C, is preheated to 652°C, while NG enters at 25°C and 10 bar. The stream 45, leaving the CALCINER, enters the SEP-05 block, where solid-vapor separation occurs. This operates similarly to SEP-01 from the AIR CONTACTOR, utilize a 0/1 logic approach. Stream 46, consisting of CaO and unreacted $CaCO_3$ (the seeds of Calcite), is cooled to 674°C before being sent to the SLAKER. Stream 47 is sent to the COMPRESSION TRAIN section in which it is cooled and further purified.

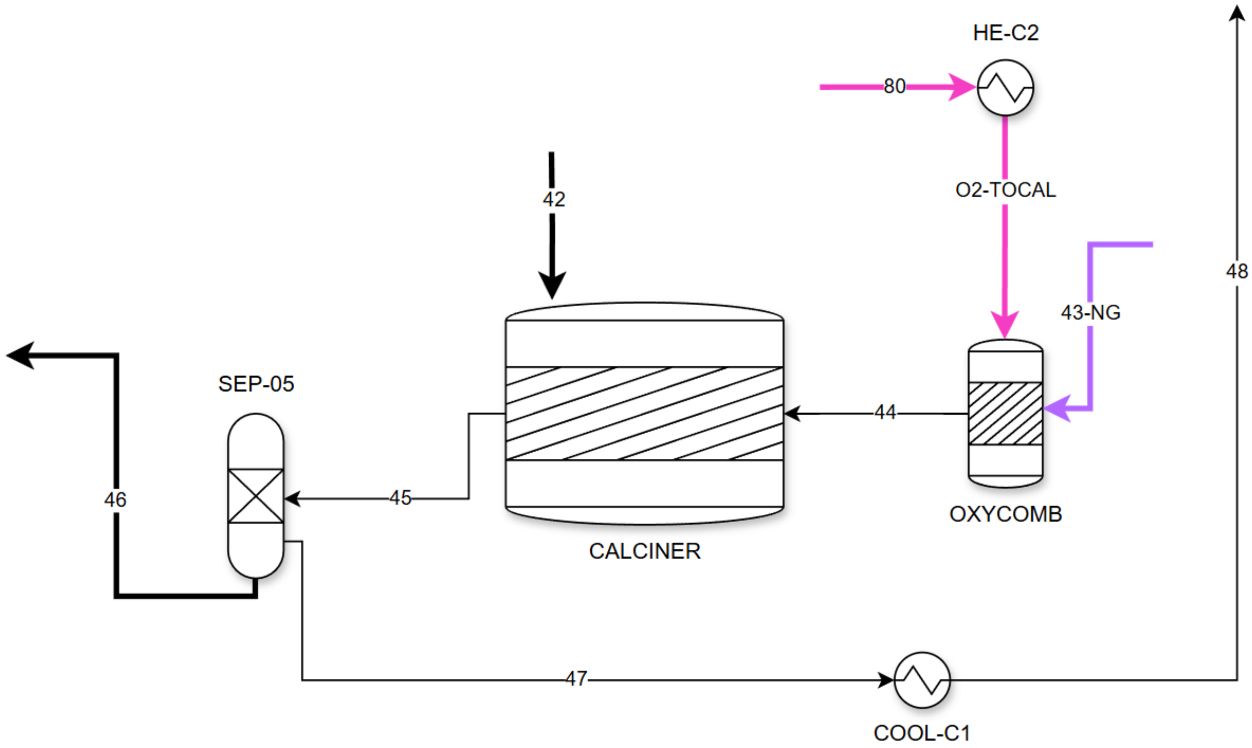

Figure 19 CALCINER Hierarchy

2.7.6 AIR SEPARATION UNIT HIERARCHY

The ASU is responsible for producing the oxygen required by the OXYCOMB. While Bianchi et al. did not model this system, Zolfaghari et al. provided their own version of this section. However, due to some missing datas, it was not possible to reproduce their model and instead it was implemented the ASU plant from Cheng et al.[54] reference while only the first stage of the air compression train was taken from Zolfaghari et al.[22].

The system starts with stream AIR-02, which, like the other air streams, is assumed to be free of argon. It is first sent to PRE-COOL, where it is cooled from 21°C to 9.5°C. The air, then, passes through the first separator, SUMP-A1, modeled using a FLASH SEP block, where an initial portion of moisture is removed.

The air continues its way via stream S3, entering a compression train composed of three pairs of compressors and intercoolers, which bring it to the target pressure of 5 bar as defined in the reference study[54]. The intercoolers in the compression train play a crucial role in reducing the work required by the compressors as the work of the compressors is directly proportional to the inlet temperature, anyway, this will be further detailed in the COMPRESSION TRAIN section. The compressors are modeled as polytropic, with efficiency calculations based on the polytropic ASME method.

The intercoolers INTCO-A1, INTCO-A2, and INTCO-A3 reduce the air temperature to 35°C after each compression stage—except for the last one—which brings the temperature down to 16°C. The cooled air then flows via stream S10 into a second separator, SUMP-A2, modeled using a SEP block, where the final moisture removal occurs.

The ASU operates via a two-stage cryogenic distillation process to separate nitrogen and oxygen with high purity. These two consecutive distillation stages enhance the separation efficiency:

1. The first stage occurs at almost ambient pressure in the Low-Pressure Column (LPC).
2. The second stage takes place at a higher pressure (5 bar) in the High-Pressure Column (HPC).

Since cryogenic temperatures are required to condense oxygen, specialized cooling is applied.

The dry air is then directed to a splitter (SPLI-ASU), where a split fraction of 22.6% is set based on Cheng et al.'s plant data[54]. The air is cooled to -179.3°C through CRYO-1 cooler and fed into the Low-Pressure Column (LPC).

The other fraction exiting SPLI-ASU is also cooled in CRYO-2 cooler and exits at -174.6°C and 5 bar. The stream S18 continue its way and feeds the HPC, entering the column as vapor from the bottom stage.

HPC is divided into 20 stages and modeled using an Equilibrium-based approach. This is chosen over a Rate-based model since no chemical reactions occur inside the column.

At the bottom of the HPC, a stream rich in oxygen exits in liquid phase at -175.73°C and 5 bar. At the top, a stream mainly composed of nitrogen exits as vapor (stream N2-VAP).

This nitrogen-rich stream is first cooled in COND-HPC, where temperature decreases from -179.03°C to -180.20°C, before entering a splitter (SEP-A2), where approximately 65% of the mass flow rate is recirculated back to the LPC top stage.

Both the HPC and LPC are modeled using RADFRAC blocks, without built-in condenser or reboiler. Instead, COND-HPC and REBO-LPC perform these functions. This approach is chosen to allow precise control over the condenser/reboiler outlet temperatures, rather than defining a fixed reflux ratio or duty requirement.

The streams N2-L2 and S20 undergo further cooling to -190.30°C and -180.7°C, respectively. These are then introduced into the LPC, where:

- N2-R enters at stage 1 (top stage)
- O2-R enters at stage 15

The LPC consists of 29 stages and operates at a pressure of 1.35 bar. At the bottom, nearly pure oxygen exits at -182.88°C.

This stream is passed through the reboiler (REBO-HPC), exiting at -181.32°C with a vapor fraction of 73%. It then enters a separator (modeled as a FLASH block), where the liquid and vapor phases are separated.

- The vapor is recycled to stage 29 of the LPC.
- The liquid exits via stream O2-P, which is heated to 93°C in HE-A1 and then sent to OXYCOMB.

At the top of the LPC, the N2-P stream exits and is warmed to 21°C, recovering cryogenic heat.

A design specification is implemented to adjust the mass flow rate of AIR-02, ensuring that the required oxygen production target is met. This oxygen target is iteratively tuned during the OXYCOMB heat balance calculations which are discussed in the CALCINER section.

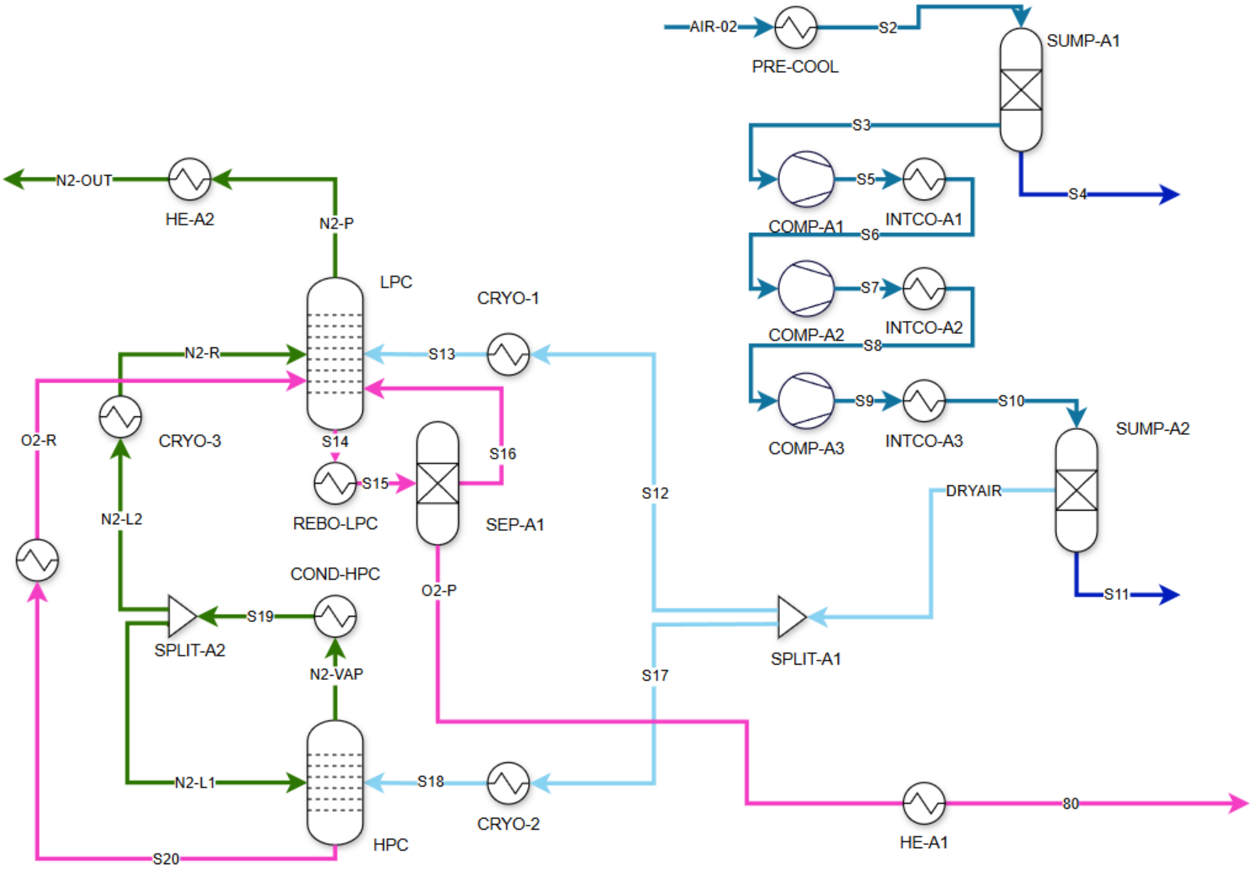

Figure 20 ASU Hierarchy

2.7.7 COMPRESSION TRAIN HIERARCHY

The COMPRESSION TRAIN is the last section traversed by CO_2 before the storage/utilization procedure. In this Hierarchy also the Knockout is accounted, modelled with a SEP block called SEP-04. The block is fed by stream 47 which comes from the calciner which is cooled down to 217 °C and then enters the knockout via stream 48. A mass flow rate of water of 531 ton/h is also provided to the knockout via stream 29. The component simply allows the hot gases to cool down and so removing the steam content which condensates. The temperature inlet in Bianchi et al. model is around 400 °C while in Zolfaghari et al. is 458 °C. It is decided to recover some heat more by reducing the temperature, and so, decreasing the heat rejected by the knockout. The block is set with 0/1 logic to separate the gaseous component from the water. The water is collected and sent to the washer via stream 29-1.

The stream 49, which now is almost pure CO_2, is passed through a series of 4 pairs of compressor intercooler until 150 bars of pressure is reached—which is the typical pressure at which CO_2 is stored.

The compressors are all assumed to be isentropic with an efficiency of 0.85 and a compression ratio of 3.5. Each intercooler between every compression stage brings the temperature back to 45 °C. As previously explained, the work of the compressor is directly proportion to the inlet temperature of the gas. This means that cooling the gas before compression reduces the work required, increasing efficiency. Nonetheless, the heat of the intercooler can eventually be recovered.

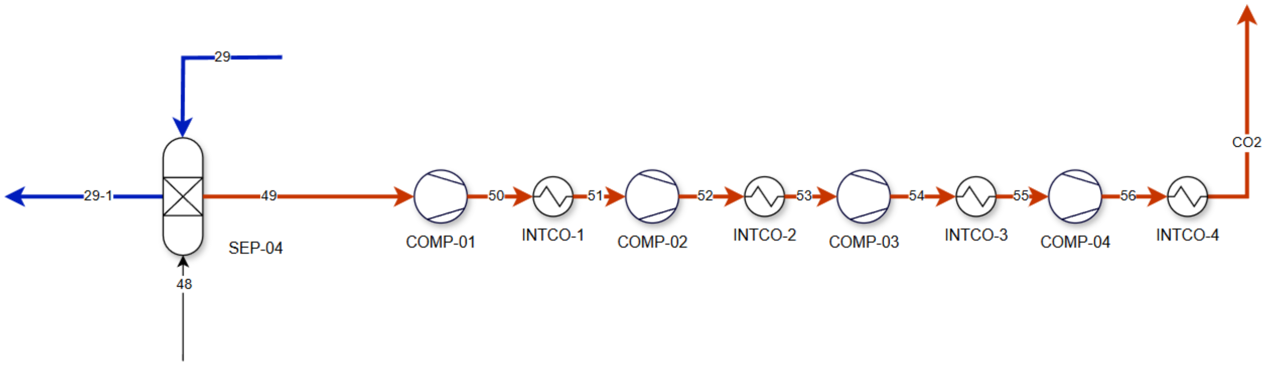

Figure 21 COMPRESSION TRAIN Hierarchy

$$W_{is} = \frac{k}{k-1} R T_{in} \left[\left(\frac{P_{out}}{P_{in}} \right)^{\frac{k-1}{k}} - 1 \right]$$

$$W_{is} \propto T_{in}$$

Where:

$$k = \frac{c_p}{c_v}$$

2.7.8 POWER ISLAND HIERARCHY

To supply the system the same gas cycle of reference[11] is implemented. The first component is a compressor which takes the inlet air and brings it to 10 bars. The inlet air is assumed to be without CO_2 for simplicity, as the biggest part of it is produced during the combustion. Then the compressed air enters GIBBS reactor fed also with 6.3 ton/h of the same NG of the CALCINER. The GIBBS reactor is a component which performs automatically the calculation related to chemistry. The chemical reactions are taken from ASPEN databank, and the equilibrium is calculated by using the operating condition provided by the user inside the block. The temperature of the combustion chamber is set to 1600 °C while the pressure is 10 bars.

Also, a design spec is implemented to control the inlet air, in this way 121 ton/h of mass flow rate for exhaust gas is reached as shown in reference. The gas is sent to a turbine modelled as isentropic which expands the exhaust gases to 1 bar and produces around 32 MW of mechanical power. The exhaust gases which leave the turbine at 892 °C are sent to a series of coolers, modelled by the block HRSG/POSTHRSG, in order to recover the heat and bring the temperature to 26 °C. The cooled gases are sent to the ABSORBER block of the AIR CONTACTOR via stream 1.

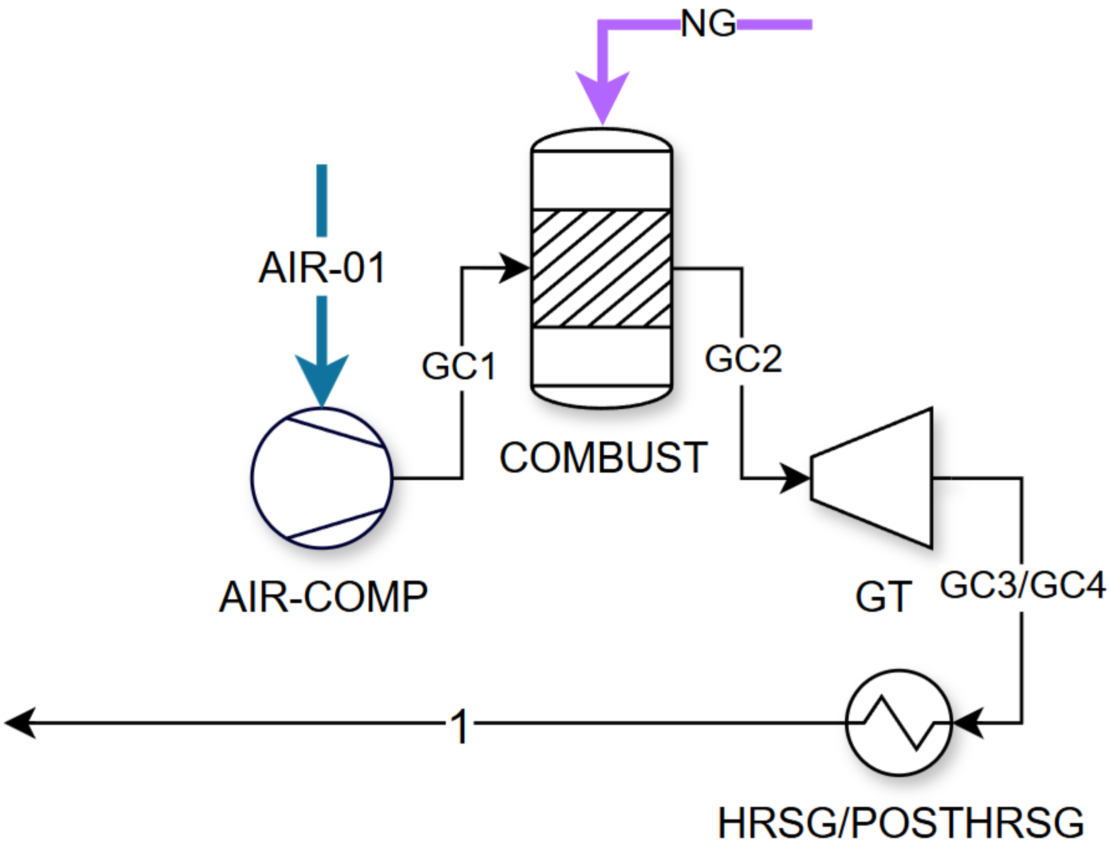

Figure 22 POWER ISLAND Hierarchy

2.7.9 STEAM CYCLE HIERARCHY

The STEAM CYCLE section has two main purposes, the first is to produce the 7 ton/h of steam required by the Slaking reaction, while the second is to recover the high-grade heat rejected by the plant to produce energy with a steam turbine. The cycle is modelled as an open loop to avoid convergence problems, so it is forced SC1-2 to be equal to SC1 in terms of temperature and pressure—because actually are the same stream. The SC1 stream is set to 3.5 bars and 137 °C and it is sent through the PUMP-42B to reach 42 bars. The water passes through a first economizer called ECO reaching 252 °C and the through an evaporator called EVA, in which complete phase transition occurs. After that 7 ton/h of steam are spilled in the SLA-SPLI block and sent to the SLAKER via stream 36-1. The steam is expanded to 1 bar using a valve before entering the SLAKER via stream 36. The remaining part is further heated in the SUPH heater block which brings the steam to 500 °C. The steam is expanded into a steam turbine to 3.5 bars and then cooled to 140 °C in the COND-SC block (condenser). The steam turbine produces 8.84 MW of mechanical power. It isn't possible to expand the steam to 1 bar because liquid under 3.5 bars start arising, giving error in the block— since droplet inside real turbines can damage the blades. Since the expanded steam remains at a higher pressure than the atmospheric one, the condenser is set to cool the stream to a temperature of 140°C, just enough to condensate almost all the steam. The cooled stream SC8 is mixed with a make-up of water which is pumped to 3.5 bars by the PUMP-4B. The two exit the mixer as stream SC1-2. To match the condition of stream SC1 the outlet vapor fraction in the condenser is iteratively adjusted.

The heat provided by ECO, EVA and SUPH come from the heat recovered by other streams as well as other heaters of other sections. The process will be better discussed in the Pinch Analysis

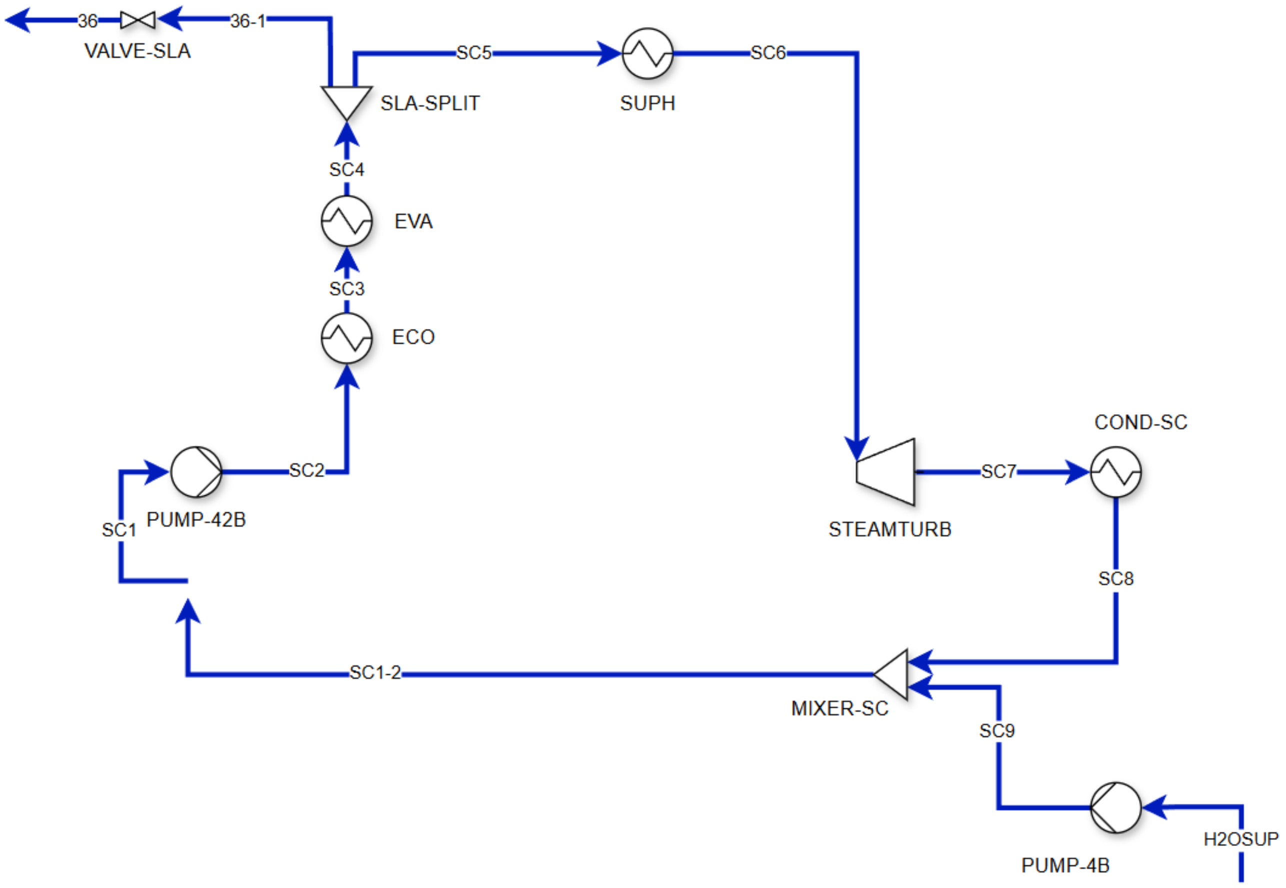

Figure 23 STEAM CYCLE Hierarchy

2.7.10 UTILIZATION FACILITY INTEGRATION

In the next step, a utilization facility is modelled and integrated along with the DAC system. The facility is a methanol production plant, based on a thermocatlytic reaction, in which hydrogen and CO_2 are made reacted togheter in a plug flow reactor.

The hydrogen is provided via electrolysis, implementig a Solid Oxide Electrolyzer. The Utilization Hierarchy incorporates the entire utilization facility. The system is modelled based on two references[28], [55], upscaling the plants proposed to handle the huge amount of CO_2 produced by the DAC. Some assumptions and variations of the original layout are made which will be discussed in this section.

Firstly the ASU component is removed as the oxygen is produced as a consequence of the electrolysis.

A big modification is implemented in the STEAM CYCLE. First of all, as we will see during the Pinch analysis of the new plant, the heat to be rejected drastically increases with the utilization facility. This because the high operating temperature of the SOEC, the compression process of recirculated gases and hydrogen, and the exothermicity of the reaction of methanol. The higher amounts of heat is used to feed the steam cycle to produce electricity. This time, due to the increasing complexity of the HEN, the HRSG is separated from the POSTHRSG cooler and used to feed directly the steam cycle. In this way the HRSG stream is fixed making the HEN design more suitable. To do this a splitter is added in the steam cycle spilling a certain amount of mass flow rate. The stream spilled is heated in the HRSG (cold side) modelled simply with a heater. To extract the right amount of water to be sent to the HRSG a design spec is used. Firstly the HRSG(hot side) available heat is calculated by cooling the flue gases of the POWER ISLAND to 147 °C. As the water after compression in PUMP-42B is at a temperature slightly less than 137°C this guarantee that the minimum temerature difference is maintened. The design spec varies the splitted fraction until the heat required in the HRSG (cold side) is equal to the one rejected by the HRSG (hot side). The spilled water is then sent to the same steam turbine in which the remaining steam heated by ECO, EVA and SUPH is expanded. Ultimately, the compression ratio of COMP-04 in the COMPRESSION TRAIN section is decreased in order to obtain 75 bars of pressure of the outlet stream. This because the methanol synthesization process work at this pressure condition.

For the modelling, due to the higher pressure involved, PENG-ROBINSON method is implemented. The facility can be divided into two main sections. In the first section hydrogen is produced via electrolysis and the oxygen produced as by-products is collected to be sent to the CALCINER Hierarchy. The second part of the facility, instead, is where the methanol is synthesized and distilled.

Figure 24 Scheme of the DAC plant coupled with the Utilization Facility modelled

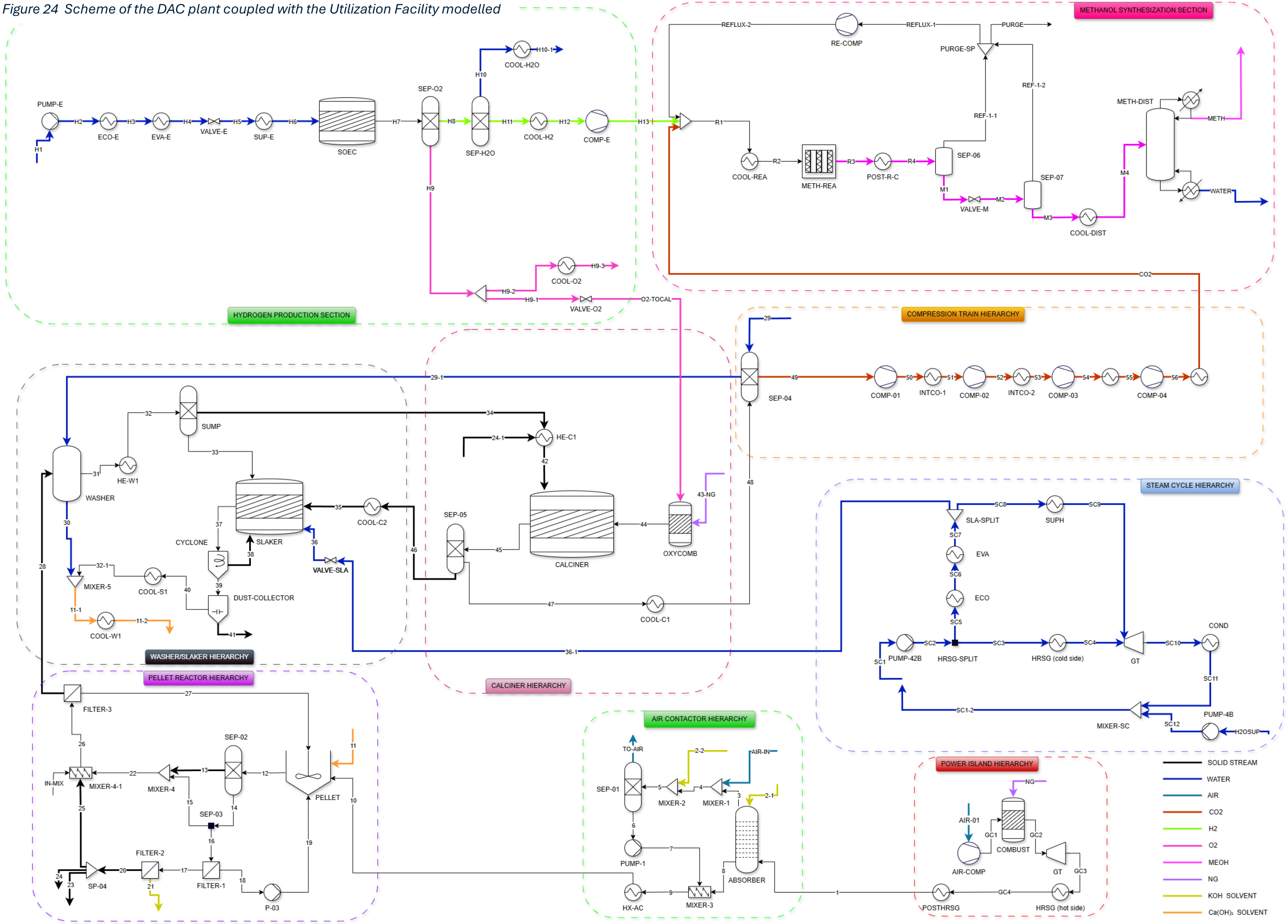

2.7.11 HYDROGEN PRODUCTION SECTION

It all starts with the PUMP-E block in which a mass flow rate of water is brought to 18 bars of pressure. The pump works with a mechanical efficiency of 0.8 as the other pumps of the system. The water is then heated up passing through two heaters, ECO-E and EVA-E, until the phase transition occurs. The steam is expanded to 15 bars of pressure, thanks to a valve, to reach the operating pressure condition of the Solid Oxide Electrolyzer (SOEC). After the expansion the steam is further heated up to 700°C. Generally, SOEC doesn't work under pressure but can benefit from it. Accounting also that the produced hydrogen will require compression, the increasing pressure of the water can be useful to reduce required work further in the plant[28]. The higher sovra-pressure imposed on the first two heaters is kept from the original layout of one of the references[28]as this is beneficial for the thermal integration. Increasing the pressure, phase transition occurs at a slightly higher temperature allowing the moving of part of the heat from the SUPH to the two heaters. As they work at lower temperature their coupling with hot streams is easier. This procedure causes a loss of 3 °C during the expansion and a slightly higher work required by the PUMP-E which can be considered negligible.

The SOEC, which is assumed to work at thermoneutral point, is modelled with a simple RSTOIC block. This doesn't allow to model the complex electrochemistry which occurs inside the cell but for our purpose the simplification is enough. Modelling a complex electrochemical system inside Aspen, in fact, can result in a very complicated task as no built-in blocks can be used. Actually, in the V14 of Aspen, a block to model PEM cells has been released. Anyway, this block is not suitable for the modelling of an SOEC which works at very different operating conditions compared to the PEM. The choice of the SOEC is due to the high electrical conversion achievable, which is between 80% and 90%, as a huge amount of hydrogen is required. As we will see, the SOEC is the component which consumes the most electricity inside the entire plant. Secondly, the high operating temperature of the SOEC can be exploited, recovering the heat of the output streams, increasing the capacity of the STEAM CYCLE.

The RSTOIC block is set to 15 bars and 700°C and the splitting of water reaction is provided with a conversion factor of 80%.

$$H_2O \rightarrow H_2 + \frac{1}{2}O_2$$

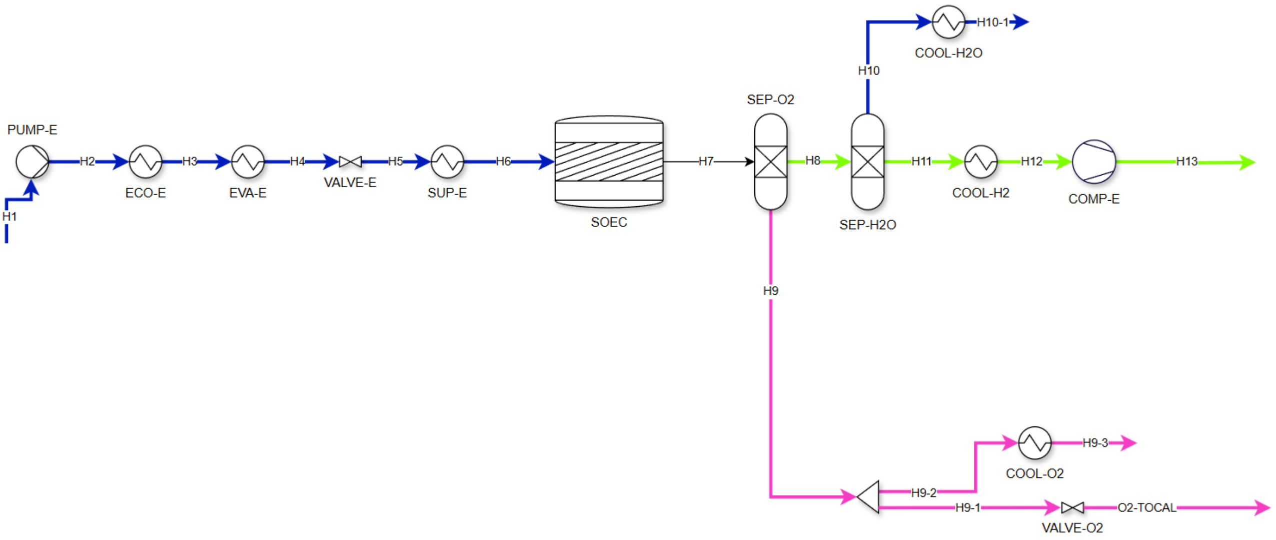

Figure 25 Hydrogen production section of the UTILIZATION Hierarchy

When the SOEC work at thermoneutral point, the heat required by the cell corresponds to the amount of the electrical power. The heat calculated by Aspen for the block is the difference between the enthalpy of the products and the reactants. So, this heat would be the electrical power required by the cell if the conversion process would occur in an ideal way without the losses. To account Faraidic losses—which occurs when part of the electrical current is wasted in unwanted chemical reactions—and to account overpotential losses, the power is computed in this way:

$$P_{SOEC} = I_{cell} V_{cell}$$

$$I_{cell} = (z\, \dot{n}_{H_2} F)/\eta_{faraidic}$$

$z = 2$ charge number of hydrogen

$\dot{n}_{H_2} = mol/s$ moles flow rate of hydrogen

$F = 96485\ C/mol$ Faraday number

$\eta_{faraidic} = 0{,}9$ Faraidic efficiency

$V_{cell} = 1{,}336\ V$

The voltage is taken from reference of an SOEC working at 700°C and is slightly higher than thermoneutral voltage (1.3 V) to account for real condition operation[56]. A faraidic efficiency is assumed to be equal to 90%.

The outlet stream coming out from the cell is sent into two separators modelled with SEP blocks. These two are fictitious components as hydrogen is produced at the cathode while the oxygen exits at the anode. The oxygen stream is sent to a splitter via stream H9, where the needed amount is separated, expanded and directly sent to the CALCINER via O2-TOCAL stream. The remaining part of the oxygen is brought to 100°C to recover the heat, as well as the stream of water separated. The hydrogen is sent to COOL-H2 block, in which is brought to 100°C, and then is compressed to 75 bars in the COMP-E block. The cooling procedure before the compression stage is done to recover heat, but also to reduce the amount of work required by the compressor and avoid overheating of the hydrogen during compression phase.

2.7.12 METHANOL SYNTHESIZETION SECTION

The hydrogen now compressed at 75 bars is mixed with CO_2 and a recirculated mass flow rate. The mixture passes through COOL-REA block in which is cooled to 270°C and then is sent to the reactor METH-REA. The methanol reactor is modelled using a PFR block which models the behavior of real plug flow reactor. First it is necessary to provide the working temperature and pressure. The temperature can be constant along with the reactor, imposed by the cooling fluid temperature or by the temperatures of inlet reactants. It is also possible to impose the temperature profile of the reactor as a function of the length. The temperature in our case is imposed as constant provided by an external cooling fluid at 270°C while the operating temperature is imposed at 75 bars. These two values are taken from reference[28] and assumed as fixed. Also, the moles flow ratio of CO_2 over the moles flow of hydrogen is taken by the same reference and fixed to 43%, which is the result of the optimization procedure of the study[28]. To achieve that a design specification is implemented which varies the inlet mass of water in Hierarchy (stream H1), to achieve the specified ratio in the stream R1. This design specification is computationally demanding due to the strong nonlinearity. In fact, the amount of CO_2 in the stream R1 is also influenced by the recirculated mass flow rate which contains the unreacted CO_2 which is function also of the hydrogen presence in the stream R1.

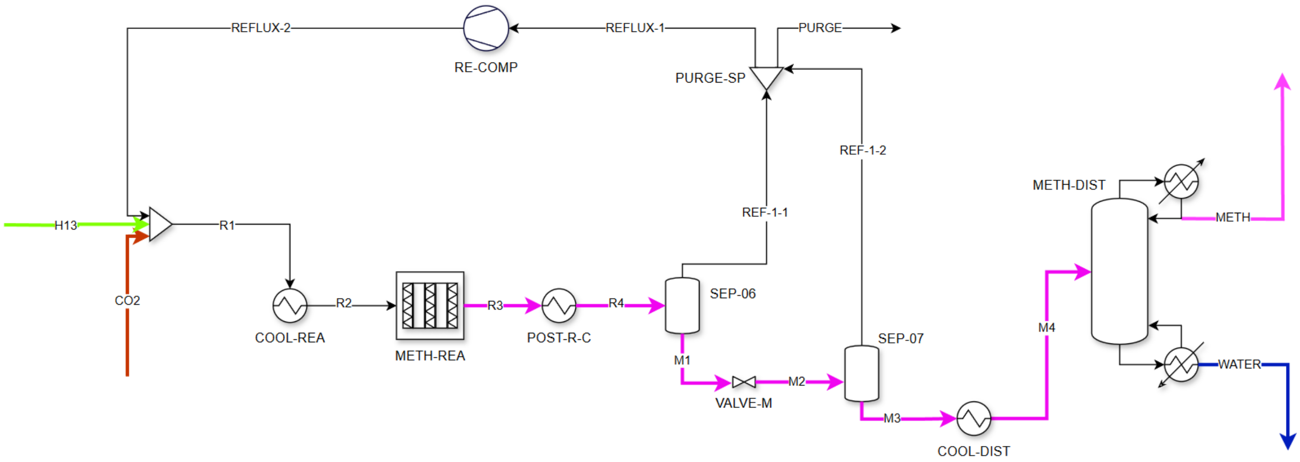

Figure 26 Methanol Synthesization section of the UTILIZATION Hierarchy

The recirculation is required as the reactor have a poor conversion efficiency with only one passage. The others parameter required by the reactor, as well as the design procedure will be explained in the successive dedicated section. The stream R3, which comes out the PFR is cooled in the POST-R-C block and then sent in a separator block modelled with a FLASH block. The gaseous stream REF-1-1, which contains mainly CO and unreacted H_2 and CO_2, is sent to PURGE-SP block, while the liquid is expanded to 2.2 bars and then moved to another FLASH block called SEP-07. Here the gaseous stream is also sent to PURGE-SP block while the crude methanol is extracted from the bottom. The PURGE-SP block is a splitter that controls the PURGE stream which is required to make the simulation converge. If all the REF-1-1 and REF1-2 streams were recirculated the mass accumulated would be so much to make the solver fail. The purge split fraction is set to 3% of the inlet mass flow but a proper sensitivity analysis will be provided in the results discussion. The REFLUX-1 stream coming from the splitter is then recompressed to 75 bars and then mixed with the inlet hydrogen and CO_2. The crude methanol coming out from the SEP-07 is cooled again to 25 °C and then is distillated using a RADFRAC block. The RADFRAC used an equilibrium-based mode and is divided in 60 plates. Built-in reboiler and condenser of the block are used. The crude methanol enters exactly at the middle of the column at stage 30 while the almost pure methanol exits from the top after the condenser block, in liquid phase. The separate water, instead, exits from the bottom and could be reused in the SOEC. Further purification process would be required as some traces of other products can be found inside. To make the RADFRAC properly work two guess values equal to 0.1 are used for the reflux ratio and distillate to feed ratio parameters. A design specification built in the block is used to varied iteratively these two parameters in order to obtain a 99.9% recovery of the inlet methanol and a purity of 99.3% of methanol in METH stream.

2.7.13 METHANOL REACTOR DESIGN

Methanol reactor is the most complex part of the entire facility as account for the complexity of the themocatalytic reaction which occurs inside. The reactor is packed with Cu/ZnO/Al_2O_3 industrial catalyst, which is one of the most used. It is implemented an LHHW kinetic model for this catalyst developed firstly by Vanden Bussche and Froment (1996) further adjusted in the work of Mignard et al.[57].

The model assumes that the methanol is mainly produced by the hydrogenation of CO_2 while the CO contributes to the methanol is negligible. For this reason, only the rate of reaction of the hydrogenation of CO_2 and the RWGS are inserted[28]. The rates of reactions are:

$$r_{CH_3OH} = \frac{k_1\left(p_{H_2}p_{CO_2}\right)[1 - \frac{1}{K_{eq1}}\frac{p_{CH_3OH}p_{H_2O}}{p_{CO_2}{p_{H_2}}^3}]}{(1 + k_2\frac{p_{H_2O}}{p_{H_2}} + k_3{p_{H_2}}^{0,5} + k_4p_{H_2O})^3}$$

$$r_{RWGS} = \frac{k_5p_{CO_2}[1 - K_{eq2}\frac{p_{CO}p_{H_2O}}{p_{CO_2}p_{H_2}}]}{1 + k_2\frac{p_{H_2O}}{p_{H_2}} + k_3{p_{H_2}}^{0,5} + k_4p_{H_2O}}$$

Where generical p_j is the partial pressure of j-esim compound and kinetic constants follows the Arrhenius form:

$$k_i = A_i\exp\left(\frac{B_i}{RT}\right)$$

	A		B	
k_1	1.07	$molbar^{-2}s^{-1}Kg_{cat}^{-1}$	36696	$Jmol^{-1}$
k_2	3453.38		$-$	
k_3	0.499	$bar^{-0,5}$	17197	$Jmol^{-1}$
k_4	$6,62\text{E} - 11$	bar^{-1}	124119	$Jmol^{-1}$
k_5	$1,22\text{E} + 10$	$molbar^{-2}s^{-1}Kg_{cat}^{-1}$	-98084	$Jmol^{-1}$

Table 3 Kinetics coefficient for the rate of reaction of Hydrogenation of CO_2 and RWGS[57]

The thermodynamic equilibrium constant, instead, are provided by Graaf et al.[58] with the following formulation:

$$log_{10}K_{eq1} = \frac{3066}{T} - 10.592$$

$$log_{10}\frac{1}{K_{eq2}} = -\frac{2073}{T} - 2029$$

Additionally, from reference[28], catalyst density of 2000 $\frac{Kg}{m^3}$, a particle size of the catalyst of 0.005 m and a bed voidage equal to 0.5 is used for the reactor. The bed voidage indicates the fraction of volume of the reactor which is available for the reactants to flow, not filled by the catalyst.

To upscale the reactor dimensions several considerations are made. Firstly, the diameter of the single tube is kept fixed equal to 0.085 m. Then from the values provided by the reference it is estimated the theoretical residence time.

The reference provides the mass flow rate of CO_2 which enters the reactor equal to 2.75 ton/h. The amount of hydrogen is estimated using the ratio of moles of hydrogen over the moles of CO_2.

$$\dot{n}_{H_2} = \dot{n}_{CO_2} * 0.43$$

The inlet mass flow rate in the reference reactor is assumed as the sum of the one of CO_2 and hydrogen computed. The mass flow is then converted to volume flow rate using the density of each component at 270°C and 75 bars. From the volume of the reactor and the inlet volume flow rate the residence time is estimated in this way:

$$t_{res} = \frac{V_{rea}}{\dot{v}_{inlet}} bedvoidage$$

This procedure overestimates slightly the residence time as part of the recirculated mixture is not accounted. In particular the CO produced.

	mass flow rate [Kg/s]	MM[g/mol]	mole flow rate [mol/s]	density at 75 bar and 270°C [kg/m^3]	volume flow rate[m^3/s]
CH3OH produced	0.35	32.04	10.92	-	-
CO2 inlet	0.76	44.01	6.01	73.09	1.05E-02
H2 inlet	0.03	2.02	13.97	3.35	8.41E-03
mixture inlet	-	-	-	-	1.89E-02

Table 4 Parameters for the evaluation of the residence time in methanol reactor of reference[28]

tubes diameter [m]	0.085
reactor lenght [m]	1.50
number of tube	30.00
available volume [m^3]	0.13
residence time theoretical [s]	6.77

Table 5 Reference methanol's reactor characteristics[28]

The dimension of our reactor is iteratively increased in order to have a very close guess value of the inlet volume flow rate from the simulation, as this parameter is a function of the volume of the reactor itself being recirculated. At some point the volume flow rate started to settle and a guess value of 11.71 m^3/s is taken. This volume flow rate is roughly 620 times the one of the reference. The first guess value of the volume of the reactor is obtained multiplying the value for the volume of the reference reactor for 620. The volume is further increased to obtain an increase in the methanol produced.

Maintaining the same proportion, which have roughly the length 3 times the diameter, would lead to a length of our reactor equal to 14.86 m. As the pressure drop is mainly related to the length, it is decided to maintain this volume having diameter and length almost equal. This represents a critical condition as a PFR with a diameter bigger than the length could be impractical in the real world. In fact, with this proportion, the heat removal procedure would become tricky, having a small area to transfer heat. Also, the flow distribution could become uneven and proper manifold before the reactor would be required. This configuration guarantees a pressure drop of 0.24 bars calculated with the Ergun equation method.

The reactor is obtained using the following formula:

$$V_{rea} = A_{rea} * L_{rea} = \frac{{D_{rea}}^3}{4}\pi$$

$$n_{tubes} = \frac{D_{rea}}{D_{tube}}$$

Tubes diameter [m]	0.085
Reactor lenght [m]	6.82
Number of tube	6434
Reactor diameter[m]	6.82

Table 6 Evaluated parameters of methanol's reactor used

2.8 PINCH ANALYSIS OVERVIEW AND PLANT THERMAL INTEGRATION

Pinch Analysis is a systematic approach to optimize energy efficiency in industrial processes, by integrating heat recovery systems. The methodology follows several key stages, ensuring that energy consumption is minimized while maximizing the recovery of waste heat.

The first step in performing Pinch Analysis involves gathering detailed thermal data on all process streams that require heating or cooling. This includes determining the mass flow rates, inlet and outlet temperatures, and effective specific heat capacities of each stream. Eventually, effective specific heat capacity and mass flow rate can be incorporated for simplicity in only one parameter, which is the product of them.

Once the thermal data is obtained, composite curve (CC) and grand composite curve (GCC) are constructed to represent the cumulative energy demand of cold streams and the cumulative energy availability of hot streams as functions of temperature. These composite curves visually depict the potential for heat recovery within the system. By analyzing the overlap between these curves, it is possible to identify the pinch point, which is the temperature at which the minimum temperature difference occurs between the hot and cold streams. The pinch point serves as a thermodynamic boundary, dividing the system into two distinct regions: above the pinch, where there is a deficit of heat requiring external heating, and below the pinch, where there is an excess of heat that needs to be removed. The minimum temperature difference can be chosen arbitrary, affecting the pinch point position and the maximum amount of heat recoverable. Low values of minimum temperature difference allows to recover more heat but as drawback heat exchanger area increases.

Minimum temperature difference can't obviously go under 0°C, as this would violate the second law of thermodynamics and common values range from 10 to 20 °C for high temperature system.

Following the identification of the pinch point, the minimum energy targets for the process are determined. This includes establishing the minimum required external heating and the minimum required external cooling. These energy targets represent the theoretical limits of energy consumption that can be achieved through optimal heat integration. These values are shown by the CC curve and correspond to the difference between the cold curve and hot curve on the x-axis. Specifically, the difference in the region below pinch point is the heat to be rejected while the difference over the pinch point is the heat to be supplied. With energy targets defined, the next step is the design of the HEN to achieve the desired heat recovery while minimizing the use of external utilities. The hot streams are coupled with cold streams until no more coupling is possible.

To maximize the performance of HEN general rules have to be satisfied:

- no heat should be transferred across the pinch point, as this would increase overall energy consumption
- Above the pinch point only heaters are acceptable, while all the hot streams must be completely satisfied by the cold streams
- Below the pinch point only coolers are acceptable, while all the cold streams must be completely satisfied by the hot streams

Additionally, a good approach is to couple streams which share similar heat capacity and delta temperatures close as possible to minimum temperatures difference. Also, starting to couple the streams from the pinch point generally allows better results in terms of network efficiency.

The synthesis of the HEN involves determining the optimal configuration of heat exchangers, heaters, and coolers to ensure efficient thermal integration. Various heuristics and optimization techniques can be applied to refine the network, example erasing of close loop inside the network and external heater/cooler can be used instead the peripheral heat exchangers of the network, which generally transfer low amount of heat [59], [60].

Our thermal integration is done using Aspen Energy Analyzer software, also developed by AspenTech. The software requires all the hot and cold streams, as input data, with their inlet and outlet temperature. It also requires a minimum temperature difference, which is chosen equal to 10 °C, and the effective heat capacity of each stream. It is also possible to give to the software the heat capacity with the mass flow rate and specific heat capacity separated.

The software automatically plots the CC and the GCC calculating the amount of heat required and the heat which have to be rejected. To account for that it is required to choose some utility streams which will be used as external sources.

Our thermal integration requires a slightly different approach from classic pinch analysis. First, many streams are involved, creating a very complex system. Secondly, the STEAM CYCLE Hierarchy is built starting from thermal integration. In this way the mass flow rate flowing in the cycle is a design parameter, which is varied to reach the configuration desired for the plant and use all the available usable heat.

The first procedure consists in analyzing all the heater/cooler blocks inside Aspen plus simulation and collecting the required data for the analysis. Only the ECO, EVA and SUPH blocks are inserted into Aspen Energy Analyzer calculating the effective cp while for the other Mcp parameter is used. It’s increased the amount of mass flow rate in the ECO, EVA and SUPH blocks until a further increase would have required the introduction of an external heat source. It is also paid attention to have the mass flow rate of SUPH with 7 ton/h less, due to the spilled for the SLAKER.

Similarly to what is done for the previous layout, a pinch analysis strategy is implemented for the new plant with the utilization section. Also, in this case no external heat is required and no pinch point is calculated by the software. The complexity of this configuration is much higher than the previous, so the modification of the STEAM CYCLE is implemented, as previously discussed, and the HEN is kept as simple as possible avoiding the splitting of the streams.

2.9 ENERGY ANALYSIS AND VALIDATION

For the Energy analysis of the systems all the electrical consumption and production are collected. Conversion efficiency from mechanical to electrical energy are assumed equal to 95%. Other component consumption not specifically modelled inside the simulation or which can't be used, are taken from Keith et al.[11] and eventually adjusted based on our consumptions. Specifically, The SLAKER, CALCINER, PELLET REACTOR, MIXERS and auxiliary components electrical requirements are added. Auxiliary component 's electrical consumption are added to address the consumption due to recirculation of cooling fluid. The consumption of the ASU is also added by taking the value from reference and linearly adjusting it based on the consumption, dividing our mass flow rate of oxygen by the one reported and multiplying it for the energy used. This procedure is done because a thermal integration problem in the ASU is detected. This will be further discussed in the results Chapter. Also, the amount of NG required by the system is collected and the energy content is estimated using the LHV equal to 43.054 Mj/kg

The reference provides a consumption of 8.81 GJ/ton-CO_2 thermally supplied or 5.26 Gj thermally and 366 KWh electrically supplied per ton-CO_2.

As no external heat is required by the plant after the thermal integration, the net electricity consumption is computed and converted into primary energy. To do that, the conversion efficiency from thermal to electrical energy is calculated using the consumption data of the reference as follows:

$$\eta = \frac{\left(\frac{366\ KWh}{0{,}277\frac{KWh}{MJ}}\right)}{8810\ Mj - 5260\ Mj} = 37\%$$

A similar value is obtained for our combined cycle, dividing the total electricity produced by the thermal energy provided by the mass flow rate of NG of the POWER ISLAND (39%).

$$\eta_{COMB-CYCLER} = \frac{P_{el,TOT,PROD}}{\dot{m}_{NG-PI} * LHV_{NG}} = 39\%$$

Another parameter calculated is the Avoided CO_2. This is the actual amount of carbon dioxide removed by the atmosphere and corresponds to the actual amount captured by the Air contactor. To compute this value, to the CO_2 available after COMPRESSION TRAIN is subtracted the CO_2 produced in the POWER ISLAND and OXYCOMB.

$$\mathrm{CO}_{2AVOIDED} = \mathrm{CO}_{2CAPTURED} - \mathrm{CO}_{2PRODUCED}$$

2.10 SENSITIVITY ANALYSIS PARAMETERS AND KPI EVALUATION

To evaluate the performance of the Utilization facility and overall plant, several parameters are adopted:

- The CO_2 conversion: a parameter calculated as the percentage of moles of CO_2 which are converted in some product.

$$CONV_{CO_2}[\%] = (1 - \frac{\dot{n}_{CO_2,OUT}}{\dot{n}_{CO_2,\mathrm{IN}}}) * 100$$

- The Selectivity toward methanol: which corresponds to the percentage of CO_2 which generates methanol, only considering the CO_2 which has reacted.

$$S_{CH_3OH}[\%] = (\frac{\dot{n}_{CH_3OH,OUT}}{\dot{n}_{CO_2,IN} - \dot{n}_{CO_2,\mathrm{OUT}}}) * 100$$

- The Yield of methanol: which is the total methanol produced over the moles of CO_2 at the inlet of the plant. This parameter actually corresponds to the product of the first two.

$$Y_{CH_3OH}[\%] = CONV_{CO_2}[\%] * S_{CH_3OH}[\%] = \frac{\dot{n}_{CH_3OH,OUT}}{\dot{n}_{CO_2,IN}} * 100$$

- The electrical efficiency of the utilization facility: which is the ratio of the chemical power produced, computed by multiplying the mass flow rate of methanol with its LHV, and the total electrical consumption of the facility, including the ones to produce the hydrogen.

$$EC[\%] = \frac{\dot{m}_{CH_3OH,OUT} * LHV_{CH_3OH}}{P_{el,UTIL-FAC}} * 100$$

These parameter are particularly usefull for the sensitivity analysis of the Methanol Reactor as it is possible to evaluate directly the performance of it analyzing the change in this parameters when certain variables—such as the reactor's volume or the PURGE stream mass flow rate—are varied.

Additionally, three Key performance indexes (KPIs) are evaluated, accounting the energy efficiencies of portion of the plant. In this way, it is possible to understand how energy efficiency decreases as more blocks are added.

First of all, the efficiency of the methanol section—which only accounts for the reactor and the distillation process—is calculated, assuming as input the hydrogen already compressed and the electricity required in this section. The output energy is instead calculated as the chemical power stored inside the methanol produced, obtained by multiplying the mass flow rate of methanol with its LHV.

$$\eta_{METHANOL-SECTION}[\%] = \frac{\dot{m}_{CH_3OH,PROD} * LHV_{CH_3OH}}{\dot{m}_{H_2,REQ} * LHV_{H_2} + P_{el,METH-SEC}} * 100$$

Then, the overall efficiency of the utilization facility is calculated in the same way. This time, as inlet power, is assumed the overall consumption of the facility, including the one of the SOEC. This parameter is slightly less than the already mentioned electrical efficiency. In fact, for the evaluation of this parameter is used the amount of methanol produced—the one contained in METH stream—while for the electricity conversion parameter is considered all the methanol generated by the reactor.

$$\eta_{UTILIZATION-FACILITY}[\%] = \frac{\dot{m}_{CH_3OH,PROD} * LHV_{CH_3OH}}{P_{el,UTIL-FAC}} * 100$$

Last KPI, the most important one, is the overall efficiency of the plant, accounting both the DAC and the utilization facility. The energy input is calculated as the sum of all the electrical contribution and the energy supplied by the NG without any conversion.

$$\eta_{OVERALL-PLANT}[\%] = \frac{\dot{m}_{CH_3OH,PROD} * LHV_{CH_3OH}}{(\dot{m}_{NG-TOT} * LHV_{NG}) + P_{el,TOT}} * 100$$

Also, the methanol Yield is re-calculated, this time using only the methanol available in stream METH. This parameter is called effective Yield.

$$Y_{CH_3OH,EFFECTIVE}[\%] = \frac{\dot{n}_{CH_3OH,PROD}}{\dot{n}_{CO_2,IN}} * 100$$

3 RESULTS

3.1 DAC PLANT

In this section the main differences and analogies of our plant with the references are shown and discussed. In particular the aspects related to heat consumed and provided by component such as the CALCINER and the SLAKER. Also, variations related to minor’s component, stream mass flow rate and composition are analyzed.

3.1.1 AIR CONTACTOR

The reference[15] states that the mixture which enters heat exchanger (HX-AC) of the Hierarchy is heated. However, based on the original plant design of Keith et al.'s work [11], it is evident that the component following the air contactor component is a cooler, even if the temperatures are not specified. Additionally, the temperature of the spent solvent exiting the absorber (31°C) of Keith et al. is comparable to that of stream 8 (31.86°C) of our plant, whereas in Bianchi et al.'s model [15], it is reported as 55°C.

This is not the only difference between our model and the references. In fact, the solvent required in our model is approximately 1.5 times higher than in Bianchi et al.'s model. When, instead, we compare the total solvent mass flow rate to Keith et al.'s work, it is about 0.15 times. Bianchi et al. explain that in the original model, some solvent storage basins are used, likely accounting for the significantly lower solvent requirement. Anyway, a higher solvent required does not significantly affect the model, resulting only in a higher amount of water and slightly higher values of the ions of the non-reacted solvent in stream 10.

3.1.2 PELLET REACTOR

Compared to the reference[15], a bigger mass flow rate in the recirculation streams (stream 19 and stream 27) is detected. This is due by the higher amount of solvent required in the AIR CONTACTOR Hierarchy. This difference, anyway, doesn’t affecte the further Hierarchies, as the the output streams are comparable with the reference work, in terms of mass flow rate and mass fraction.

Also, a slight difference in composition and mass flow rate of the stream 11-2 and 11 is noticeable. These streams actually are the same one but are modelled separately for the reasons explained in Chapter 2.

These differences are mainly due to the inefficiency of the slaker reactor; in fact, a portion of the CaO cannot be converted into calcium hydroxide.

Due to the variation apported to the stream 23 and 24, explained in previosly in the Chapter 2, some differences can be found an will be analyzed. For many components it will be provided the results for both the configurations, with and without the modification of these two streams.

The PELLET block, due to the endothermicity of the reaction, requires 33.5 MW of heat at 25°C.

3.1.3 WASHER AND SLAKER

The reaction occurring in the SLAKER block is strongly exothermic; in fact, the SLAKER, in the first configuration (stream 23 and 24 maintained as reference[15], [22]), produced roughly 43.7 MW of heat, very close to the 45 MW reported in the reference[15]. After the changes of the streams 23 and 24 in the PELLET REACTOR the heat produced by the SLAKER block increased to 60.46 MW due to the higher amount of reactants involved. Additionally, around 24 ton/h of unreacted CaO is collected by the DUST-COLLECTOR, which is almost the same value reported by Keith et al.[11]. This loss explains the difference between stream 11-2 and stream 11 already explained. To account for this a proper make-up of Calcium oxide would be required.

3.1.4 CALCINER

The CALCINER requires 10.8 ton/h of NG, in Bianchi et al.[15] plant while, instead, in Keith et al. the required NG is 13.4 ton/h. The oxygen is instead fixed at 58 ton/h in both the references.

As previously mentioned, both the values used for NG and oxygen are adjusted to match the requirement of the CALCINER.

The optimized values in the configuration where Calcite disposal is kept as Bianchi et al. resulted in:

- Oxygen flow rate: 39.4 ton/h
- NG flow rate: 10.9 ton/h
- Heat produced: 118.232 MW

With heat output slightly higher than required for the CALCINER, and the residual oxygen in stream 44 minimal equal to 1.5% in mass fraction.

After the changes of the Calcite disposal (stream 23 and 24), instead, the following values are obtained:

- Oxygen flow rate: 54.6 ton/h
- NG flow rate: 15.0 ton/h
- Heat produced: 162.90 MW

With even lower oxygen traces in the output stream 44, around 0.4% in mass fraction.

The CALCINER block requires, in the final configuration, 162.88 MW of heat.

The first case, in which disposed fines of calcite are higher, gives results comparable to the ones obtained by the two references[15], [22]. The second case, instead, gives values much more similar to Keith et al.[11]. In this last case some differences are noticeable. In particular, NG mass flow rate is slightly higher while oxygen mass flow rate is smaller. This is mainly due to the fact that we used NG instead of pure methane. Being the LHV of methane bigger than NG, to achieve the same thermal energy output a smaller value is requested. The reference[11], also, probably accounted incomplete combustion phenomena by providing an amount of oxygen slightly higher than the stoichiometric one, which explains this difference.

From now on, only the case with corrected stream 23 and stream 24 will be discussed.

3.1.5 ASU

As already mentioned, the current ASU configuration is unable to fully recover cryogenic heat while maintaining a $\Delta T_{min} = 10°C$. This results in an unrecovered cryogenic heat load of 6.5 MW, which must be externally supplied. With a typical cryogenic cycle COP of 0.1, this translates to an electricity consumption of 65 MW, excluding auxiliary system power. This energy demand is unreasonably high, making the plant unviable. Consequently, for the final energy analysis, the energy consumption values are adopted from Keith et al. reproportioning the consumption linearly based on our values of oxygen required.

Since the ASU integration is not a primary objective of this study, this design is kept to provide a general overview on how cryogenic air separation unit works.

The main reason for the heat recovery limitation is the close temperature approach of the hot and cold streams, preventing effective thermal coupling. Specifically:

- The HPC condenser and LPC reboiler could not be thermally integrated, which is a common heat recovery strategy in most ASUs.
- Pressurized streams cooling is usually partially achieved by expanding them to LPC pressure, reducing the cryogenic heat demand and enhancing thermal integration between feed streams and product streams.

3.1.6 POWER ISLAND AND STEAM CYCLE

For instance, the mechanical power produced by gas and steam turbines are reported in this paragraph. Gas one produces 32 MW of mechanical power while the STEAMTURB produces 8.84 MW. No other results related to POWER ISLAND are discussed here as it remains very similar to the references[15], [22]. The STEAM CYCLE is instead discussed in a more detailed way in the pinch analysis. Anyway, this last Hierarchy can't be compared directly to the references as a different design Is used.

3.1.7 UTILIZATION INTEGRATION IMPACT

The facility integration, as previously said, change the plant structure and some variations can be detected in the main Hierarchies. First of all, the ASU component became useless as oxygen is produced, as consequence, during the electrolysis. The amount of oxygen produced is much larger than the one required so no other external contribution is required. The oxygen produced by the SOEC is 100% pure, which impact the CO2 stream purity and others aspects. In details, it's possible to note that no changes in the AIR CONTACTOR and PELLET REACTOR Hierarchies are detected. This because the open loop approach is used, which allow to maintain fixed the composition of the solvent streams. Almost negligible variation are present in the WASHER/SLAKER Hierarchy and a small variation can be detected in the CALCINER Hierarchy. In the CALCINER, the mass flow rate of oxygen is slightly less than the base case, as no nitrogen and CO_2 are present inside the stream. Aditionally, the oxygen stream, which come out from the SOEC, is directly sent to the CALCINER without any cooling procedure. The temperature of the feeding oxygen is the same of the working temperature of the SOEC, equal to 700°C. These two changes increase the heat generated inside the OXYCOMB which became roughly 1 MW higher than the one required by the CALCINER. It is decided to maintain the same amount of NG as the difference is relatively small. Anyway, a possible decreasing of the NG required by the CALCINER would be possible. Small variation of CO_2 available is noticeble, in fact as no CO_2 is cointaned in the oxygen stream, less CO_2 comes out the calciner. As we will see this variation is very small. A variation of roghly 2 ton/h in the CO2 output stream is instead present, in fact, even if almost no variation is present in the CO_2 available the nitrogen content is reduced a lot thanks the removal of ASU. This lead to slighlty less mass flow rate and higher purity of the CO2 stream. This is particularly beneficial as the gases in the CO2 stream are very difficult to be removed and can affect negativly the purity of methanol produced.

3.2 METHANOL SENSITIVITY ANALYSIS

This section provide a sensitivity analysis of the parameters introduced to evaluate the performance of the methanol reactor. In particular, variation of the Yield of methanol, CO_2 conversion, selectivity toward methanol and mass flow rate of methanol are analyzed in different scenarios, comparing them to variation of the volume of the reactor or variation of the percentage of mass purged in the methanol synthesization section.

The first graph shows the total amount of methanol produced as function of the volume flow rate. This graph is usefull to understand the previosly discussed design of methanol reactor.

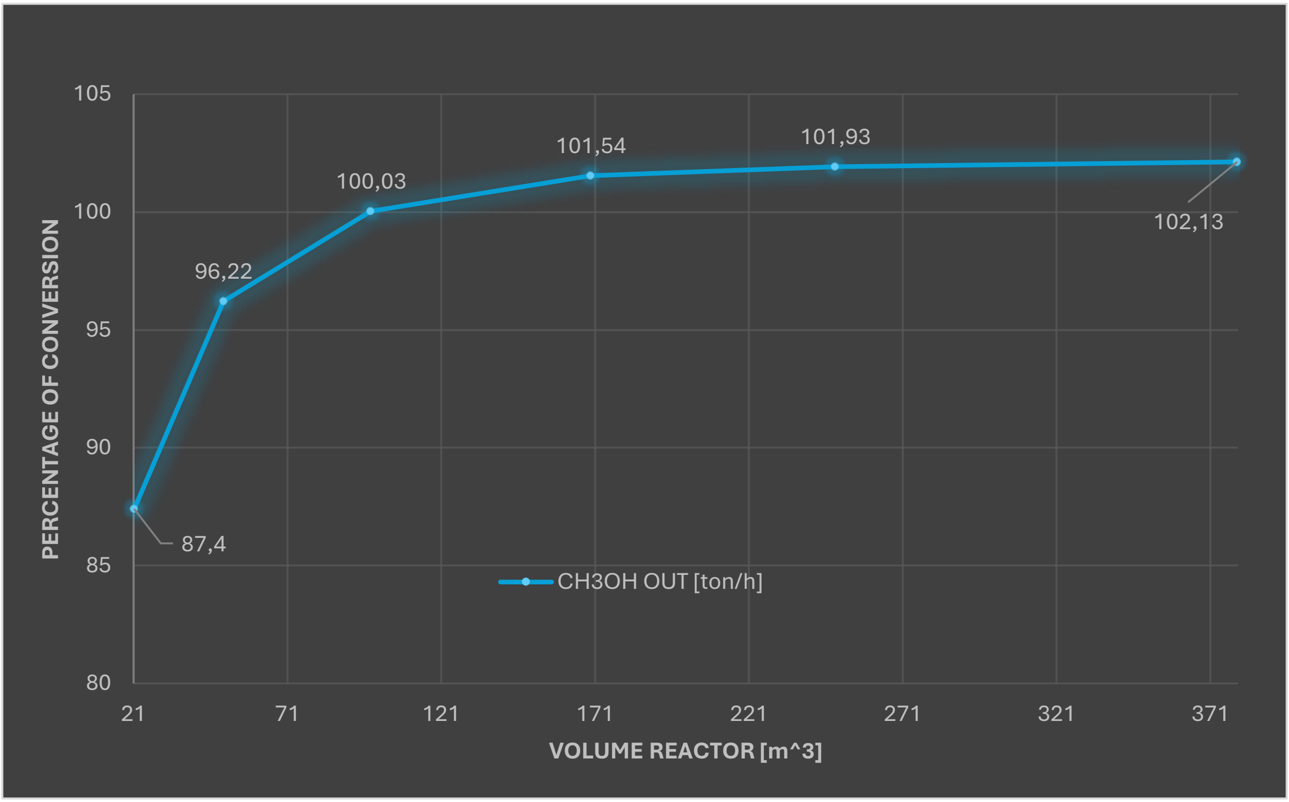

Figure 27 Sensitivity analysis of methanol produced by the reactor as function of the reactor's volume

A residence time of 11.55 seconds is calculated by Aspen for the current configuration, which corresponds to 249 m^3. Even if this value is much bigger than the residence time calculated from reference(around 7 seconds) an increase of the volume the reactor would be possible with a consequently increase of the methanol produced. Anyway, the increase is to small and not worthy compared to the increasing of the size. To give an idea, increasing both the diameter and length of

roughly 1 meter the total amount of methanol produced would rise to 102.10 ton/h compared to the actual 101.95 ton/h. The increasing of the volume would be around 100 m^3.
In further studies eventual reduction of the volume could be considered to account an economic optimization.

The second sensitivity analys is conducted variyng firstly the length of the reactor maintening the number of tube fixed. Then is done exact the same but this time length is kept fixed. Our configuration is marked by the orange point.

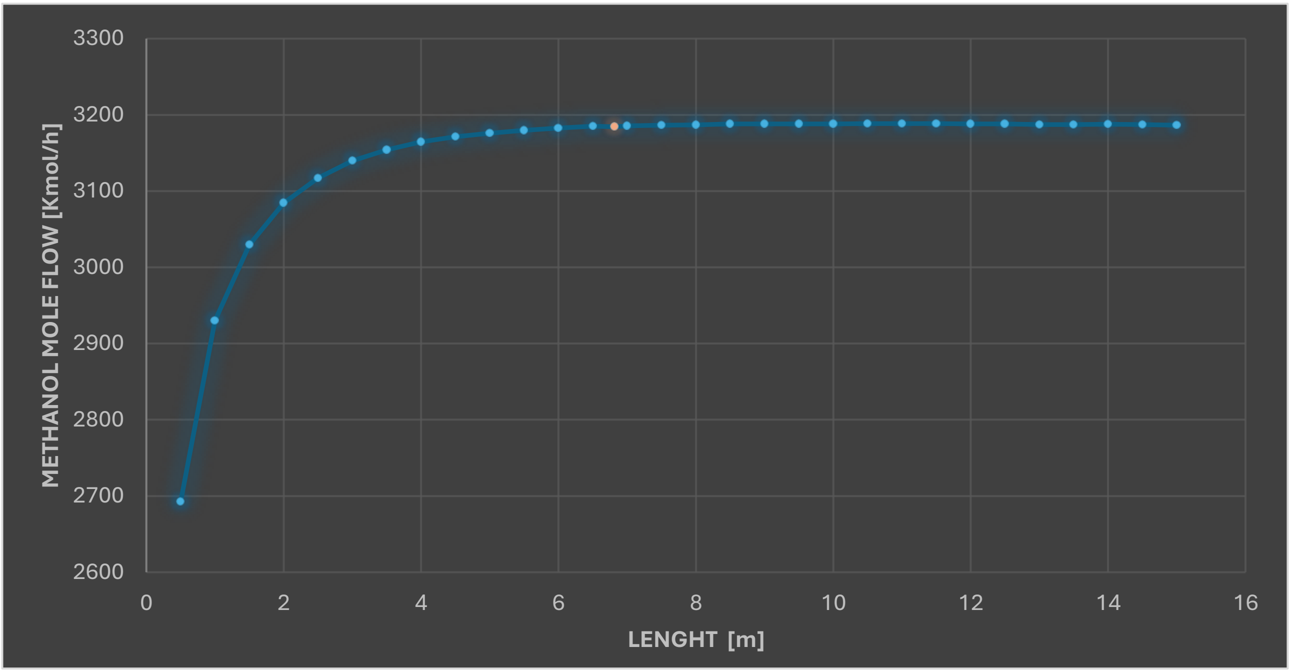

Figure 28 Sensitivity analysis of methanol produced as function of the lenght of the reactor

The sensitivity analysis of the length shows that after 6 meter, the reactor does not increase the production of methanol and the profile is almost asyntotic.

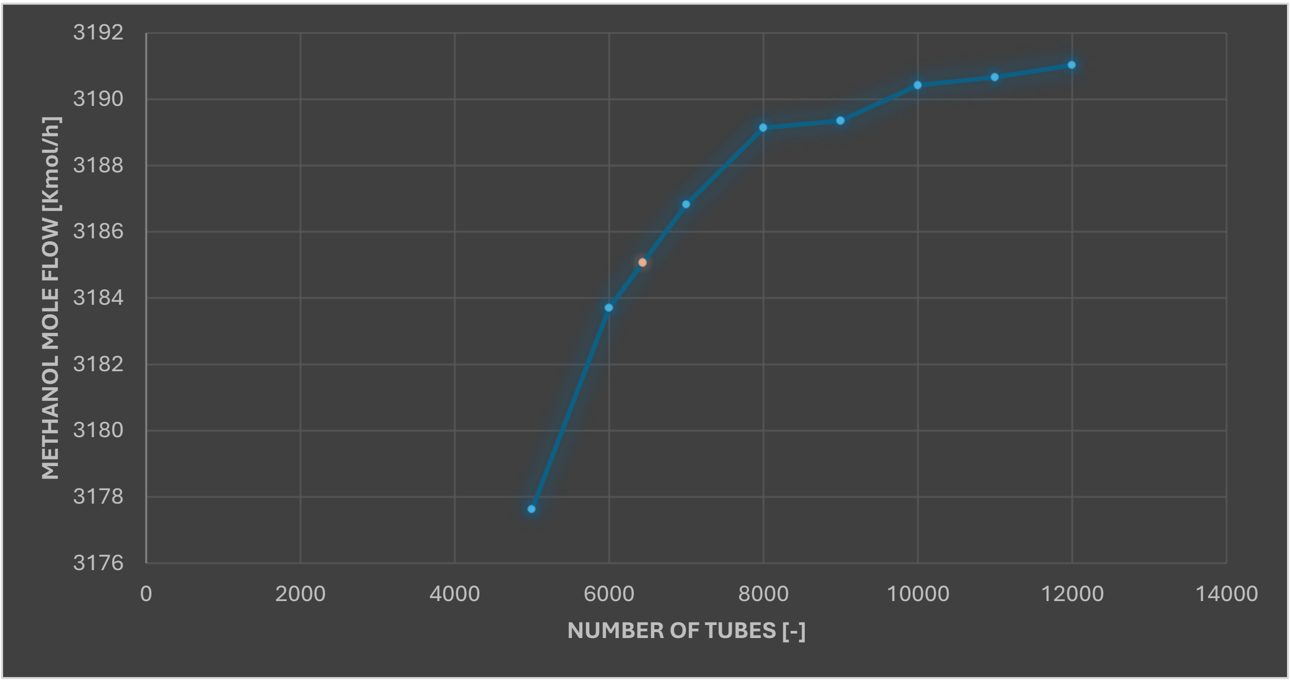

Figure 29 Sensitivity analysis of methanol produced by the reactor as function of the number of tubes of the reactor

The sensitivity analysis of the number of tubes, instead, shows that until 12000 tubes there is still a gain of productivity. Nonetheless, it is decided to keep the number of tubes at 6434 as an increase of them would require also an increase of the length to maintain the geometry proportion. As previously said, even though an increase of both parameters would be possible the gain obtained, compared to the increase in the volume of the reactor, would not be worthy. This sensitivity analysis shows that the reactor, only from a conversion efficiency point of view, benefits from geometry with larger diameter compared to length. This is also another reason behind the choice of our geometry since imposing the two-parameter equal is the best option which does not compromise the heat removal operation.

The third sensitivity analysis shows similar behavior of the first graph in which a similar one is conducted for the total amount of methanol produced by the reactor. This time the three conversion parameters are ploted as function of the volume of the methanol’s reactor.

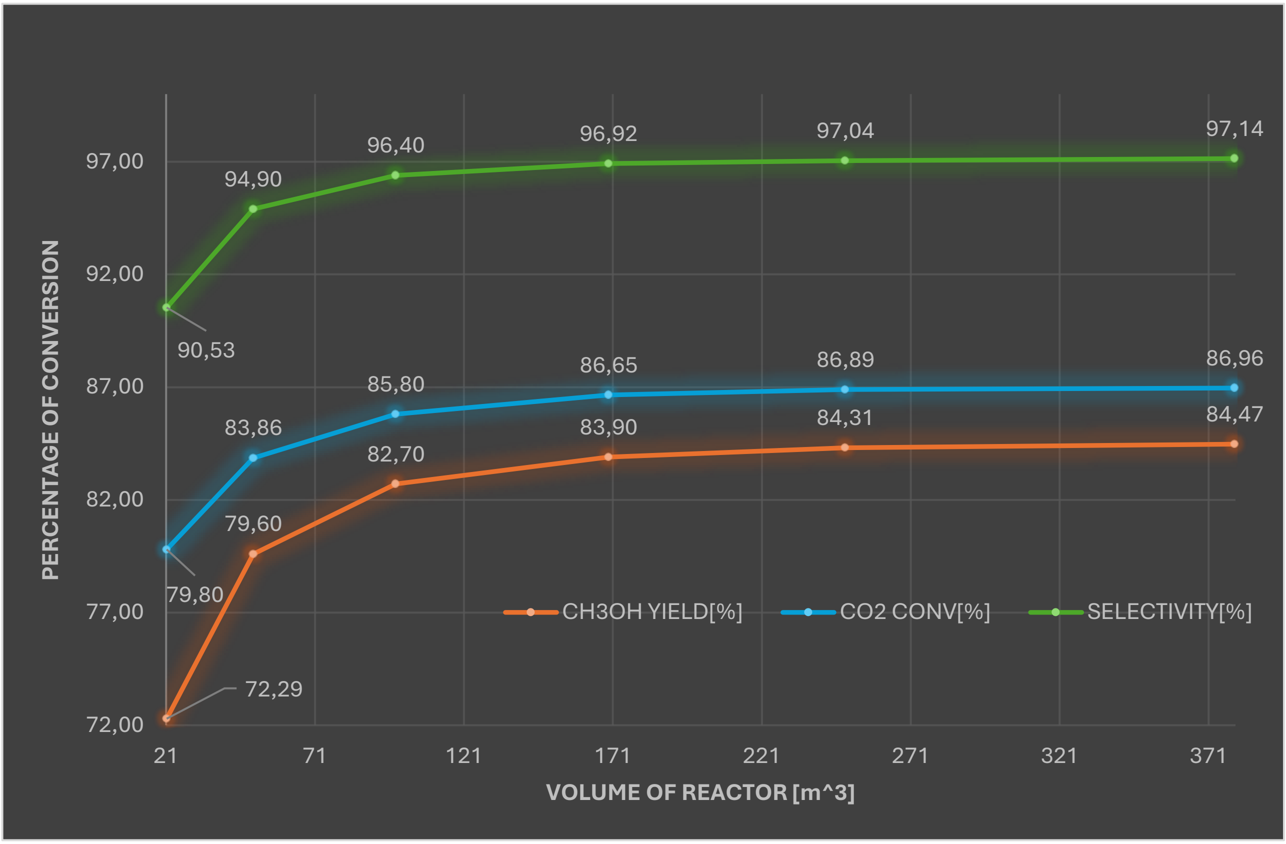

Figure 30 Sensitivity analysis of conversion parameters as function of the reactor's volume

The three profiles are almost asymptotic and very similar from a qualitative perspective. As the volume increases, the difference between the three profiles diminishes even if this behavior is not so marked. After 249 m^3, which corresponds to our choice, there is no more gain and the difference between the three parameters remains the same. With the current configuration a value of Yield of methanol equal to 84.31%, a CO_2 conversion of 86.89% and a selectivity towards methanol of 97.04% are obtained.

The last two sensitivity analysis are conducted varying this time the mass flow rate purge and keeping constant the volume of reactor.

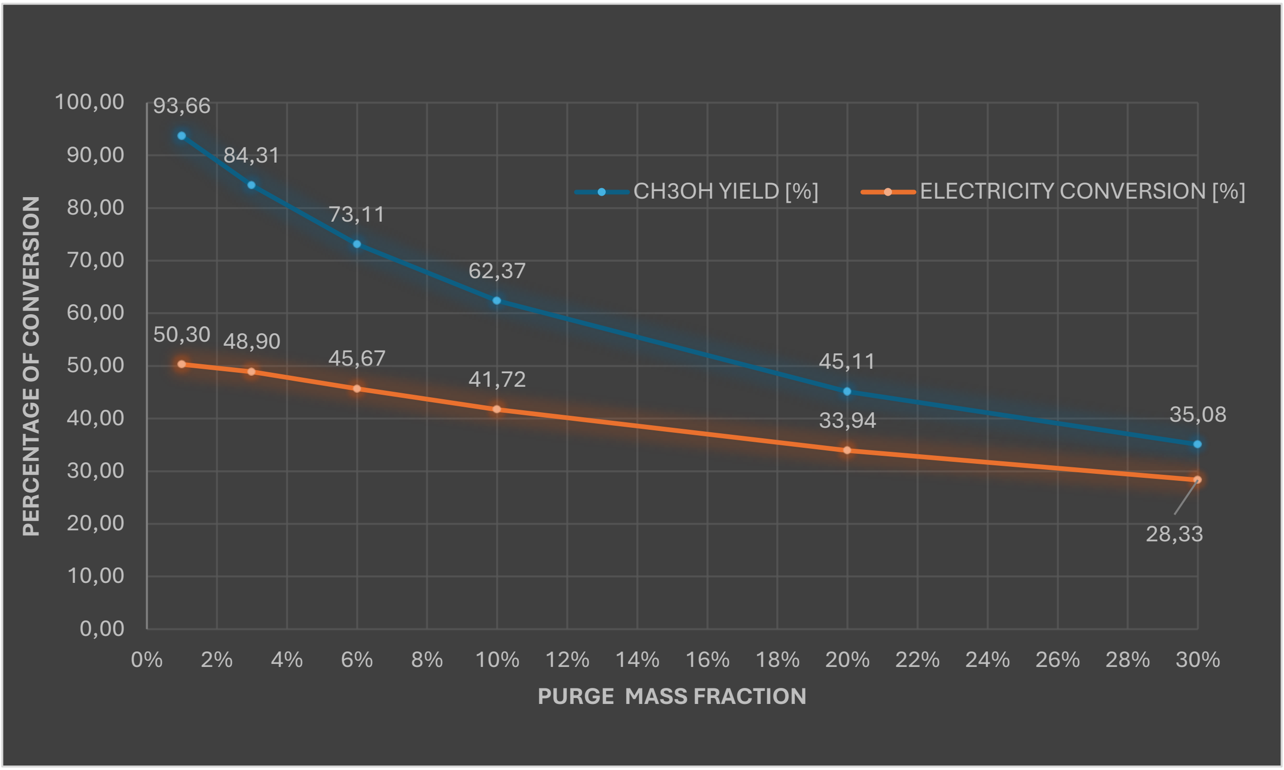

Figure 32 Sensitivity analysis of Methanol's Yield and Electrical conversion as function of the mass purged

All the parameters analyzed are also strongly related to the mass fraction purged, in fact, increasing the purge stream mass flow rate, the Yield drop relatively fast as well as the electrical efficiency. A sensitivity analysis of the parameters related to the purge stream is provided below.

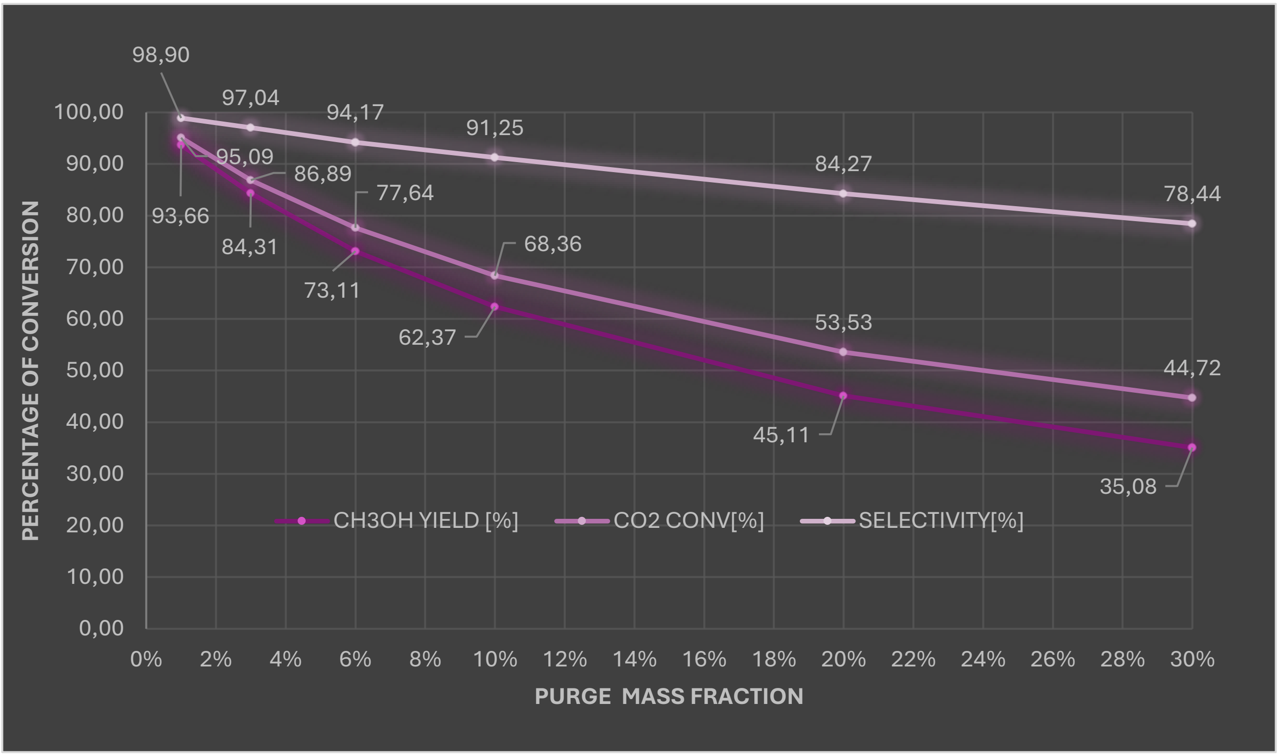

Figure 31 Sensitivity analysis of the conversion parameters as function of the mass purged

As we can see, with only 1% of mass purged a very high Yield of methanol is obtain almost equal to 94%. The maximum electrical conversion achievable, following the trend, is slightly higher than 50%. To maintain realistic values, similar to the one from another study [55], 3% of purge is adopted for the final configuration as reported in the methanol synthetization section.

The last sensitivity analysis is conducted using the three conversion parameters related to the mass flow rate purged.

The three trends follow different patterns and tend to almost converge at one point as the purge mass flow rate decreases. This is in accordance with the hypothesis on which the model is built. Being, in fact, the RWGS not so advantaged by the catalyst, the difference between the yield, the CO_2 conversion and the selectivity is mainly due to the amount of unreacted CO_2. While increasing the volume at a certain point would not lead to further gain in terms of more CO_2 reacted, no mass flow rate purged would lead to an almost complete reaction of the CO_2 with the consequence of the small possible difference between the parameters. In this scenario, CO_2 conversion would be almost 100% while the Selectivity and the Yield would be almost the same.

3.3 THERMAL INTEGRATION

This section shows the results obtained by the application of the Pinch analysis methodology. This includes the CC and GCC curves as well as the HEN for both the plants.

3.3.1 STANDALONE DAC PLANT

The first one treated is the standalone DAC plant.

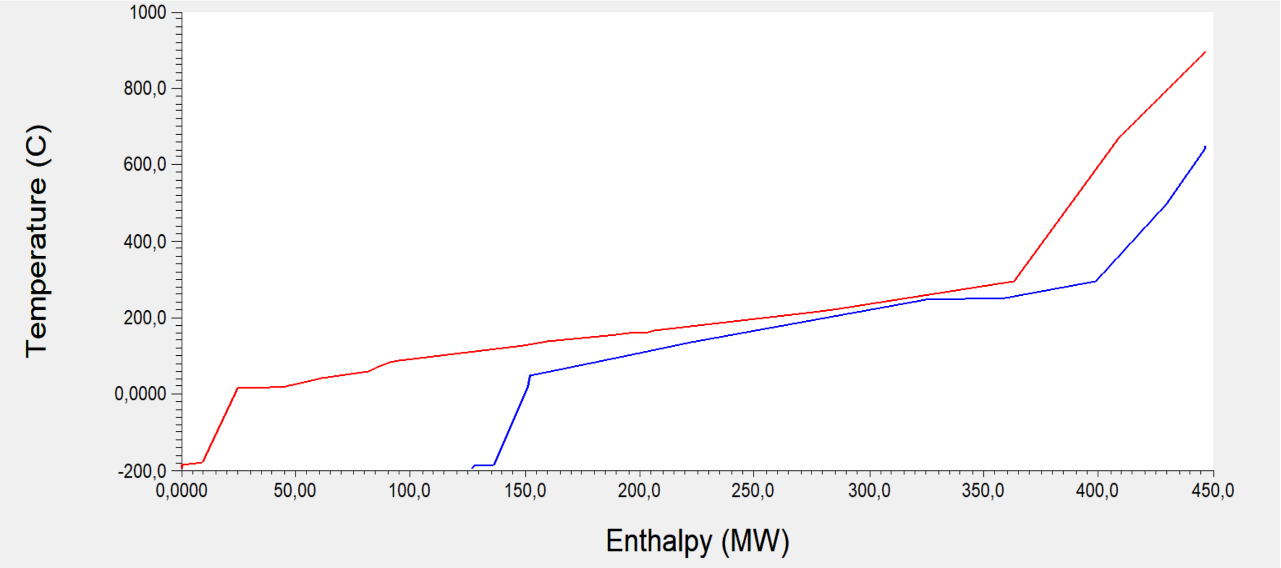

Figure 33 Composite Curve of the Standalone DAC plant

Without the three heaters from the STEAM CYCLE, the GCC curve showed that no heat is required externally, and a huge amount of heat have to be rejected. This also creates the result that no pinch point is present for that configuration.
The CC shown represents the final configuration obtained and, as it is possible to see from the graph, the theoretical amount of heat recoverable is equal to 316.2 MW. This can be seen graphically as the span on the x-axis covered by the blue curve.

In the GCC, the touching of the y-axis by the curve in two points, depict the fact that all the high-grade heat is recovered. This is the direct consequence of the procedure applied, in which the mass flow rate of the STEAM CYCLE is progressively increased. The procedure has been discussed in detail in the Chapter 2.
Even if theoretically it is possible to recover all the heat specified by the software, the resulting HEN would be too complex leading to an almost unsolvable problem. To gain some degree of freedom an external utility, accounting for the heat generated by the SLAKER, is inserted. The HEN is built trying to leave the unsatisfied heat demand in a temperature range below 300°C, in our case in the EVA stream.
At the end we obtain a configuration where only 4.6 MW are provided by the SLAKER, while the rest is provided by the hot streams.

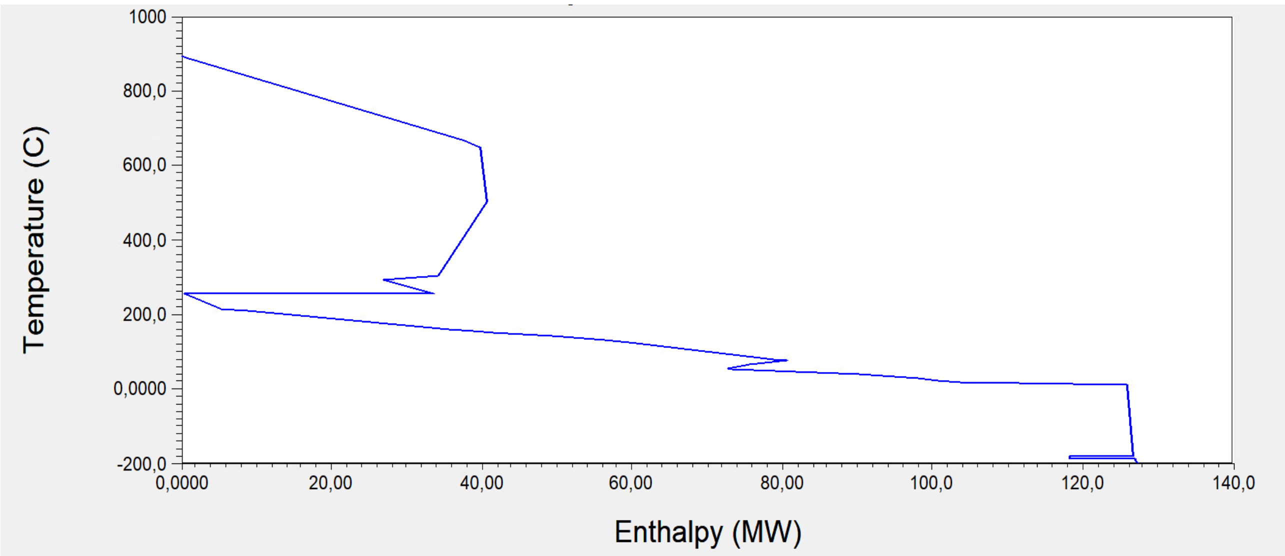

Figure 34 Gran Composite curve of the Standalone DAC plant

We are able to feed the STEAM CYCLE with a total mass flow rate of 68 ton/h of water using this configuration.

Accounting the heat to be rejected, the unsatisfied hot streams are coupled with a cold stream utility which represented an external cold source. The power required for cooling is not accounted in the final energy balance as it is assumed to use cooling towers and other passive systems fed by cold water from natural resources.

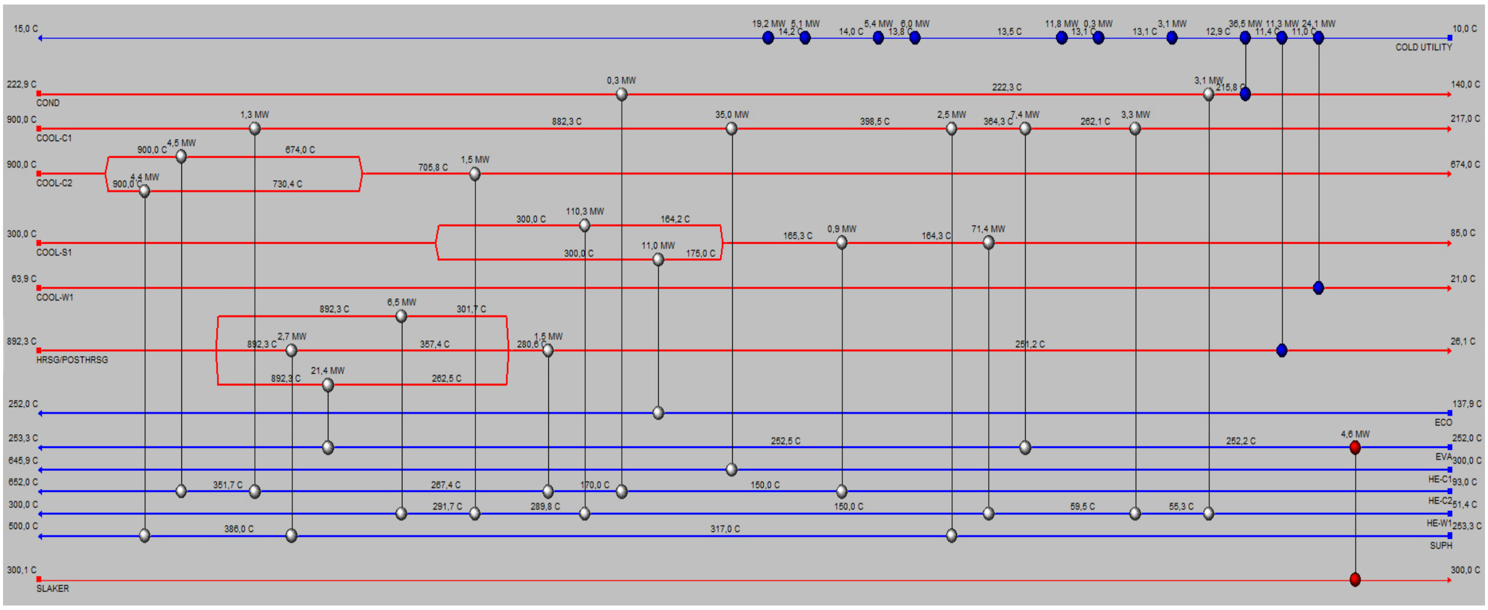

Figure 35 HEN of Standalone DAC plant

Also, the ASU is present in this analysis and the unsatisfied cryogenic streams are coupled to a very low temperature utility. Anyway, as previously explained in the ASU section, this consumption will not be considered and general consumption from Keith et al. will be used instead.

HEN shows quite good performance with an increasing demand of cooling of 3.6% compared to optimum configuration. Also, the number of units are slightly higher with a 25% increase compared to the optimum configuration calculated by the software. It is possible, including the ASU, to recover

311.6 MW of heat, this means that the heat given by the SLAKER accounts only for 1.5% of the theoretical recoverable heat (316.2 MW).

For clarity reasons, the HEN maps show only the stream which actively participates in the heat recovery procedure, the totally unrecoverable streams are connected to the cold utility but hidden. This includes the intercoolers and the HX-AC. Additionally, the HEN map portion related to ASU is provided separately. The elements inside the model which requires heat are all satisfied except for the PELLET block, which requires roughly 33.5 MW at 25 °C. Assuming to have to supply the heat, this could be done using the heat from the COMPRESSION TRAIN intercoolers and the stream related to COOL-W1. This last one produces a big amount of heat which can’t be recovered as it is at low grade. The remaining part of the heat required by the PELLET block could be supplied by the SLAKER. The tables provided below show all the HX used in the Pinch methodology with: streams coupled, inlet and outlet temperature (for both sides), minimum temperature difference (for both sides) and load.

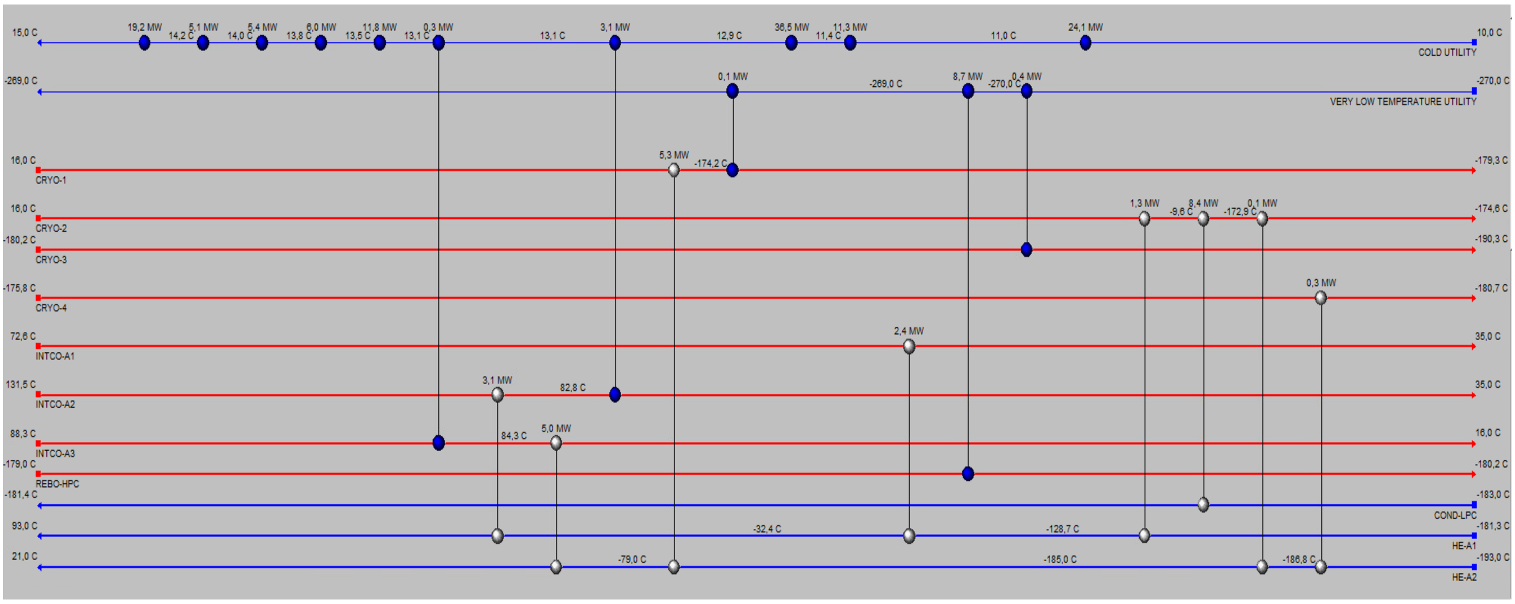

Figure 36 HEN of The ASU

HX-ID	COLD STREAMS	COLD T_in[°C]	COLD T_out[°C]	HOT STREAMS	HOT T_in[°C]	HOT T_out[°C]
E-102	HE-A1	-181,3	-128,7	CRYO-2	16,0	-9,6
E-521	HE-W1	55,3	59,5	COOL-C1	262,1	217,0
E-106	COND-LPC	-183,0	-181,4	CRYO-2	-9,6	-172,9
E-527	HE-W1	289,8	291,7	COOL-C2	705,8	674,0
E-511	SUPH	253,3	317,0	COOL-C1	398,5	364,3
E-509	ECO	137,9	252,0	COOL-S1	300,0	175,0
E-514	HE-W1	59,5	150,0	COOL-S1	164,3	85,0
E-507	HE-C2	170,0	267,4	HRSG/POSTHRSG	280,6	251,2
E-129	HE-A1	-32,4	93,0	INTCO-A2	131,5	82,8
E-510	HE-C1	300,0	645,9	COOL-C1	882,3	398,5
E-120	HE-A2	-186,8	-185,0	CRYO-2	-172,9	-174,6
E-109	HE-A2	-193,0	-186,8	CRYO-4	-175,8	-180,7
E-506	HE-C2	267,4	351,7	COOL-C1	900,0	882,3
E-508	HE-W1	150,0	289,8	COOL-S1	300,0	164,2
E-504	SUPH	317,0	386,0	HRSG/POSTHRSG	892,3	357,4

E-502	EVA	252,5	253,3	HRSG/POSTHRSG	892,3	262,5
E-512	EVA	252,2	252,5	COOL-C1	364,3	262,1
E-101	HE-A2	-185,0	-79,0	CRYO-1	16,0	-174,2
E-522	HE-W1	51,4	55,3	COND	222,3	215,8
E-133	HE-A2	-79,0	21,0	INTCO-A3	84,3	16,0
E-497	SUPH	386,0	500,0	COOL-C2	900,0	730,4
E-499	HE-C2	351,7	652,0	COOL-C2	900,0	674,0
E-501	HE-W1	291,7	300,0	HRSG/POSTHRSG	892,3	301,7
E-123	HE-A1	-128,7	-32,4	INTCO-A1	72,6	35,0
E-513	HE-C2	93,0	150,0	COOL-S1	165,3	164,3
E-515	HE-C2	150,0	170,0	COND	222,9	222,3

Table 7 HX of the Standalone DAC plant's Pinch analysis pt.1

HX-ID	**LOAD [MW]**	**DT min HOT [°C]**	**DT min COLD [°C]**
E-102	1,3	144,7	171,7
E-521	3,3	202,6	161,7
E-106	8,4	171,8	10,1
E-527	1,5	414,1	384,2
E-511	2,5	81,5	111,0
E-509	11,0	48,0	37,1
E-514	71,4	14,3	25,5
E-507	1,5	13,2	81,2
E-129	3,1	38,5	115,2
E-510	35,0	236,5	98,5
E-120	0,1	12,1	12,2
E-109	0,3	11,0	12,3
E-506	1,3	548,3	614,9
E-508	110,3	10,2	14,2
E-504	2,7	506,3	40,4
E-502	21,4	639,0	10,0
E-512	7,4	111,8	9,9
E-101	5,3	95,0	10,8
E-522	3,1	166,9	164,4
E-133	5,0	63,3	95,0
E-497	4,4	400,0	344,4
E-499	4,5	248,0	322,3
E-501	6,5	592,3	10,0
E-123	2,4	104,9	163,7
E-513	0,9	15,3	71,3
E-515	0,3	52,9	72,3

Table 8 HX of the Standalone DAC plant's Pinch analysis pt.2

3.3.2 DAC AND UTILIZATION FACILITY COUPLED

Similarly to the previous plant, for the one coupled with the utilization facility, it is obtained a HEN not able to recover all the theoretical heat. The missing part is provided by the SLAKER as it is at a temperature below 300°C. The heat required by the SLAKER results in 11.7 MW which increases the cooling demand by 25% compared to the target. Anyway, with this configuration it is possible to recover 603.1 MW, so the lost heat is only 1.9% of the recoverable theoretical target (614.8 MW). The huge amount of heat results also in an increase of the mass flow rate of the STEAMCYCLE which reaches 151 ton/h, allowing a mechanical output power of the steam turbine of roughly 25 MW.

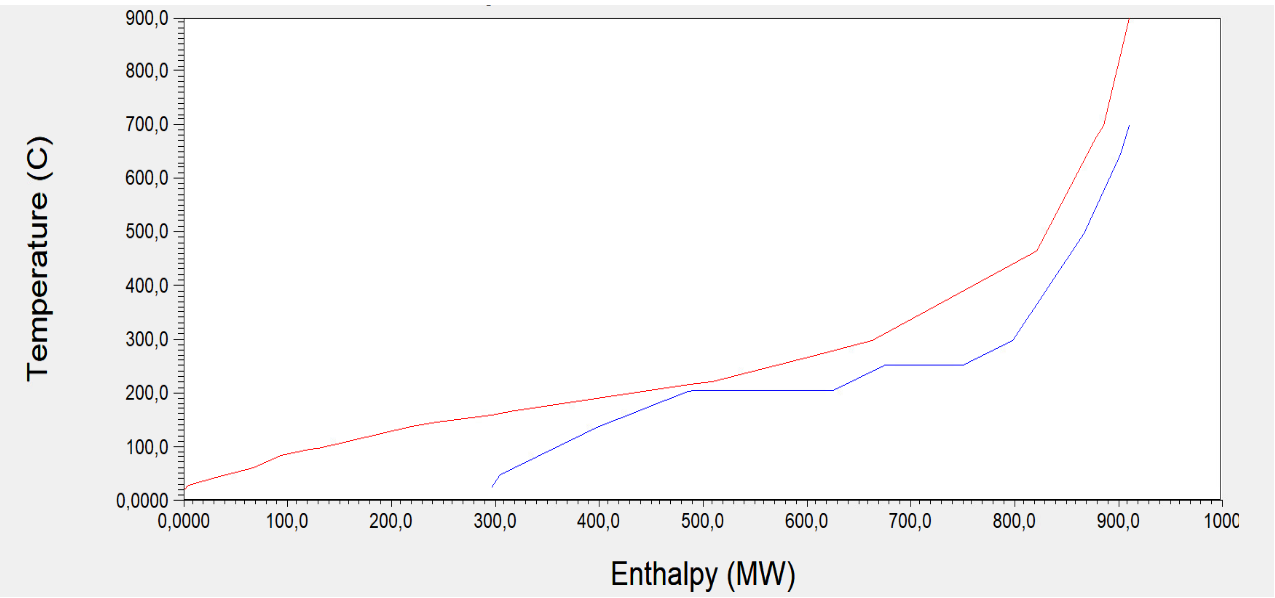

Figure 37 Composite Curve of the coupled DAC plant

The cooling, also here, is assumed to be provided by cooling towers and passive cooling systems using cold water from a river or a pond. Part of the low-grade heat can be used to feed the PELLET REACTOR, as described in the other pinch analysis, while the rest can be given by the SLAKER. The methanol

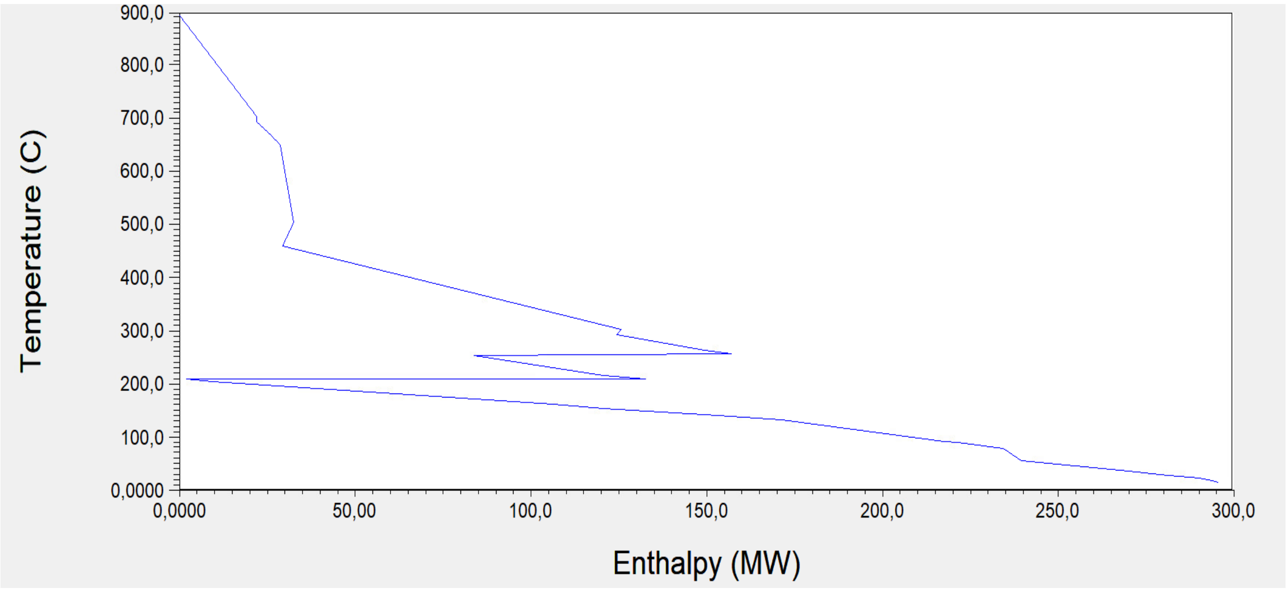

Figure 38 Gran Composite Curve of the coupled DAC plant

distillation column has the reboiler and the condenser respectively requiring 66.5 MW of heat to be supplied and 60.5 MW of heat to be removed. While the condenser can simply be refrigerated as the other streams, the heat required by the reboiler is around 100°C.

As the methanol reactor produces 54 MW of heat at 270 °C this can be used to feed partially the reboiler. The other part can be supplied by the SLAKER.

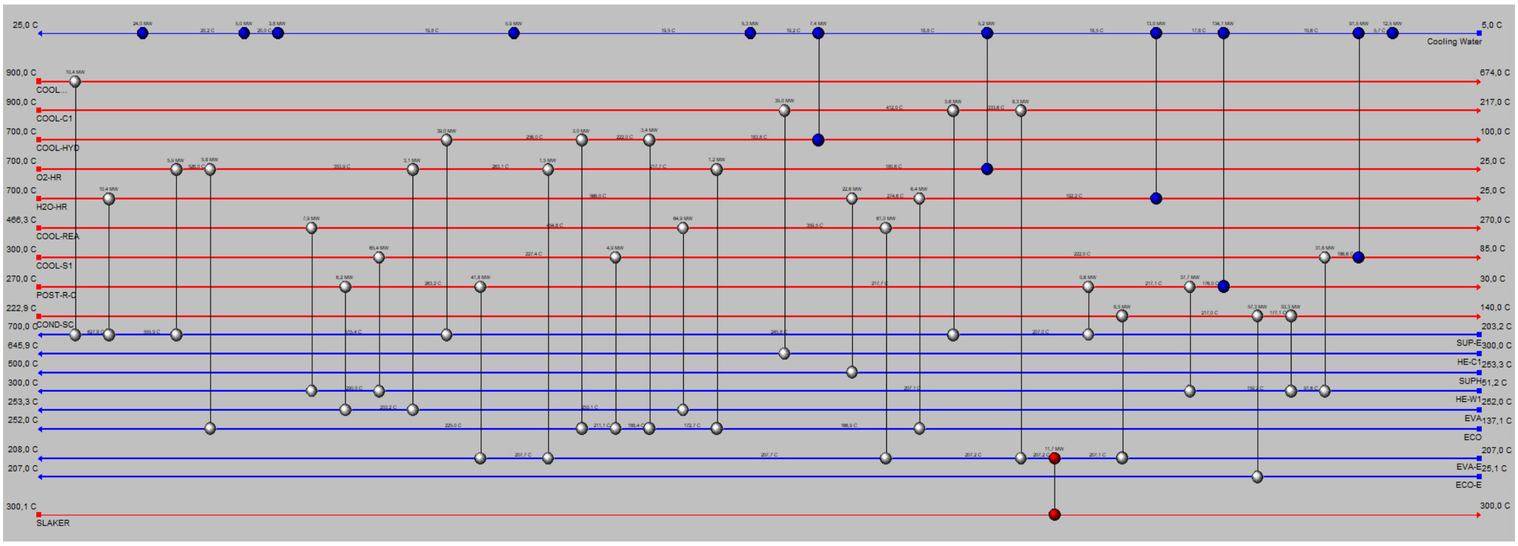

Figure 39 HEN of the coupled DAC plant

In the HEN, only the streams which participate in the heat recovery procedure are shown for clarity reasons. Below, two tables are provided which show all the HX of the HEN with their specification. In particular: temperature inlet of both sides, streams' temperature difference of both sides and duty of the HX.

HX-ID	COLD STREAMS	COLD T_in[°C]	COLD T_out[°C]	HOT STREAMS	HOT T_in[°C]	HOT T_out[°C]
E-271	EVA-E	207,2	207,2	COOL-C1	333,6	217,2
E-231	HE-C1	300,0	645,9	COOL-C1	900,0	412,0
E-233	SUP-E	515,4	555,9	O2-HR	700,0	526,0
E-242	HE-W1	290,0	300,0	COOL-REA	466,3	454,8
E-249	EVA	253,2	253,3	POST-R-C	270,0	263,2
E-253	EVA-E	207,7	207,7	O2-HR	263,1	217,7
E-236	ECO	211,1	225,0	COOL-HYD	256,0	222,0
E-230	SUP-E	627,8	700,0	COOL-C2	900,0	674,0
E-247	ECO	188,4	211,1	COOL-S1	227,4	222,0
E-243	HE-W1	207,1	290,0	COOL-S1	300,0	227,4
E-252	EVA	253,1	253,2	O2-HR	353,9	263,1
E-216	SUP-E	203,2	207,0	POST-R-C	217,7	217,1
E-214	ECO-E	25,1	207,0	COND-SC	217,0	177,1
E-220	EVA-E	207,0	207,1	COND-SC	222,9	217,0
E-248	ECO	225,0	252,0	O2-HR	526,0	353,9
E-238	SUPH	253,3	500,0	H2O-HR	566,0	274,6
E-257	EVA-E	207,2	207,7	COOL-REA	359,5	270,0
E-225	ECO	172,7	188,4	COOL-HYD	222,0	183,8

E-223	ECO	137,1	166,9	H2O-HR	274,6	192,2
E-270	SUP-E	207,0	245,8	COOL-C1	412,0	333,6
E-234	SUP-E	245,8	515,4	COOL-HYD	700,0	256,0
E-232	SUP-E	555,9	627,8	H2O-HR	700,0	566,0
E-250	EVA-E	207,7	208,0	POST-R-C	263,2	217,7
E-256	EVA	252,0	253,1	COOL-REA	454,8	359,5
E-218	HE-W1	91,6	159,2	COND-SC	177,1	140,0
E-222	HE-W1	159,2	207,1	POST-R-C	217,1	176,0
E-224	ECO	166,9	172,7	O2-HR	217,7	180,6
E-267	HE-W1	51,2	91,6	COOL-S1	222,0	186,6

Table 9 HX of the coupled DAC plant's Pinch analysis pt.1

HX-ID	**LOAD [MW]**	**DT min HOT [°C]**	**DT min COLD [°C]**
E-271	8,3	126,4	10,0
E-231	35,0	254,1	112,0
E-233	5,9	144,1	10,6
E-242	7,9	166,3	164,8
E-249	6,2	16,7	10,0
E-253	1,5	55,4	10,0
E-236	3,0	31,0	10,9
E-230	10,4	200,0	46,2
E-247	4,9	16,3	33,6
E-243	65,4	10,0	20,3
E-252	3,1	100,7	10,0
E-216	0,6	10,7	13,9
E-214	57,3	10,0	152,0
E-220	8,5	15,9	10,0
E-248	5,8	274,0	128,9
E-238	22,6	66,0	21,3
E-257	61,0	151,8	62,8
E-225	3,4	33,6	11,1
E-223	6,4	107,7	55,1
E-270	5,6	166,2	126,6
E-234	39,0	184,6	10,2
E-232	10,4	72,2	10,1
E-250	41,8	55,2	10,0
E-256	64,9	201,6	107,5
E-218	53,3	17,9	48,4
E-222	37,7	10,0	16,8
E-224	1,2	45,0	13,7
E-267	31,8	130,4	135,4

Table 10 HX of the coupled DAC plant's Pinch analysis pt.2

3.4 ENERGY ANALYSIS AND VALIDATION

3.4.1 STANDALONE DAC PLANT

HIERARCHY	COMP-ID	MECH ENERGY[MW]	ELECTICAL ENERGY[MW]	NG-REQ[ton/h]
	AIR-COMP	9,79	10,31	
	COMBUST			6,30
	GT	-32,51	-30,88	
AIRCONT		9,60	10,11	
	PUMP-1	1,25E-02	1,32E-02	
PELLET REACTOR	PUMP-2	2,23E-01	2,35E-01	
CALCINER	CALCINER			15,02
ASU	ASU (Keith et al.)	12,18	12,82	
STEAMC	PUMP-42B	1,04E-01	1,09E-01	
	PUMB-4B	6,12E-04	6,44E-04	
	STEAMTURB	-8,84	-8,40	
COMP-TRAIN	COMP-01	4,94	5,19	
	COMP-02	4,75	5,00	
	COMP-03	4,56	4,80	
	COMP-04	3,97	4,18	
OTHERS COMPONENTS NOT ACCOUNTED IN THE SIMULATION WHICH CONSUMES ELECTRICY (from Keith et al.)				
	AUX		2,60	
	MIXERS		0,50	
	SLAKER		3,60	
	CALCINER		0,80	
	PELLET REACTOR		3,40	

Table 11 Component's power required and produced of Standalone DAC plant

The energy analysis shows a total electrical consumption of 63.66 MW while the net one is 24.38 MW.

The reference provides a consumption of 8.81 GJ/ton-CO_2 thermally supplied or 5.26 Gj thermally provided, and 366 KWh electrically supplied per ton-CO_2. A total amount of energy of 6.95 Gj/ton-CO_2 is calculated for our DAC. This corresponds to 21.1% less energy than Keith et al. plant, similarly to the 19.6% less energy found by Bianchi et al. The possible difference in the outcome can be seen in different aspects.

First of all, our CALCINER is modelled as adiabatic, not accounting for heat losses. Even though in reference a small loss is specified, the found value of NG almost matches in terms of energy. The big factor can rely on the pinch analysis methodology applied. In fact, the strategy adopted is highly aggressive, aiming to recover all the heat of the plant. Additionally, our HXs are assumed as ideal. In the real world, many of the matches made during the pinch analysis could reveals impractical, especially the ones involving solid streams. Also, a minimum temperature difference of 10°C could results in a too big area required by the HXs, making the capital cost of the plant to high and so force to waste part of the heat to make the plant viable.

A second estimation is done, this time using the avoided CO_2. This corresponds to the actual CO_2 removed from the air without considering the one produced to make the plant work. Another version of the plant is provided by the reference in which all the energy requirements are satisfied electrically by external sources. In that case the plant would produce an amount of CO_2 equal to the one avoided and so, for this reason, weighting the consumption of our model on the avoided CO_2 could represent an interesting parameter. Doing so, the consumption of plant rise to 10.09 Gj/ton-CO_2, 14% higher than the ones stated by Keith et al.

TOT ELECTRICAL CONSUMPTION [MW]	63,66
NET ELECTRICAL CONSUMPTION [MW]	24,38
HEAT PROVIDED (provided interally by NG) [Gj/h]	918,00
HEAT PROVIDED (provided interally by NG) [MW]	254,29
SPECIFIC ELECTRICAL POWER REQUIRED CO2 CAPTURED [MWh/ton-CO2]	0,15
SPECIFIC HEAT REQUIRED CO2 CAPTURED [Gj/ton-CO2]	5,52
SPECIFIC HEAT REQUIRED CO2 CAPTURED [MWh/ton-CO2]	1,53
SPECIFIC ELECTRICAL POWER REQUIRED CO2 AVOIDED [MWh/ton-CO2]	0,21
SPECIFIC HEAT REQUIRED CO2 AVOIDED [Gj/ton-CO2]	8,02
TOTAL HEAT REQUIRED CONVERTING ELECTRICITY WEIGHTED PER CO2 CAPTURED [Gj/ton-CO2]	**6,95**
TOTAL HEAT REQUIRED CONVERTING ELECTRICITY WEIGHTED PER CO2 AVOIDED [Gj/ton-CO2]	**10,09**
CLAIMED TOTAL HEAT REQUIRED BY REF (keith et al.) [Gj/ton-CO2]	**8,81**
MINIMUM THEORETICAL ENERGY REQUIRED [Gj/ton-CO2]	**0,45**
PERCENTAGE DIFFERNCE FROM REF CO2 CAPTURED (Keith et al.)	**-21,1%**
PERCENTAGE DIFFERNCE FROM REF CO2 AVOIDED (Keith et al.)	**14,5%**
BIANCHI et al. PERCENTAGE DIFFERENCE FROM REF(Keith et al.)	**-19,6%**
CO2 CAPTURED [ton/h]	166,19
CO2 AVOIDED [ton/h]	114,50
GAS CYCLE EFFICIENCY	27%
COMBINED CYCLE EFFICIENCY	39%

Table 12 Energy analysis parameters Standalone DAC plant

A second analysis is conducted on the results, to account for the mass balance of the plant. As explained in the Hierarchies, a too high waste of Calcite is used in the simulation of Bianchi et al. which led to big difference in his amount of CO_2 captured and available. To assess this problem, the values of CO_2 mass flow rate is first taken from Keith et al. reference. The total CO_2 captured is estimated by summing the amount collected by the AIR CONTACTOR and the ABSORBER with the amount produced during the oxycombustion. Then the value of output CO_2 is confronted with the first computed. The values found show a higher amount in available stream, possibly due by truncation error of the reported data. It is assumed that the available amount and the captured one have almost to be equal as the mass losses inside the reference plant are all accounted by proper make-up. Then, the data from our simulation are extrapolated and analyzed showing an error of -0.12% in the outlet stream compared to the captured, which is considered acceptable. The difference in mass between the results of this study and the reference is mainly due by the higher amount captured by the absorber—as our flue gas of the POWER ISLAND are richer in CO_2. Other minor impact can be addressed to the oxygen stream from the ASU—which in our case contains trace of CO_2—and the usage of NG instead of pure methane—which also contains CO_2 inside. All the collected data are summed in the table below.

CO2 CAPTURED IN AIR CONTACTOR HIERARCHY(keith et al.) [ton/h]	127,71
CO2 PRODUCED DURING OXYCOMBUSTION (keith et al.)[ton/h]	36,80
TOT CO2 (keith et al.) [ton/h]	164,51
ACTUALLY AVAILABLE (keith et al) [ton/h]	166,08
CO2 CAPTURED IN AIR CONTACTOR HIERARCHY [ton/h]	129,47
CO2 PRODUCED DURING OXYCOMBUSTION[ton/h]	36,92
TOT CO2[ton/h]	166,39
ACTUALLY AVAILABLE [ton/h]	166,19
PERCENTAGE DIFFERENCE IN AVAILABLE CO2	0,12%
MASS DIFFERENCE [kg/h]	199,30
AVOIDED CO2 [ton/h]	114,50

Table 13 CO_2mass balance error estimation

3.4.2 DAC AND UTILIZATION FACILITY COUPLED

HIERARCHY	COMP-ID	MECH ENERGY[MW]	ELECTICAL ENERGY[MW]	NG-REQ[ton/h]
	AIR-COMP	9,79	10,31	
	COMBUST			6,302
	GT	-32,51	-30,88	
AIRCONT		9,60	10,11	
	PUMP-1	1,25E-02	1,32E-02	
PELLET REACTO	PUMP-2	2,23E-01	2,35E-01	
CALCINER	CALCINER			15,02
STEAMC	PUMP-42B	1,04E-01	1,09E-01	
	PUMB-4B	6,12E-04	6,44E-04	
	STEAMTURB	-25,37	-24,10	
COMPTRAIN	COMP-01	4,84	5,09	
	COMP-02	4,66	4,91	
	COMP-03	4,47	4,71	
	COMP-04	1,57	1,65	
OTHERS COMPONENTS NOT ACCOUNTED IN THE SIMULATION WHICH CONSUMES ELECTRICY (from Keith et al.)				
	AUX		2,60	
	MIXERS		0,50	
	SLAKER		3,60	
	CALCINER		0,80	
	PELLET REACTOR		3,40	
UTILIZATION	SOEC		850,64	
	COMP-E		23,88	
	PUMP-E		1,43E-01	
	RE-COMP		262,00	

Table 14 Component's power required and produced of coupled DAC plant

Finally, a comprehensive energy analysis of the overall new plant is conducted. Energy consumption is computed and weighted by the methanol produced while, instead, consumption per unit of CO_2 is not accounted. This is because—since the energy requirement has significantly increased—direct comparisons with DAC references would not be meaningful.

One notable observation is the slight reduction in the CO2 stream mass flow rate exiting the COMPRESSION TRAIN, which has decreased from 169.26ton/h to167.28 ton/h, resulting in a total captured CO_2 of 166.052 ton/h. As previously mentioned, the amount CO_2 in the outlet stream remains largely unchanged; the primary difference lies in its purity, which now reaches 99% by mass. The total amount of methanol produced is 100.76 ton/h.

The total energy consumption—mainly supplied electrically—is nearly two orders of magnitude higher than in previous cases equal to 1184.63 MW. This is primarily due to the significant energy demand of the SOEC and RE-COMP blocks, which must process a large recirculated mass flow.

Focusing only on the DAC unit, its energy requirement has decreased, mainly due to the removal of the ASU and the lower outlet pressure of COMP-04—which has reduced the energy consumption of the COMPRESSION TRAIN.

The three, previously mentioned, main KPIs are finally evaluated and compared, to assess the effective performance of the plant and gain insight of the worthiness of coupling the facility with the DAC plant.

All the results are reported in the table below.

TOT ELECTRICAL CONSUMPTION [MW]	1184,63
NET ELECTRIC CONSUMPTION [MW]	1128,68
HEAT PROVIDED (provided interally by NG) [Mj/h]	917998,25
HEAT PROVIDED (provided interally by NG) [MW]	254,29
CO2 CAPTURED [ton/h]	166,05
METHANOL PODUCED [ton/h]	100,76
EFFECTIVE CH3OH YIELD	**83,32%**
HYDROGEN PRODUCE BY SOEC [ton/h]	21,58
NET AVAILABLE OXYGEN PRODUCED BY SOEC [ton/h]	119,49
METHANOL LHV [Mj/kg]	19,90
CHEMICAL POWER PRODUCED [MW]	556,98
SOEC EFFICIENCY	84,5%
METHANOL SECTION EFFICIENCY	**54,60%**
UTILIZATION FACILITY EFFICIENCY	**48,30%**
OVERALL PLANT EFFICIENCY	**40,27%**

Table 15 Energy analysis parameters coupled DAC plant

As it's possible to note, considering the methanol section, the energy efficiency decreases of about 14.3% going from the methanol section to the total overall plant, while, instead, going from the only facility to the overall plant the reduction is only of 8%.

Also the effective Yield of methanol is roughly 1% less than Yield of methanol due to the wasted part in the distillation process and in the purge.

4 CONCLUSIONS

The integration of DAC with methanol synthesis offers an interesting pathway for producing carbon-neutral fuels. Nonetheless, this approach presents notable challenges. Methanol production, primarily driven by hydrogen generation via electrolysis, is the dominant source of the plant's energy consumption, since electrolysis is inherently energy-intensive. Incorporating DAC leads to a relatively modest efficiency reduction—around 8% compared to a standalone methanol plant—but provides significant benefits, including consistent CO_2 availability and access to revenue streams from carbon markets.

While CO_2 can be sourced as a byproduct from various industrial processes—such as biogas facilities—at little to no cost, these sources typically offer limited and inconsistent CO_2 volumes. Such constraints hinder large-scale methanol production and can undermine the economic viability of the investment. DAC addresses this limitation by ensuring a continuous and abundant CO_2 supply, essential for sustained industrial-scale operations. Additionally, the system's ability to generate income through emissions trading and carbon credits enhances its financial appeal.
However, this solution is not without drawbacks. Both the DAC and methanol production facilities require significant capital investments on their own; when combined at large scales, the initial costs can become prohibitive. Moreover, the substantial energy demand—primarily due to hydrogen production—necessitates careful planning and reliable access to affordable, renewable energy sources.

Successful industrial deployment of this integrated system will hinge on minimizing operational expenses through strategic site selection and securing cost-effective renewable energy. To thoroughly assess the viability of this approach, future research should focus on:

- Comprehensive economic analysis to evaluate capital expenditures, operating costs, and potential carbon market revenues.
- Site selection studies to identify locations rich in renewable energy resources with suitable infrastructure.
- Policy and market assessments to explore incentives, subsidies, and carbon pricing mechanisms.
- Investor engagement strategies to attract funding for high-impact, long-term sustainable project

BIBLIOGRAPHY

[1] M. Filonchyk, M. P. Peterson, L. Zhang, V. Hurynovich, and Y. He, “Greenhouse gases emissions and global climate change: Examining the influence of CO2, CH4, and N2O,” *Science of The Total Environment*, vol. 935, p. 173359, Jul. 2024, doi: 10.1016/J.SCITOTENV.2024.173359.

[2] K. Calvin *et al.*, “IPCC, 2023: Climate Change 2023: Synthesis Report. Contribution of Working Groups I, II and III to the Sixth Assessment Report of the Intergovernmental Panel on Climate Change [Core Writing Team, H. Lee and J. Romero (eds.)]. IPCC, Geneva, Switzerland.,” Jul. 2023. doi: 10.59327/IPCC/AR6-9789291691647.

[3] “The Paris Agreement | UNFCCC.” Accessed: Dec. 10, 2024. [Online]. Available: https://unfccc.int/process-and-meetings/the-paris-agreement

[4] “What is needed to track progress of emissions reductions under the Paris Agreement? | Climate Action Tracker.” Accessed: Dec. 10, 2024. [Online]. Available: https://climateactiontracker.org/publications/what-needed-track-progress-emissions-eductions-under-paris-agreement/

[5] “Transforming our world: the 2030 Agenda for Sustainable Development | Department of Economic and Social Affairs.” Accessed: Dec. 13, 2024. [Online]. Available: https://sdgs.un.org/2030agenda

[6] “Strategic Energy Technology Plan.” Accessed: Dec. 13, 2024. [Online]. Available: https://energy.ec.europa.eu/topics/research-and-technology/strategic-energy-technology-plan_en

[7] I. Energy Agency, “Technology Perspectives Energy Special Report on Carbon Capture Utilisation and Storage CCUS in clean energy transitions.” [Online]. Available: www.iea.org/t&c/

[8] E. Hanson, C. Nwakile, and V. O. Hammed, “Carbon Capture, Utilization, and Storage (CCUS) Technologies: Evaluating the Effectiveness of Advanced CCUS Solutions for Reducing CO2 Emissions,” *Results in Surfaces and Interfaces*, vol. 33, no. 11, p. 100381, Dec. 2024, doi: 10.1016/j.rsurfi.2024.100381.

[9] M. Bui *et al.*, “Carbon capture and storage (CCS): The way forward,” May 01, 2018, *Royal Society of Chemistry*. doi: 10.1039/c7ee02342a.

[10] P. Styring, D. Jansen, and S. Røkke, “Oxy-fuel combustion for CO_2 capture: Technologies and cost.,” *International Journal of Greenhouse Gas Control*, vol. 5, pp. 1031–1039, 2011.

[11] D. W. Keith, G. Holmes, D. St. Angelo, and K. Heidel, “A Process for Capturing CO2 from the Atmosphere,” *Joule*, vol. 2, no. 8, pp. 1573–1594, Aug. 2018, doi: 10.1016/j.joule.2018.05.006.

[12] K. S. Lackner, S. Brennan, J. M. Matter, A.-H. A. Park, A. Wright, and B. van der Zwaan, “The urgency of the development of CO2 capture from ambient air.,” *Proc Natl Acad Sci U S A*, vol. 109, no. 33, pp. 13156–62, Aug. 2012, doi: 10.1073/pnas.1108765109.

[13] “The Global CO2 Initiative, ‘Carbon dioxide Utilization (CO2U) – ICEF Roadmap 2.0,’ 2017.”.

[14] K. Z. House, A. C. Baclig, M. Ranjan, E. A. Van Nierop, J. Wilcox, and H. J. Herzog, “Economic and energetic analysis of capturing CO 2 from ambient air,” 2011, doi: 10.1073/pnas.1012253108/-/DCSupplemental.

[15] Bianchi Stefano, Lanzini Andrea, and Buffo Giulio, “Process modelling of a Direct Air Capture (DAC) system based on the Kraft process,” 2018. Accessed: Feb. 23, 2025. [Online]. Available: http://webthesis.biblio.polito.it/id/eprint/9262

[16] A. Sodiq *et al.*, “A review on progress made in direct air capture of CO2,” Feb. 01, 2023, *Elsevier B.V.* doi: 10.1016/j.eti.2022.102991.

[17] J. Hack, N. Maeda, and D. M. Meier, “Review on CO2Capture Using Amine-Functionalized Materials,” *ACS Omega*, vol. 7, no. 44, pp. 39520–39530, Nov. 2022, doi: 10.1021/ACSOMEGA.2C03385/ASSET/IMAGES/LARGE/AO2C03385_0004.JPEG.

[18] F. Sabatino, A. Grimm, F. Gallucci, M. van Sint Annaland, G. J. Kramer, and M. Gazzani, “A comparative energy and costs assessment and optimization for direct air capture technologies,” *Joule*, vol. 5, no. 8, pp. 2047–2076, Aug. 2021, doi: 10.1016/j.joule.2021.05.023.

[19] M. Fasihi, O. Efimova, and C. Breyer, “Techno-economic assessment of CO2 direct air capture plants,” *J Clean Prod*, vol. 224, pp. 957–980, Jul. 2019, doi: 10.1016/J.JCLEPRO.2019.03.086.

[20] V. Gutknecht, S. Ó. Snæbjörnsdóttir, B. Sigfússon, E. S. Aradóttir, and L. Charles, “Creating a carbon dioxide removal solution by combining rapid mineralization of CO2 with direct air capture,” *Energy Procedia*, vol. 146, pp. 129–134, Jul. 2018, doi: 10.1016/J.EGYPRO.2018.07.017.

[21] B. Dutcher, M. Fan, and A. G. Russell, “Amine-based CO2 capture technology development from the beginning of 2013-A review,” *ACS Appl Mater Interfaces*, vol. 7, no. 4, pp. 2137–2148, Feb. 2015, doi: 10.1021/AM507465F.

[22] Z. Zolfaghari, A. Aslani, R. Zahedi, and S. Kazzazi, “Simulation of carbon dioxide direct air capture plant using potassium hydroxide aqueous Solution: Energy optimization and CO2 purity enhancement,” *Energy Conversion and Management: X*, vol. 21, Jan. 2024, doi: 10.1016/j.ecmx.2023.100489.

[23] “A Wall of Fans Cleans Air - ASME.” Accessed: Feb. 26, 2025. [Online]. Available: https://www.asme.org/topics-resources/content/a-wall-of-fans-cleans-air

[24] G. Holmes and D. W. Keith, “An air–liquid contactor for large-scale capture of CO2 from air,” *Philosophical Transactions of the Royal Society A: Mathematical, Physical and Engineering Sciences*, vol. 370, no. 1974, pp. 4380–4403, Sep. 2012, doi: 10.1098/RSTA.2012.0137.

[25] K. Heidel, D. Keith, A. Singh, and G. Holmes, “Process design and costing of an air-contactor for air-capture,” *Energy Procedia*, vol. 4, pp. 2861–2868, Jan. 2011, doi: 10.1016/J.EGYPRO.2011.02.192.

[26] C. A. Obasanjo, G. Gao, J. Crane, V. Golovanova, F. P. García de Arquer, and C. T. Dinh, “High-rate and selective conversion of CO2 from aqueous solutions to hydrocarbons,” *Nature Communications 2023 14:1*, vol. 14, no. 1, pp. 1–12, Jun. 2023, doi: 10.1038/s41467-023-38963-y.

[27] V. Barbarossa and G. Vanga, “Metanazione della CO 2 con H 2”.

[28] D. Parigi, “Technical and Economical comparison between synthetic Methanol and Methane,” Apr. 2018.

[29] B. Varandas, M. Oliveira, C. Andrade, and A. Borges, “Thermodynamic Equilibrium Analysis of CO2 Methanation through Equilibrium Constants: A Comparative Simulation Study,” *Physchem 2024, Vol. 4, Pages 258-271*, vol. 4, no. 3, pp. 258–271, Jul. 2024, doi: 10.3390/PHYSCHEM4030018.

[30] H. M. Chang and I. V. Zenyuk, “Membrane electrode assembly design to prevent CO2 crossover in CO2 reduction reaction electrolysis,” *Communications Chemistry 2023 6:1*, vol. 6, no. 1, pp. 1–3, Jan. 2023, doi: 10.1038/s42004-022-00806-0.

[31] “Methanol from CO2: a technology and outlook overview.” Accessed: Feb. 20, 2025. [Online]. Available: https://www.digitalrefining.com/article/1002891/methanol-from-co2-a-technology-and-outlook-overview

[32] “About Methanol | Methanol Institute.” Accessed: Feb. 20, 2025. [Online]. Available: https://www.methanol.org/about-methanol/

[33] G. Cau *et al.*, “Approfondimenti preliminari su tecnologie e processi di sintesi di metano, metanolo e dimetiletere (DME) mediante idrogenazione catalitica della CO 2.”

[34] N. J. Azhari *et al.*, “Methanol synthesis from CO2: A mechanistic overview,” *Results in Engineering*, vol. 16, p. 100711, Dec. 2022, doi: 10.1016/J.RINENG.2022.100711.

[35] G. Bozzano and F. Manenti, “Efficient methanol synthesis: Perspectives, technologies and optimization strategies,” *Prog Energy Combust Sci*, vol. 56, pp. 71–105, Sep. 2016, doi: 10.1016/J.PECS.2016.06.001.

[36] G. Pacchioni, “From CO2 to Methanol on Cu/ZnO/Al2O3 Industrial Catalyst. What Do We Know about the Active Phase and the Reaction Mechanism?,” *ACS Catal*, vol. 14, no. 4, pp. 2730–2745, Feb. 2024, doi: 10.1021/ACSCATAL.3C05669/ASSET/IMAGES/MEDIUM/CS3C05669_0015.GIF.

[37] T. A. Atsbha, T. Yoon, P. Seongho, and C. J. Lee, “A review on the catalytic conversion of CO2using H2for synthesis of CO, methanol, and hydrocarbons,” *Journal of CO2 Utilization*, vol. 44, Feb. 2021, doi: 10.1016/J.JCOU.2020.101413.

[38] X. M. Liu, G. Q. Lu, Z. F. Yan, and J. Beltramini, “Recent Advances in Catalysts for Methanol Synthesis via Hydrogenation of CO and CO2,” *Ind Eng Chem Res*, vol. 42, no. 25, pp. 6518–6530, Dec. 2003, doi: 10.1021/IE020979S.

[39] M. K. Awasthi, R. K. Rai, S. Behrens, and S. K. Singh, “Low-temperature hydrogen production from methanol over a ruthenium catalyst in water,” *Catal Sci Technol*, vol. 11, no. 1, pp. 136–142, Jan. 2021, doi: 10.1039/D0CY01470B.

[40] E. Catizzone, C. Freda, G. Braccio, F. Frusteri, and G. Bonura, “Dimethyl ether as circular hydrogen carrier: Catalytic aspects of hydrogenation/dehydrogenation steps,” *Journal of Energy Chemistry*, vol. 58, pp. 55–77, Jul. 2021, doi: 10.1016/J.JECHEM.2020.09.040.

[41] P. Nieuwenhuis and P. Wells, “Powertrain and fuel,” *The Automotive Industry and the Environment*, pp. 73–86, Jan. 2003, doi: 10.1016/B978-1-85573-713-6.50009-3.

[42] M. Grzesik and J. Skrzypek, “Chemical equilibria in direct synthesis of dimethyl ether,” *Stud Surf Sci Catal*, vol. 122, pp. 407–410, Jan. 1999, doi: 10.1016/S0167-2991(99)80173-6.

[43] M. L. Y. Riu, M. Ye, and C. C. Cummins, “Alleviating Strain in Organic Molecules by Incorporation of Phosphorus: Synthesis of Triphosphatetrahedrane,” *J Am Chem Soc*, vol. 143, no. 40, pp. 16354–16357, Oct. 2021, doi: 10.1021/JACS.1C07959.

[44] Z. Song, D. Han, M. Yang, J. Huang, X. Shao, and H. Li, “Formic acid formation via direct hydration reaction (CO + H2O → HCOOH) on magnesia-silver composite,” *Appl Surf Sci*, vol. 607, p. 155067, Jan. 2023, doi: 10.1016/J.APSUSC.2022.155067.

[45] H. Renon and J. M. Prausnitz, “Local compositions in thermodynamic excess functions for liquid mixtures,” *AIChE Journal*, vol. 14, no. 1, pp. 135–144, Jan. 1968, doi: 10.1002/AIC.690140124.

[46] C. -C Chen, H. I. Britt, J. F. Boston, and L. B. Evans, “Local composition model for excess Gibbs energy of electrolyte systems. Part I: Single solvent, single completely dissociated electrolyte systems,” *AIChE Journal*, vol. 28, no. 4, pp. 588–596, Jul. 1982, doi: 10.1002/AIC.690280410.

[47] A. Smahi, O. Authier, M. Kanniche, L. Grandjean, and C. Bouallou, “Thermodynamic Analysis of CO2 Absorption in Aqueous MDEA-PZ Solution Using ELECNRTL and ENRTL-RK Models,” *Chem Eng Trans*, vol. 103, pp. 631–636, 2023, doi: 10.3303/CET23103106.

[48] G. Soave, “20 years of Redlich-Kwong equation of state,” *Fluid Phase Equilib*, vol. 82, no. C, pp. 345–359, 1993, doi: 10.1016/0378-3812(93)87158-W.

[49] “Peng-Robinson EOS (1976) | PNG 520: Phase Behavior of Natural Gas and Condensate Fluids.” Accessed: Jan. 23, 2025. [Online]. Available: https://www.e-education.psu.edu/png520/m11_p2.html

[50] A. H. Harvey and F. L. Smith, “Avoid Common Pitfalls when using Henry’s Law,” 2007. Accessed: Jan. 24, 2025. [Online]. Available: https://www.nist.gov/publications/avoid-common-pitfalls-when-using-henrys-law

[51] F. Isa, H. Zabiri, N. Harun, A. M. Shariff, N. K. S. Ng, and M. A. A. Afian, “Simulation Comparison Between Equilibrium and Rate-Based Approach for CO2 Removal Via Promoted K2CO3 with Glycine,” in *E3S Web of Conferences*, EDP Sciences, Jul. 2021. doi: 10.1051/e3sconf/202128703005.

[52] J. D. Seader, E. J. Henley, and D. K. Roper, “(CBE3233) Separation Process Principles 3e,” *Separation process principles* , pp. 670–725, 2011, Accessed: Jan. 24, 2025. [Online]. Available: https://www.academia.edu/28435059/_CBE3233_Separation_Process_Principles_3e

[53] “Langmuir-Hinshelwood-Hougen-Watson(LHHW) model”.

[54] M. Cheng, P. Verma, Z. Yang, and R. L. Axelbaum, “Flexible cryogenic air separation unit—An application for low-carbon fossil-fuel plants,” *Sep Purif Technol*, vol. 302, 2022, doi: 10.1016/j.seppur.2022.122086.

[55] F. Calogero, “Methanol synthesis through CO2 hydrogenation: reactor and process modeling,” Dec. 2018.

[56] C. Wu, Q. Zhu, B. Dou, Z. Fu, J. Wang, and S. Mao, “Thermodynamic analysis of a solid oxide electrolysis cell system in thermoneutral mode integrated with industrial waste heat for hydrogen production,” *Energy*, vol. 301, p. 131678, Aug. 2024, doi: 10.1016/J.ENERGY.2024.131678.

[57] D. Mignard, M. Sahibzada, J. M. Duthie, and H. W. Whittington, “Methanol synthesis from flue-gas CO2 and renewable electricity: a feasibility study,” *Int J Hydrogen Energy*, vol. 28, no. 4, pp. 455–464, Apr. 2003, doi: 10.1016/S0360-3199(02)00082-4.

[58] G. GRAAF, P. SIJTSEMA, E. STAMHUIS, and G. JOOSTEN, “CHEMICAL-EQUILIBRIA IN METHANOL SYNTHESIS,” *Chem Eng Sci*, vol. 41, no. 11, pp. 2883–2890, 1986, Accessed: Feb. 23, 2025. [Online]. Available: https://research.rug.nl/en/publications/chemical-equilibria-in-methanol-synthesis

[59] L. March, “Introduction to Pinch Technology,” 1998, Accessed: Feb. 18, 2025. [Online]. Available: www.linnhoffmarch.com

[60] I. C. . Kemp, “Pinch Analysis and Process Integration : a User Guide on Process Integration for the Efficient Use of Energy,” p. 415, 2011.

APPENDIX

AIR CONTACTOR HIERARCHY-STANDALONE DAC													
STREAM-ID	1	2_1	2_2	3	4	5	6	7	8	9	10	AIR-IN	TO-AIR
Mass flow rate[ton/h]	121,00	250,85	4543,36	99,30	250099,30	254642,66	7374,33	7374,33	272,56	7646,89	7646,89	250000,00	247268,33
Temperature [°C]	26,10	21,00	21,00	43,00	21,01	21,89	21,32	21,33	31,86	21,64	19,20	21,00	21,32
Pressure [bar]	1	1	1	1	1	1	0,95	1	1	1	1	1	0,95
Mass Fractions													
O2	0,021071	0	0	0,025671	0,230674	0,226558	0	0	1,98E-06	7,07E-08	7,07E-08	0,230755	0,233315
CO2	0,127546	4,16E-14	4,16E-14	0,016455	0,000622	0,000156	9,27E-08	9,27E-08	0,000231	2,07E-07	1,93E-07	0,000616	0,000161
H2O	0,108674	0,886879	0,886879	0,052923	0,01564	0,031318	0,919227	0,919227	0,841085	0,916442	0,916443	0,015625	0,004838
KOH	0	0	0	0	0	0	0	0	0	0	0	0	0
K2CO3	0	0	0	0	0	0	0	0	0	0	0	0	0
N2	0,742709	0	0	0,904951	0,753064	0,739628	0	0	3,62E-05	1,29E-06	1,29E-06	0,753004	0,761686
H3O+	0	6,03E-17	6,03E-17	0	0	2,34E-15	2,73E-13	2,73E-13	1,42E-11	4,02E-13	3,59E-13	0	0
K+	0	0,071318	0,071318	0	0	0,001272	0,043939	0,043939	0,065639	0,044713	0,044713	0	0
HCO3-	0	2,63E-06	2,63E-06	0	0	0,00018	0,006142	0,006142	0,083881	0,008923	0,00892	0	0
OH-	0	0,016921	0,016921	0	0	2,86E-07	1,15E-05	1,15E-05	3,29E-07	7,79E-06	6,96E-06	0	0
CO3--	0	0,02488	0,02488	0	0	0,000888	0,03068	0,03068	0,009125	0,029913	0,029916	0	0
CACO3	0	0	0	0	0	0	0	0	0	0	0	0	0
CA(OH)2	0	0	0	0	0	0	0	0	0	0	0	0	0
CAO	0	0	0	0	0	0	0	0	0	0	0	0	0
CA++	0	0	0	0	0	0	0	0	0	0	0	0	0
CAOH+	0	0	0	0	0	0	0	0	0	0	0	0	0
KOH(S)	0	0	0	0	0	0	0	0	0	0	0	0	0
CACO3(S)	0	0	0	0	0	0	0	0	0	0	0	0	0
K2CO3(S)	0	0	0	0	0	0	0	0	0	0	0	0	0
CH4	3,36E-22	0	0	0	0	0	0	0	0	0	0	0	0
C2H6	2,88E-37	0	0	0	0	0	0	0	0	0	0	0	0
CAO(S)	0	0	0	0	0	0	0	0	0	0	0	0	0
AR	0	0	0	0	0	0	0	0	0	0	0	0	0

PELLET REACTOR HIERARCHY pt.1-STANDALONE DAC													
STREAM-ID	10	11	12	13	14	15	16	17	18	19	20	21	22
Mass flow rate[ton/h]	7646,89	769,98	81559,86	197,8252	81362,03	81,36203	81280,67	8214,097	73066,57	73066,57	95,58832	8118,508	279,1872
Temperature [°C]	19,20	21,00	25,00	25,00241	25,00241	25,00241	25,00241	25,00245	25,00245	25,00537	25,00253	25,00253	25,00242
Pressure [bar]	1	1	1	1	1	1	1	0,9	0,9	1	1	1	1
Mass Fractions													
O2	0,000541	0	0,005408	0	0,005408	5,41E-06	0,005403	0,00054	0,004863	0,004863	0	0,00054	5,41E-06
CO2	0,001477	1,29E-18	8,44E-09	0	8,44E-09	8,44E-12	8,43E-09	8,43E-10	7,59E-09	7,59E-09	0	8,43E-10	8,44E-12
H2O	7007,936	543,62	75747,44	0	75747,44	75,74744	75671,69	7567,169	68104,52	68104,52	0	7567,169	75,74744
KOH	0	0	0	0	0	0	0	0	0	0	0	0	0
K2CO3	0	0	0	0	0	0	0	0	0	0	0	0	0
N2	0,00988	0	0,098841	0	0,098841	9,88E-05	0,098742	0,009874	0,088868	0,088868	0	0,009874	9,88E-05
H3O+	2,75E-09	1,65E-13	2,47E-11	0	2,47E-11	2,47E-14	2,47E-11	2,47E-12	2,22E-11	2,22E-11	0	2,47E-12	2,47E-14
K+	341,9142	5,350115	3474,044	0	3474,044	3,474044	3470,57	347,057	3123,513	3123,513	0	347,057	3,474044
HCO3-	68,21379	8,62E-10	2,33E-01	0	0,233137	0,000233	0,232904	0,02329	0,209613	0,209641	0	0,023291	0,000233
OH-	0,053236	61,01631	813,2586	0	813,2586	0,813259	812,4454	81,24454	731,2008	731,2008	0	81,24454	0,813259
CO3--	228,7607	0,000187	1231,265	0	1231,265	1,231265	1230,033	123,0033	1107,03	1107,03	0	123,0033	1,231265
CACO3	0	0	0	0	0	0	0	0	0	0	0	0	0
CA(OH)2	0	0	0	0	0	0	0	0	0	0	0	0	0
CAO	0	0	0	0	0	0	0	0	0	0	0	0	0
CA++	0	22,92405	0,001392	0	0,001392	1,39E-06	0,00139	0,000139	0,001251	0,001251	0	0,000139	1,39E-06
CAOH+	0	131,6771	0,003798	0	0,003798	3,80E-06	0,003794	0,000379	0,003415	0,003415	0	0,000379	3,80E-06
KOH(S)	0	0	0	0	0	0	0	0	0	0	0	0	0
CACO3(S)	0	5,389689	293,5092	197,8252	95,684	0,095684	95,58832	95,58832	0	0	95,58832	1,81E-08	197,9209
K2CO3(S)	0	0	0	0	0	0	0	0	0	0	0	0	0
CH4	0,00E+00	0	0	0	0	0	0	0	0	0	0	0	0
C2H6	0,00E+00	0	0	0	0	0	0	0	0	0	0	0	0
CAO(S)	0	0	0	0	0	0	0	0	0	0	0	0	0
AR	0	0	0	0	0	0	0	0	0	0	0	0	0

PELLET REACTOR HIERARCHY pt.2-STANDALONE DAC							
STREAM-ID	23	24	25	26	27	28	IN-MIX
Mass flow rate[ton/h]	3,447	21,79775	70,34357	359,4581	81,26635	278,1917	9,92725
Temperature [°C]	25,00253	25,00253	25,00253	24,94133	24,94221	24,94221	21
Pressure [bar]	1	1	1	1	1	1	1
Mass Fractions							
O2	0	0	0	5,41E-06	5,41E-06	0	0
CO2	0	0	0	8,38E-12	8,38E-12	0	0
H2O	0	0	0	75,74744	75,74744	0	0
KOH	0	0	0	0	0	0	0
K2CO3	0	0	0	0	0	0	0
N2	0	0	0	9,88E-05	9,88E-05	0	0
H3O+	0	0	0	2,46E-14	2,46E-14	0	0
K+	0	0	0	3,474044	3,474044	0	0
HCO3-	0	0	0	0,000233	0,000233	0	0
OH-	0	0	0	0,813258	0,813258	0	0
CO3--	0	0	0	1,231265	1,231265	0	0
CACO3	0	0	0	0	0	0	0
CA(OH)2	0	0	0	0	0	0	0
CAO	0	0	0	0	0	0	0
CA++	0	0	0	1,39E-06	1,39E-06	0	0
CAOH+	0	0	0	3,80E-06	3,80E-06	0	0
KOH(S)	0	0	0	0	0	0	0
CACO3(S)	3,447	21,79775	70,34357	278,1917	0	278,1917	9,92725
K2CO3(S)	0	0	0	0	0	0	0
CH4	0	0	0	0	0	0	0
C2H6	0	0	0	0	0	0	0
CAO(S)	0	0	0	0	0	0	0
AR	0	0	0	0	0	0	0

WASHER/SLAKER HIERARCHY pt.1-STANDALONE DAC													
STREAM-ID	11_1	11_2	28	29	30	31	32	32_1	33	34	35	36	37
Mass flow rate[ton/h]	711,52	711,52	278,19	558,11	335,56	500,74	500,74	375,96	222,55	278,19	170,72	7,00	401,37
Temperature [°C]	63,93	21,00	24,94	54,09992	51,39672	51,39672	300	85	300	300	674	198,4733	300
Pressure [bar]	1	1	1	1	1	1	1	1	0,9	0,9	1	1	1
Mass Fractions													
O2	0	0	0	0	0	0	0	0	0	0	0	0	0
CO2	3,39E-19	2,33E-21	0,00E+00	3,57E-06	3,57E-06	7,94E-09	1,71E-06	6,29E-19	3,86E-06	0	0	0	1,16E-12
H2O	0,73083	0,73083	0	0,999996	0,999996	0,444441	0,444443	0,490592	0,999996	0	0	1	0,459536
KOH	0	0	0	0	0	0	0	0	0	0	0	0	0
K2CO3	0	0	0	0	0	0	0	0	0	0	0	0	0
N2	0	0	0	0	0	0	0	0	0	0	0	0	0
H3O+	5,57E-15	3,06E-16	0,00E+00	1,25E-07	1,02E-07	7,87E-12	0	6,91E-15	0	0	0	0	1,38E-17
K+	0	0	0	0	0	0	0	0	0	0	0	0	0
HCO3-	9,06E-12	1,35E-12	0,00E+00	3,99E-07	4,84E-07	6,54E-06	0	7,27E-12	0	0	0	0	2,39E-12
OH-	0,069823	0,07307	0	1,78E-10	1,86E-10	5,02E-07	0	0,12627	0	0	0	0	0,120226
CO3--	1,94E-07	2,45E-07	0	4,23E-12	6,12E-12	5,27E-07	0	2,33E-07	0	0	0	0	4,43E-07
CACO3	0	0	0	0	0	0	0	0	0	0	0	0	0
CA(OH)2	0	0	0	0	0	0	0	0	0	0	0	0	0
CAO	0	0	0	0	0	0	0	0	0	0	0	0	0
CA++	0,0235	0,031151	0	0	5,13E-08	3,09E-06	0	0,030635	0	0	0	0	0,033288
CAOH+	0,167408	0,156509	0	0	2,42E-14	8,03E-09	0	0,336539	0	0	0	0	0,308693
KOH(S)	0	0	0	0	0	0	0	0	0	0	0	0	0
CACO3(S)	0,008439	0,008439	1	0	0	0,555548	0,555556	0,015963	0	1	0,035144	0	0,016522
K2CO3(S)	0	0	0	0	0	0	0	0	0	0	0	0	0
CH4	0,00E+00	0	0	0	0	0	0	0	0	0	0	0	0
C2H6	0,00E+00	0	0	0	0	0	0	0	0	0	0	0	0
CAO(S)	0	0	0	0	0	0	0	0	0	0	0,964856	0	0,061734
AR	0	0	0	0	0	0	0	0	0	0	0	0	0

WASHER/SLAKER HIERARCHY pt.2-STANDALONE DAC						
STREAM-ID	38	39	40	41	42	24_1
Mass flow rate[ton/h]	1,10	400,27	375,96	24,31	299,99	21,80
Temperature [°C]	300	300	300	300	645,88	25
Pressure [bar]	1	1	1	1	1	1
Mass Fractions						
O2	0	0	0	0	0	0
CO2	0	1,16E-12	1,23E-12	0	0	0
H2O	0	0,4608	0,490592	0	0	0
KOH	0	0	0	0	0	0
K2CO3	0	0	0	0	0	0
N2	0	0	0	0	0	0
H3O+	0	0	1,47E-17	0	0	0
K+	0	0	0	0	0	0
HCO3-	0	0	2,55E-12	0	0	0
OH-	0	0	0,128351	0	0	0
CO3--	0	0	4,73E-07	0	0	0
CACO3	0	0,014994	0	0	0	0
CA(OH)2	0	0,463478	0	0	0	0
CAO	0	0	0	0	0	0
CA++	0	0	0,035538	0	0	0
CAOH+	0	0	0,329555	0	0	0
KOH(S)	0	0	0	0	0	0
CACO3(S)	0,572312	0	0,015963	0	1	1
K2CO3(S)	0	0	0	0	0	0
CH4	0	0	0	0	0	0
C2H6	0	0	0	0	0	0
CAO(S)	0,427688	0,060728	0	1	0	0
AR	0	0	0	0	0	0

CALCINER HIERARCHY-STANDALONE DAC									
STREAM-ID	42	43_NG	44	45	46	47	48	O2-TOCAL	80
Mass flow rate[ton/h]	299,99	15,02	68,60	368,59	170,72	197,87	197,87	53,58	53,58
Temperature [°C]	645,88	25,00	900,00	900,00	900,00	900,00	217,00	652,00	93,00
Pressure [bar]	1	10	1	1	1	1	1	1	1
Mass Fractions									
O2	0	0	0,003923	0,00073	0	0,00136	0,00136	0,963055	0,963055
CO2	0,00E+00	7,50E-02	5,38E-01	0,450897	0	0,839919	0,839919	0,002634	0,002634
H2O	0	0	0,417011	0,077611	0	0,144572	0,144572	0	0
KOH	0	0	0	0	0	0	0	0	0
K2CO3	0	0	0	0	0	0	0	0	0
N2	0	0,064	0,040812	0,007596	0	0,014149	0,014149	0,034311	0,034311
H3O+	0,00E+00	0,00E+00	0,00E+00	0	0	0	0	0	0
K+	0	0	0	0	0	0	0	0	0
HCO3-	0,00E+00	0,00E+00	0,00E+00	0	0	0	0	0	0
OH-	0	0	0	0	0	0	0	0	0
CO3--	0,00E+00	0,00E+00	0	0	0	0	0	0	0
CACO3	0	0	0	0	0	0	0	0	0
CA(OH)2	0	0	0	0	0	0	0	0	0
CAO	0	0	0	0	0	0	0	0	0
CA++	0	0	0	0	0	0	0	0	0
CAOH+	0	0	0	0	0	0	0	0	0
KOH(S)	0	0	0	0	0	0	0	0	0
CACO3(S)	1	0	0	0,016278	0,035144	0	0	0	0
K2CO3(S)	0	0	0	0	0	0	0	0	0
CH4	0,00E+00	0,796	0	0	0	0	0	0	0
C2H6	0,00E+00	0,065	0	0	0	0	0	0	0
CAO(S)	0	0	0	0,446889	0,964856	0	0	0	0
AR	0	0	0	0	0	0	0	0	0

ASU HIERARCHY pt.1-STANDALONE DAC

STREAM-ID	AIR-02	DRY-AIR	N2-L1	N2-L2	N2-OUT	N2-P	N2-R	N2-VAP	O2-P	O2-R	S2	S3	S4
Mass flow rate[ton/h]	229,19	225,61	115,61	61,08	172,03	172,03	61,08	176,70	53,58	113,54	229,19	226,94	2,25
Temperature [°C]	16,00	21,00	16,00	-180,20	-180,20	21,00	-192,99	-190,30	-179,03	-181,39	9,50	9,50	9,50
Pressure [bar]	5,00	1,00	5,00	5	5	1	1,35	5	5	1,35	1	1	1
Mass Fractions													
O2	0,230755	0,234418	2,12E-05	2,12E-05	0,00748	0,00748	2,12E-05	2,12E-05	0,963055	0,360529	0,230755	0,23304	6,33E-07
CO2	6,16E-04	6,25E-04	4,83E-71	4,83E-71	5,82E-40	5,82E-40	4,83E-71	4,83E-71	0,002634	0,000962	0,000616	0,000622	9,44E-09
H2O	0,015625	0	0	0	0	0	0	0	0	0	0,015625	0,00588	0,999999
KOH	0	0	0	0	0	0	0	0	0	0	0	0	0
K2CO3	0	0	0	0	0	0	0	0	0	0	0	0	0
N2	0,753004	0,764956	0,999979	0,999979	0,99252	0,99252	0,999979	0,999979	0,034311	0,638509	0,753004	0,760458	5,86E-08
H3O+	0,00E+00	0,00E+00	0,00E+00	0	0	0	0	0	0	0	0	0	0
K+	0	0	0	0	0	0	0	0	0	0	0	0	0
HCO3-	0,00E+00	0,00E+00	0,00E+00	0	0	0	0	0	0	0	0	0	0
OH-	0	0	0	0	0	0	0	0	0	0	0	0	0
CO3--	0,00E+00	0,00E+00	0	0	0	0	0	0	0	0	0	0	0
CACO3	0	0	0	0	0	0	0	0	0	0	0	0	0
CA(OH)2	0	0	0	0	0	0	0	0	0	0	0	0	0
CAO	0	0	0	0	0	0	0	0	0	0	0	0	0
CA++	0	0	0	0	0	0	0	0	0	0	0	0	0
CAOH+	0	0	0	0	0	0	0	0	0	0	0	0	0
KOH(S)	0	0	0	0	0	0	0	0	0	0	0	0	0
CACO3(S)	0	0	0	0	0	0	0	0	0	0	0	0	0
K2CO3(S)	0	0	0	0	0	0	0	0	0	0	0	0	0
CH4	0,00E+00	0	0	0	0	0	0	0	0	0	0	0	0
C2H6	0,00E+00	0	0	0	0	0	0	0	0	0	0	0	0
CAO(S)	0	0	0	0	0	0	0	0	0	0	0	0	0
AR	0	0	0	0	0	0	0	0	0	0	0	0	0

ASU HIERARCHY pt.2-STANDALONE DAC

STREAM-ID	S5	S6	S7	S8	S9	S10	S11	S12	S13	S14	S15	S16	S17	S18	S19	S20
Mass flow rate[ton/h]	226,94	226,94	226,94	226,94	226,94	226,94	1,33	50,99	50,99	198,12	198,12	144,54	174,62	174,62	176,70	113,54
Temperature [°C]	72,56	35,00	131,49	35,00	88,34	16,00	16,00	16,00	-179,30	-183,02	-181,39	-181,39	16,00	-174,60	-180,20	-175,76
Pressure [bar]	1,67	1,67	3,33	3,33	5,00	5,00	5,00	5,00	5,00	1,35	1,35	1,35	5,00	5,00	5,00	5,00
Mass Fractions																
O2	0,23304	0,23304	0,23304	0,23304	0,23304	0,23304	0	0,234418	0,234418	0,904411	0,904411	0,882676	0,234418	0,234418	2,12E-05	0,360529
CO2	0,000622	0,000622	0,000622	0,000622	0,000622	0,000622	0	0,000625	0,000625	0,000712	0,000712	1,12E-07	0,000625	0,000625	4,83E-71	0,000962
H2O	0,00588	0,00588	0,00588	0,00588	0,00588	0,00588	1	0	0	0	0	0	0	0	0	0
KOH	0	0	0	0	0	0	0	0	0	0	0	0	0	0	0	0
K2CO3	0	0	0	0	0	0	0	0	0	0	0	0	0	0	0	0
N2	0,760458	0,760458	0,760458	0,760458	0,760458	0,760458	0	0,764956	0,764956	0,094877	0,094877	0,117324	0,764956	0,764956	0,999979	0,638509
H3O+	0	0	0	0	0	0	0	0	0	0	0	0	0	0	0	0
K+	0	0	0	0	0	0	0	0	0	0	0	0	0	0	0	0
HCO3-	0	0	0	0	0	0	0	0	0	0	0	0	0	0	0	0
OH-	0	0	0	0	0	0	0	0	0	0	0	0	0	0	0	0
CO3--	0	0	0	0	0	0	0	0	0	0	0	0	0	0	0	0
CACO3	0	0	0	0	0	0	0	0	0	0	0	0	0	0	0	0
CA(OH)2	0	0	0	0	0	0	0	0	0	0	0	0	0	0	0	0
CAO	0	0	0	0	0	0	0	0	0	0	0	0	0	0	0	0
CA++	0	0	0	0	0	0	0	0	0	0	0	0	0	0	0	0
CAOH+	0	0	0	0	0	0	0	0	0	0	0	0	0	0	0	0
KOH(S)	0	0	0	0	0	0	0	0	0	0	0	0	0	0	0	0
CACO3(S)	0	0	0	0	0	0	0	0	0	0	0	0	0	0	0	0
K2CO3(S)	0	0	0	0	0	0	0	0	0	0	0	0	0	0	0	0
CH4	0	0	0	0	0	0	0	0	0	0	0	0	0	0	0	0
C2H6	0	0	0	0	0	0	0	0	0	0	0	0	0	0	0	0
CAO(S)	0	0	0	0	0	0	0	0	0	0	0	0	0	0	0	0
AR	0	0	0	0	0	0	0	0	0	0	0	0	0	0	0	0

COMPRESSION TRAIN HIERARCHY-STANDALONE DAC											
STREAM-ID	29	48	49	50	51	52	53	54	55	56	CO2
Mass flow rate[ton/h]	529,50	197,87	169,26	169,26	169,26	169,26	169,26	169,26	169,26	169,26	169,26
Temperature [°C]	21,00	217,00	54,10	168,45	45,00	158,30	45,00	161,69	45,00	166,74	45,00
Pressure [bar]	1	1	1	3,50	3,50	12,25	12,25	42,88	42,88	150,06	150,06
Mass Fractions											
O2	0	0,00136	1,59E-03	0,00159	0,0015899	0,0015899	0,00159	0,00159	0,00159	0,00159	0,00159
CO2	0,00E+00	8,40E-01	9,82E-01	0,98187	0,9818697	0,9818697	0,98187	0,98187	0,98187	0,98187	0,98187
H2O	1	0,144572	0	0	0	0	0	0	0	0	0
KOH	0	0	0	0	0	0	0	0	0	0	0
K2CO3	0	0	0	0	0	0	0	0	0	0	0
N2	0	0,014149	0,0165404	0,01654	0,0165404	0,0165404	0,01654	0,01654	0,01654	0,01654	0,01654
H3O+	1,63E-09	0,00E+00	0,00E+00	0	0	0	0	0	0	0	0
K+	0	0	0	0	0	0	0	0	0	0	0
HCO3-	0,00E+00	0,00E+00	0,00E+00	0	0	0	0	0	0	0	0
OH-	1,46E-09	0	0	0	0	0	0	0	0	0	0
CO3--	0,00E+00	0,00E+00	0	0	0	0	0	0	0	0	0
CACO3	0	0	0	0	0	0	0	0	0	0	0
CA(OH)2	0	0	0	0	0	0	0	0	0	0	0
CAO	0	0	0	0	0	0	0	0	0	0	0
CA++	0	0	0	0	0	0	0	0	0	0	0
CAOH+	0	0	0	0	0	0	0	0	0	0	0
KOH(S)	0	0	0	0	0	0	0	0	0	0	0
CACO3(S)	0	0	0	0	0	0	0	0	0	0	0
K2CO3(S)	0	0	0	0	0	0	0	0	0	0	0
CH4	0,00E+00	0	0	0	0	0	0	0	0	0	0
C2H6	0,00E+00	0	0	0	0	0	0	0	0	0	0
CAO(S)	0	0	0	0	0	0	0	0	0	0	0
AR	0	0	0	0	0	0	0	0	0	0	0

POWER ISLAND-STANDALONE DAC						
STREAM-ID	AIR-01	GC-1	GC-2	GC-3	NG	1
Mass flow rate[ton/h]	114,70	114,70	121,00	121,00	6,30	121,00
Temperature [°C]	20,00	315,39	1600,00	892,32	25,00	26,10
Pressure [bar]	1	10	10	1	10	1
Mass Fractions						
O2	0,21	0,21	0,0210707	0,021071	0	0,0210707
CO2	0	0	0,1275462	0,127546	0,075	0,1275462
H2O	0,01	0,01	0,1086743	0,108674	0	0,1086743
KOH	0	0	0	0	0	0
K2CO3	0	0	0	0	0	0
N2	0,78	0,78	0,7427088	0,742709	0,064	0,7427088
H3O+	0	0	0	0	0	0
K+	0	0	0	0	0	0
HCO3-	0	0	0	0	0	0
OH-	0	0	0	0	0	0
CO3--	0	0	0	0	0	0
CACO3	0	0	0	0	0	0
CA(OH)2	0	0	0	0	0	0
CAO	0	0	0	0	0	0
CA++	0	0	0	0	0	0
CAOH+	0	0	0	0	0	0
KOH(S)	0	0	0	0	0	0
CACO3(S)	0	0	0	0	0	0
K2CO3(S)	0	0	0	0	0	0
CH4	0	0	3,36E-22	3,36E-22	0,796	3,36E-22
C2H6	0	0	2,88E-37	2,88E-37	0,065	2,88E-37
CAO(S)	0	0	0	0	0	0
AR	0	0	0	0	0	0

STEAM CYCLE-STANDALONE DAC												
STREAM-ID	SC-1	SC-1-2	SC-2	SC-3	SC-4	SC-5	SC-6	SC-7	SC-8	SC-9	H2O-SUP	36-1
Mass flow rate[ton/h]	68,00	68,00	68,00	68,00	68,00	61,00	61,00	61,00	61,00	7,00	7,00	7,00
Temperature [°C]	136,50	135,32	137,08	252,00	253,30	253,30	500,00	222,68	140,07	25,02	25,00	253,30
Pressure [bar]	3,50	3,50	42,00	42,00	42,00	42,00	42,00	3,50	3,50	3,50	1,00	42,00
Mass Fractions												
O2	0	0	0	0	0	0	0	0	0	0	0	0
CO2	0	0	0	0	0	0	0	0	0	0	0	0
H2O	1	1	1	1	1	1	1	1	1	1	1	1
KOH	0	0	0	0	0	0	0	0	0	0	0	0
K2CO3	0	0	0	0	0	0	0	0	0	0	0	0
N2	0	0	0	0	0	0	0	0	0	0	0	0
H3O+	0	0	0	0	0	0	0	0	0	0	0	0
K+	0	0	0	0	0	0	0	0	0	0	0	0
HCO3-	0	0	0	0	0	0	0	0	0	0	0	0
OH-	0	0	0	0	0	0	0	0	0	0	0	0
CO3--	0	0	0	0	0	0	0	0	0	0	0	0
CACO3	0	0	0	0	0	0	0	0	0	0	0	0
CA(OH)2	0	0	0	0	0	0	0	0	0	0	0	0
CAO	0	0	0	0	0	0	0	0	0	0	0	0
CA++	0	0	0	0	0	0	0	0	0	0	0	0
CAOH+	0	0	0	0	0	0	0	0	0	0	0	0
KOH(S)	0	0	0	0	0	0	0	0	0	0	0	0
CACO3(S)	0	0	0	0	0	0	0	0	0	0	0	0
K2CO3(S)	0	0	0	0	0	0	0	0	0	0	0	0
CH4	0	0	0	0	0	0	0	0	0	0	0	0
C2H6	0	0	0	0	0	0	0	0	0	0	0	0
CAO(S)	0	0	0	0	0	0	0	0	0	0	0	0
AR	0	0	0	0	0	0	0	0	0	0	0	0

UTILIZATION FACILITY pt.1-COUPLED DAC															
STREAM-ID	CO2	H1	H2	H3	H4	H5	H6	H7	H8	H9	H10	H11	H12	H13	H9-1
Mass flow rate[ton/h]	167,28	240,89	240,89	240,89	240,89	240,89	240,89	240,89	69,74	171,15	48,18	21,56	21,56	21,56	51,60
Temperature [°C]	45,00	25,00	25,12	207,00	208,00	203,19	700,00	700,00	700,00	700,00	700,00	700,00	100,00	371,92	700,00
Pressure [bar]	75	1	18	18	18,28	15	15	15	15	15	15	15	15	75	15
Mass Fractions															
O2	0,001615	0	0	0	0	0	0	0,710481	0	1	0	0	0	0	1
CO2	0,992638	0	0	0	0	0	0	0	0	0	0	0	0	0	0
H2O	0	1	1	1	1	1	1	0,2	0,690802	0	1	0	0	0	0
KOH	0	0	0	0	0	0	0	0	0	0	0	0	0	0	0
K2CO3	0	0	0	0	0	0	0	0	0	0	0	0	0	0	0
N2	0,005746	0	0	0	0	0	0	0	0	0	0	0	0	0	0
H3O+	0	0	0	0	0	0	0	0	0	0	0	0	0	0	0
K+	0	0	0	0	0	0	0	0	0	0	0	0	0	0	0
HCO3-	0	0	0	0	0	0	0	0	0	0	0	0	0	0	0
OH-	0	0	0	0	0	0	0	0	0	0	0	0	0	0	0
CO3--	0	0	0	0	0	0	0	0	0	0	0	0	0	0	0
CACO3	0	0	0	0	0	0	0	0	0	0	0	0	0	0	0
CA(OH)2	0	0	0	0	0	0	0	0	0	0	0	0	0	0	0
CAO	0	0	0	0	0	0	0	0	0	0	0	0	0	0	0
CA++	0	0	0	0	0	0	0	0	0	0	0	0	0	0	0
CAOH+	0	0	0	0	0	0	0	0	0	0	0	0	0	0	0
KOH(S)	0	0	0	0	0	0	0	0	0	0	0	0	0	0	0
CACO3(S)	0	0	0	0	0	0	0	0	0	0	0	0	0	0	0
K2CO3(S)	0	0	0	0	0	0	0	0	0	0	0	0	0	0	0
CH4	0	0	0	0	0	0	0	0	0	0	0	0	0	0	0
C2H6	0	0	0	0	0	0	0	0	0	0	0	0	0	0	0
CAO(S)	0	0	0	0	0	0	0	0	0	0	0	0	0	0	0
AR	0	0	0	0	0	0	0	0	0	0	0	0	0	0	0
CH3OH	0	0	0	0	0	0	0	0	0	0	0	0	0	0	0
H2	0	0	0	0	0	0	0	0,089519	0,309198	0	0	1	1	1	0
CO	0	0	0	0	0	0	0	0	0	0	0	0	0	0	0

UTILIZATION FACILITY pt.2-COUPLED DAC																		
STREAM-ID	H9-2	H9-3	R1	R2	R3	R4	REF-1-1	REF-1-2	REFLUX-2	REFLUX-3	M1	M2	M3	M4	METH	WATER	O2-TOCAL	PURGE
Mass flow rate[ton/h]	119,55	119,55	1072,16	1072,16	1072,16	1072,16	5,73	5,73	883,32	883,32	167,24	167,24	161,51	161,51	101,58	59,94	51,60	27,32
Temperature [°C]	700,00	25,00	467,31	270,00	270,00	30,00	31,00	31,00	17,37	526,75	30,00	30,67	31,00	25,00	37,39	98,99	700,28	17,37
Pressure [bar]	15	10	75	75	74,76	74,82	2,2	2,2	2,2	75	74,82	2,2	2,2	2,2	1	1	1	2,2
Mass Fractions																		
O2	1	1	0,008397	0,008397	0,008397	0,008397	0,001477	0,001477	0,009887	0,009887	5,12E-05	5,12E-05	6,20E-07	6,20E-07	9,86E-07	1,10E-120	1	0,009887
CO2	0	0	0,79097	0,79097	0,656412	0,656412	0,944617	0,944617	0,772087	0,772087	0,036404	0,036404	0,004188	0,004188	0,006659	1,80E-91	0	0,772089
H2O	0	0	0,000487	0,000487	0,055567	0,055567	0,005017	0,005017	0,000591	0,000591	0,353194	0,353194	0,365544	0,365544	0,001205	0,9830158	0	0,000591
KOH	0	0	0	0	0	0	0	0	0	0	0	0	0	0	0	0	0	0
K2CO3	0	0	0	0	0	0	0	0	0	0	0	0	0	0	0	0	0	0
N2	0	0	0,029885	0,029885	0,029885	0,029885	0,001556	0,001556	0,035186	0,035186	5,35E-05	5,35E-05	1,86E-07	1,86E-07	2,95E-07	3,63E-136	0	0,035185
H3O+	0	0	0	0	0	0	0	0	0	0	0	0	0	0	0	0	0	0
K+	0	0	0	0	0	0	0	0	0	0	0	0	0	0	0	0	0	0
HCO3-	0	0	0	0	0	0	0	0	0	0	0	0	0	0	0	0	0	0
OH-	0	0	0	0	0	0	0	0	0	0	0	0	0	0	0	0	0	0
CO3--	0	0	0	0	0	0	0	0	0	0	0	0	0	0	0	0	0	0
CACO3	0	0	0	0	0	0	0	0	0	0	0	0	0	0	0	0	0	0
CA(OH)2	0	0	0	0	0	0	0	0	0	0	0	0	0	0	0	0	0	0
CAO	0	0	0	0	0	0	0	0	0	0	0	0	0	0	0	0	0	0
CA++	0	0	0	0	0	0	0	0	0	0	0	0	0	0	0	0	0	0
CAOH+	0	0	0	0	0	0	0	0	0	0	0	0	0	0	0	0	0	0
KOH(S)	0	0	0	0	0	0	0	0	0	0	0	0	0	0	0	0	0	0
CACO3(S)	0	0	0	0	0	0	0	0	0	0	0	0	0	0	0	0	0	0
K2CO3(S)	0	0	0	0	0	0	0	0	0	0	0	0	0	0	0	0	0	0
CH4	0	0	0	0	0	0	0	0	0	0	0	0	0	0	0	0	0	0
C2H6	0	0	0	0	0	0	0	0	0	0	0	0	0	0	0	0	0	0
CAO(S)	0	0	0	0	0	0	0	0	0	0	0	0	0	0	0	0	0	0
AR	0	0	0	0	0	0	0	0	0	0	0	0	0	0	0	0	0	0
CH3OH	0	0	0,004699	0,004699	0,099788	0,099788	0,044064	0,044064	0,005703	0,005703	0,610185	0,610185	0,630267	0,630267	0,992134	0,0169842	0	0,005703
H2	0	0	0,084257	0,084257	0,066129	0,066129	0,001042	0,001042	0,077858	0,077858	3,57E-05	3,57E-05	3,43E-08	3,43E-08	5,46E-08	9,82E-152	0	0,077857
CO	0	0	0,081306	0,081306	0,083822	0,083822	0,002226	0,002226	0,098688	0,098688	7,64E-05	7,64E-05	1,34E-07	1,34E-07	2,14E-07	5,45E-144	0	0,098688

STEAM CYCLE- COUPLED DAC															
STREAM-ID	36-1	H2O-SUP	SC-1	SC-1-2	SC-2	SC-3	SC-4	SC-5	SC-6	SC-7	SC-8	SC-9	SC-10	SC-11	SC-12
Mass flow rate[ton/h]	7,00	7,00	182,10	182,10	182,10	38,10	38,10	143,99	143,99	143,99	136,99	136,99	175,10	175,10	7,00
Temperature [°C]	253,3	25	136,5	135,7723	137,08457	137,08457	500	137,0846	252	253,3	253,3	500	222,6808	140,065	25,01722
Pressure [bar]	42	1	3,5	3,5	42	42	42	42	42	42	42	42	3,5	3,5	3,5
Mass Fractions															
O2	0	0	0	0	0	0	0	0	0	0	0	0	0	0	0
CO2	0	0	0	0	0	0	0	0	0	0	0	0	0	0	0
H2O	1	1	1	1	1	1	1	1	1	1	1	1	1	1	1
KOH	0	0	0	0	0	0	0	0	0	0	0	0	0	0	0
K2CO3	0	0	0	0	0	0	0	0	0	0	0	0	0	0	0
N2	0	0	0	0	0	0	0	0	0	0	0	0	0	0	0
H3O+	0	0	0	0	0	0	0	0	0	0	0	0	0	0	0
K+	0	0	0	0	0	0	0	0	0	0	0	0	0	0	0
HCO3-	0	0	0	0	0	0	0	0	0	0	0	0	0	0	0
OH-	0	0	0	0	0	0	0	0	0	0	0	0	0	0	0
CO3--	0	0	0	0	0	0	0	0	0	0	0	0	0	0	0
CACO3	0	0	0	0	0	0	0	0	0	0	0	0	0	0	0
CA(OH)2	0	0	0	0	0	0	0	0	0	0	0	0	0	0	0
CAO	0	0	0	0	0	0	0	0	0	0	0	0	0	0	0
CA++	0	0	0	0	0	0	0	0	0	0	0	0	0	0	0
CAOH+	0	0	0	0	0	0	0	0	0	0	0	0	0	0	0
KOH(S)	0	0	0	0	0	0	0	0	0	0	0	0	0	0	0
CACO3(S)	0	0	0	0	0	0	0	0	0	0	0	0	0	0	0
K2CO3(S)	0	0	0	0	0	0	0	0	0	0	0	0	0	0	0
CH4	0	0	0	0	0	0	0	0	0	0	0	0	0	0	0
C2H6	0	0	0	0	0	0	0	0	0	0	0	0	0	0	0
CAO(S)	0	0	0	0	0	0	0	0	0	0	0	0	0	0	0
AR	0	0	0	0	0	0	0	0	0	0	0	0	0	0	0
CH3OH	0	0	0	0	0	0	0	0	0	0	0	0	0	0	0
H2	0	0	0	0	0	0	0	0	0	0	0	0	0	0	0
CO	0	0	0	0	0	0	0	0	0	0	0	0	0	0	0